

USING GEOPHYSICAL CONSTRAINTS TO DETERMINE GROUNDWATER  
TRAVEL TIMES, SEAFLOOR ARRIVAL LOCATIONS, AND SALTWATER  
CONCENTRATIONS FOR TRANSITION ZONE DEPTHS AT UNDERGROUND  
NUCLEAR DETONATIONS ON AMCHITKA ISLAND

Presented to the Faculty  
of the University of Alaska Fairbanks

in Partial Fulfillment of the Requirements  
for the Degree of

DOCTOR OF PHILOSOPHY

By

Anna M. Wagner, M. Sc.

Fairbanks, Alaska

August 2007

UMI Number: 3286627

Copyright 2008 by  
Wagner, Anna M.

All rights reserved.

### INFORMATION TO USERS

The quality of this reproduction is dependent upon the quality of the copy submitted. Broken or indistinct print, colored or poor quality illustrations and photographs, print bleed-through, substandard margins, and improper alignment can adversely affect reproduction.

In the unlikely event that the author did not send a complete manuscript and there are missing pages, these will be noted. Also, if unauthorized copyright material had to be removed, a note will indicate the deletion.

**UMI**<sup>®</sup>

---

UMI Microform 3286627

Copyright 2008 by ProQuest Information and Learning Company.

All rights reserved. This microform edition is protected against unauthorized copying under Title 17, United States Code.

ProQuest Information and Learning Company  
300 North Zeeb Road  
P.O. Box 1346  
Ann Arbor, MI 48106-1346

USING GEOPHYSICAL CONSTRAINTS TO DETERMINE GROUNDWATER  
TRAVEL TIMES, SEAFLOOR ARRIVAL LOCATIONS, AND SALTWATER  
CONCENTRATIONS FOR TRANSITION ZONE DEPTHS AT UNDERGROUND  
NUCLEAR DETONATIONS ON AMCHITKA ISLAND

By

Anna M. Wagner

RECOMMENDED: Martyr Unsworth

[Signature]

John P. Eichelberger

[Signature]

[Signature]

Advisory Committee Chair

[Signature]

Chair, Department of Civil and Environmental Engineering

APPROVED: [Signature]

Dean, College of Engineering and Mines

[Signature]  
Dean of the Graduate School

Aug 13, 2007  
Date

## Abstract

There is a great amount of radioactive material in the subsurface of Amchitka Island as a result from underground nuclear testing performed between 1965 and 1971. It is unknown how long it will take for the radionuclides to travel to the seafloor and the marine environment or where possible seepage zones will occur. The contaminant transport is greatly affected by the location of the transition zone (TZ) and the effective porosity, which were both determined by magnetotellurics (MT) in 2004. The hypothesis of this study was as follows: the groundwater travel times and seafloor arrival locations, can be estimated through groundwater modeling, with the location of the transition zone being estimated by magnetotellurics. An additional hypothesis is as follows: saltwater concentration for a TZ and the general subsurface characteristics can be quantified with groundwater modeling, using geophysical constraints in combination with saltwater and hydraulic head measurements.

The groundwater travel times were estimated with groundwater modeling using the transition zone location as determined by MT. Shortest groundwater travel times are 1,200 and 2,100 years, at Long Shot and Cannikin respectively. At Long Shot, a decreased groundwater travel time of up to 55 % could be seen when an enhanced hydraulic conductivity was included at the location of an assumed andesite sill layer. The seafloor arrival locations can be up to 1,000 and 2,100 m offshore at Long Shot and Cannikin respectively but will most likely occur closer to shore. This study was also successful at establishing the general characteristics of the subsurface by using geophysical constraints in combination with saltwater and hydraulic head measurements. The subsurface at Long Shot is isotropic or has mild anisotropy ratio of 1:2, which confirms the study by Fenske (1972). As represented in this study, this method has been shown to be valuable in determining the saltwater concentration of the TZ as determined by MT and can thus be used in further studies of islands and coastal areas.

## Table of Contents

	Page
Signature Page.....	i
Title Page.....	ii
Abstract.....	iii
Table of Contents.....	iv
List of Figures.....	vii
List of Tables.....	ix
Acknowledgements.....	x
<b>Chapter 1 Introduction.....</b>	<b>1</b>
<b>Chapter 2 Hypothesis.....</b>	<b>4</b>
<b>Chapter 3 Amchitka Island.....</b>	<b>8</b>
3.1. Geology.....	9
3.1.1. Geology at the Long Shot site.....	10
3.1.2. Geology at the Cannikin site.....	11
3.2. Hydrology.....	11
3.2.1. Hydrology at the Long Shot site.....	13
3.2.2. Hydrology at the Cannikin site.....	14
3.2.3. Location of the freshwater – saltwater transition zone.....	15
<b>Chapter 4 Underground Nuclear detonations.....</b>	<b>20</b>
4.1.1. Effects from the Long Shot explosion.....	21
4.1.2. Effects from the Cannikin explosion.....	22
<b>Chapter 5 Previous groundwater models.....</b>	<b>25</b>
5.1. Long Shot.....	25

5.2. Cannikin .....	26
<b>Chapter 6 Methods .....</b>	<b>28</b>
6.1. Model parameters .....	32
6.1.1. Long Shot groundwater modeling parameters .....	34
6.1.2. Cannikin groundwater modeling parameters .....	34
<b>Chapter 7 Results .....</b>	<b>37</b>
7.1. Long Shot.....	37
7.1.1. Simulated and measured shapes of TZ.....	37
7.1.2. Saltwater concentration distribution throughout the TZ.....	38
7.1.3. Simulated and measured saltwater concentrations .....	38
7.1.4. Simulated and measured environmental heads.....	39
7.1.5. Seafloor arrival locations .....	43
7.1.6. Groundwater travel times.....	43
7.1.7. Andesite sill layer.....	50
7.2. Cannikin .....	54
7.2.1. Simulated and measured shapes of TZ.....	54
7.2.2. Saltwater concentration distributions throughout the TZ.....	54
7.2.3. Simulated and measured saltwater concentrations .....	56
7.2.4. Simulated and measured environmental heads.....	56
7.2.5. Seafloor arrival locations .....	57
7.2.6. Groundwater travel times.....	58
7.2.7. Cannikin Lake and Rubble Chimney.....	63
7.3. Saltwater concentration distribution for the TZ .....	65
7.4. Groundwater table constraint .....	66
<b>Chapter 8 Discussions .....</b>	<b>68</b>
8.1. Long Shot.....	68

8.1.1. Shapes of the transition zone .....	68
8.1.2. Saltwater concentration distribution of the TZ.....	68
8.1.3. Comparing measured and simulated saltwater concentrations....	69
8.1.4. Comparing measured and simulated environmental heads .....	70
8.1.5. Seafloor arrival locations .....	70
8.1.6. Groundwater travel times.....	71
8.1.7. Andesite sill layer.....	73
8.2. Cannikin .....	74
8.2.1. Shapes of the transition zone .....	74
8.2.2. Saltwater concentration distribution for the TZ.....	75
8.2.3. Comparing measured and simulated saltwater concentration .....	75
8.2.4. Comparing measured and simulated environmental heads.....	76
8.2.5. Seafloor arrival locations .....	77
8.2.6. Groundwater travel times.....	77
8.2.7. Cannikin Lake and Rubble Chimney.....	81
8.3. Determining saltwater concentrations for the transition zones .....	82
8.4. Groundwater table constraint .....	82
8.5. Groundwater travel times compared to earlier studies .....	83
<b>Chapter 9 Conclusions .....</b>	<b>86</b>
<b>Chapter 10 Further work .....</b>	<b>93</b>
<b>Chapter 11 References.....</b>	<b>96</b>

## List of Figures

	Page
Figure 1.1 Location map of Amchitka Island.....	1
Figure 3.1 Amchitka Island and the MT profiles shown as. ....	9
Figure 3.2 Illustration of island hydrology showing the freshwater lens. ....	16
Figure 3.3 Flow pattern (solid lines) for a homogeneous and.....	16
Figure 3.4 a) Total dissolved salinity (TDS) measurements at Long Shot. ....	18
Figure 3.5 Electrical resistivity models of the a) Long Shot .....	19
Figure 4.1 Cannikin Lake that was created from the Cannikin .....	23
Figure 6.1 Topography at a) Long Shot and b) Cannikin.....	28
Figure 6.2 Location of the MT measurement stations (Unsworth et .....	29
Figure 6.3 Schematic cross-section with geometry and boundary conditions of	32
Figure 6.4 Effective porosity distributions as determined by magnetotellurics at	34
Figure 6.5 Illustration of topography and Cannikin Lake. The dotted.....	36
Figure 7.1 Simulated and measured saltwater concentrations for Long Shot.....	39
Figure 7.2 Simulated and measured environmental head measurements at.....	40
Figure 7.3 Shapes of the TZ (solid line) at Long Shot .....	41
Figure 7.4 Travel paths at Long Shot for different anisotropy.....	43
Figure 7.5 Comparison between longitudinal dispersivities and its affect.....	45
Figure 7.6 Recharge and hydraulic conductivity plotted versus groundwater.....	48
Figure 7.7 Recharge and hydraulic conductivity plotted versus groundwater.....	50
Figure 7.8 Shape of transition zones for the andesite sill .....	52
Figure 7.9 Total width of sills plotted versus groundwater travel .....	53
Figure 7.10 Travel paths and seafloor arrival locations for different .....	53
Figure 7.11 Shapes of the TZ (solid line) for isotropic .....	55
Figure 7.12 Measured and simulated saltwater concentrations for Cannikin.....	56
Figure 7.13 Simulated and measured environmental head measurements at....	57
Figure 7.14 Travel paths at Cannikin for particles originating at.....	58
Figure 7.15 Groundwater travel paths at Cannikin for different dispersivities.....	60

Figure 7.16 Recharge and hydraulic conductivity plotted versus groundwater...	62
Figure 7.17 Recharge and hydraulic conductivity plotted versus groundwater...	63
Figure 7.18 Shape of transition zones for a) an isotropic .....	65
Figure 7.19 Topography (thick line) and groundwater table (thick dashed line) .	67

## List of Tables

	Page
Table 3.1 Recharge and hydraulic conductivities at Long Shot (LS), Cannikin, .	14
Table 7.1 Saltwater concentration distributions throughout the TZ for Long.....	42
Table 7.2 Calculated travel times from the bottom of the cavity .....	47

## Acknowledgements

I would like to express gratitude to my advisor, Dr. David Barnes for introducing me to this project, and for giving me the opportunity to pursue my PhD. His help and encouragement led to the submission of this thesis. I also owe a great deal of gratitude to Dr. Martyn Unsworth (University of Alberta) for his constant support, guidance and encouragement. Martyn has provided magnetotelluric results and he gave me the opportunity to join the Amchitka research expedition in 2004. Furthermore I would like to extend appreciations to Dr. David Kosson (Vanderbilt University), Dr. John Eichelberger and Dr. Larry Hinzman, who have given me advice and support throughout my studies.

I gratefully acknowledge financial support from the Consortium for Risk Evaluation with Stakeholder Participation II (CRESP), the Inland Northwest Research Alliance (INRA), University of Alaska Fairbanks (UAF) Graduate School, and U.S. Department of Energy (DOE) under Award No. DE-FG26-00NT40938 to the Institute for Responsible Management, and Water and Environmental Research Center (WERC). However, any opinions, findings, conclusions, or recommendations expressed herein are those of the author and do not necessarily reflect the views of CRESP, INRA, UAF Graduate School, U.S DOE, or WERC. The Amchitka bathymetry data were provided courtesy of Robert Aguirre, Zygmunt Kowalik, and Mark Johnson. Thanks to all colleagues at Civil and Environmental Engineering at UAF and WERC. Especially thanks to Dr. John Zarling (UAF) who has been my mentor in many ways. I would also like to thank Ben Rostron and Carl Mendoza at the University of Alberta.

I am deeply indebted to friends and family for their encouragements throughout my studies. I would especially like to thank Anna Liljedahl for providing me with help and support throughout my time as a PhD student. Wes, you are everything to me, and Ronja, you are my forever sunshine.

I would like to dedicate this PhD thesis to my Mom and Dad; they have always given me love and support and without them I would not be here today.

## Chapter 1 Introduction

Underground nuclear testing on Amchitka Island in the 1960s and 1970s released large amounts of radioactive material in the subsurface. The island was chosen for the tests due to its remoteness (Figure 1.1) (Merritt, 1973), its favorable geology for containment of radionuclides, and its proximity to the eastern coast of what was then the Soviet Union (U.S. AEC 1971). The first explosion, Long Shot, was detonated at 701 m below ground surface (mbgs) (654 m below sea level (mbsl)) on October 29, 1965, with an announced yield of 80 kt. Its purpose was to investigate the seismic detection of nuclear tests as a part of the U.S. Department of Defense Vela Uniform program (U.S Army Corps of Engineers and USGS, 1965; DOE, 2000). Milrow, the second nuclear explosion, was detonated on October 2, 1969, with a yield of 1 Mt at 1218 mbgs and was a calibration explosion for Cannikin, a 5 Mt detonation. Cannikin was detonated 1728 mbsl (1791 mbgs) on November 6, 1971 (USGS, 1970; Merritt and Fuller, 1977). The detonation was a part of the weapons-testing program of the U.S. Department of Energy (DOE, formerly the U.S. Atomic Energy Commission) (Claassen, 1978).

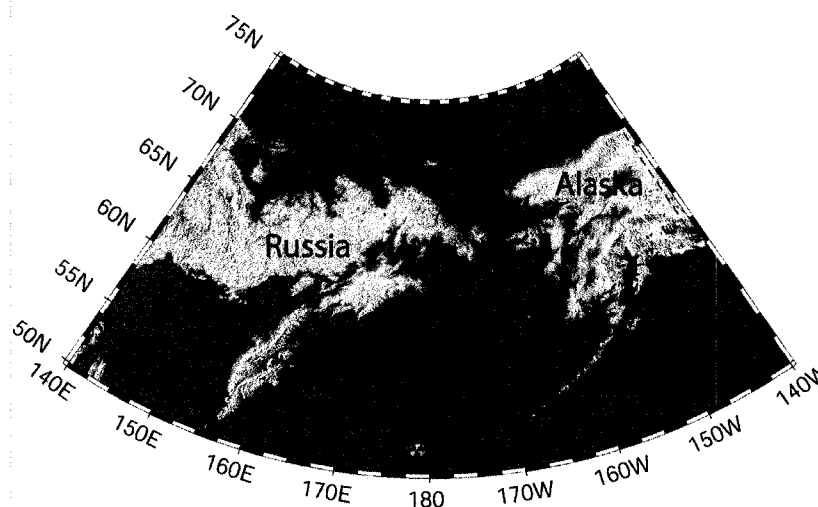


**Figure 1.1** Location map of Amchitka Island.

The nuclear explosions on Amchitka Island are not subject to the Comprehensive Environmental Response, Compensation, and Liability Act (CERCLA) (DOE, 2006a). However, Alaska Department of Environmental Conservation (ADEC) and DOE agreed to conduct remediation activities to appropriate cleanup standards on the mud pits used to contain drilling muds resulting from drilling each explosion's emplacement hole (DOE, 2006a). Removing the radionuclides from the nuclear explosion cavities is not technically feasible; therefore, a long-term monitoring of the island to ensure and protect human health from possible radioactivity from the nuclear explosions was needed (DOE, 2006b).

The Consortium for Risk Evaluation with Stakeholders Participation (CRESP) conducted an independent scientific assessment of Amchitka Island based on a request from the State of Alaska to provide a basis for long-term stewardship. As a result of the CRESP study (Powers et al., 2005). Amchitka is entering a long-term surveillance and maintenance phase and transferred to the responsibility of the DOE's Office of Legacy Management, which will oversee all monitoring and any future response actions (DOE, 2006a). A Long-Term Surveillance and Maintenance Plan (LTSMP) of Amchitka Island is being developed where details of the monitoring strategy including species to be sampled, frequency and method of collection, and radionuclides to be analyzed will be provided. Foodstuff and biota monitoring will be included in a regular periodic monitoring. Results from groundwater modeling and independent science studies will guide regular groundwater and surface water monitoring. At this time, DOE has determined that biota will be sampled at an interval of five years and at the same time interval an on-site inspection of the mud pit caps and other physical and institutional controls will be conducted (DOE, 2006a).

The rate of groundwater flow ultimately controls the radionuclide migration away from the explosion cavity (Kersting, 1996). Groundwater travel time depends on several parameters such as the hydraulic conductivity, rate of

recharge, location of the freshwater – saltwater transition zone (TZ), macrodispersivity, anisotropy, and effective porosity. As a part of the CRESP study, an extensive geophysical, and biological research expedition to Amchitka Island was carried out in 2004 (Powers et al., 2005). A part of the geophysical investigation was to locate the freshwater – saltwater TZ with magnetotellurics (MT) and to determine the effective porosities at the nuclear detonation sites (Unsworth et al., 2007). The objective of the research presented in this dissertation was to: determine groundwater travel times from Long Shot and Cannikin to the marine environment, determine seafloor arrival locations where radionuclides may enter the marine environment, and establish the general subsurface characteristics of the two sites and approximate a range of saltwater concentration for the freshwater – saltwater TZ as determined by MT. Radionuclide transport results in longer travel times compared to groundwater transport due to dissolution, precipitation, aqueous complexation, and sorption involved at radionuclide movement. In an environmental and human health perspective, investigating the groundwater travel time gives the shortest possible travel time to the marine environment, which is why the radionuclide transport was not investigated in this study.

## Chapter 2 Hypothesis

There is ongoing concern about the potential release of radionuclides into the marine environment at Amchitka Island. Even though there have been other studies estimating the groundwater travel time on Amchitka Island (U.S. Army Corps of Engineers and USGS, 1965; Ballance, 1970; Fenske, 1972; Wheatcraft, 1995; Hassan et al., 2002), they all reported a great uncertainty due to the limited information available. With recently gathered information by Unsworth et al (2007) of the location of the freshwater – saltwater transition zone and the effective porosity (both of which influence the groundwater travel time significantly), a study was needed to investigate whether this information could be used to decrease the uncertainty of the groundwater travel time. The focus of this doctoral dissertation is on the Long Shot and Cannikin test sites with the hypothesis as follows: the groundwater travel times and seafloor arrival locations, can be estimated through groundwater modeling, with the location of the transition zone being estimated by magnetotellurics. An additional hypothesis is as follows: saltwater concentration for a TZ and the general subsurface characteristics can be quantified with groundwater modeling, using geophysical constraints in combination with saltwater and hydraulic head measurements.

To investigate this hypothesis, a deterministic finite element groundwater model was created for the Long Shot and Cannikin sites. The location of the freshwater – saltwater TZ is directly related to the elevation of the water table above sea level and subsurface characteristics such as dispersivity and anisotropy. The groundwater travel time decreases with an increase in freshwater lens thickness and the freshwater lens thickness increases with an increase in groundwater table elevation. A high groundwater table across the island will result in a shorter groundwater travel time compared to if the island has a lower groundwater table. If the groundwater table is fixed, the location of the freshwater – saltwater TZ will be fixed for scenarios having the same anisotropy and

dispersivity; changing the hydraulic conductivity or recharge rate will only affect the groundwater travel time and not the location of the TZ. On Amchitka Island the groundwater table is located within a few meters of the ground surface (Gonzalez, 1977; Merritt and Fuller, 1977). When considering the effect that the groundwater table has on groundwater travel time, the shortest groundwater travel time would be for a groundwater table located close to the ground surface. In this study the groundwater table was thus fixed to a meter below ground surface. Several scenarios were simulated using different dispersivities and anisotropies in order to see how the shape of the transition zones would match the shape of the transition zone as determined by MT. Furthermore, the saltwater concentration distribution at the nuclear device emplacement hole and at the depths of the transition zone as determined by MT were investigated. Simulated hydraulic heads and saltwater concentrations were also compared to measured values obtained by U.S. Army Corps of Engineers and USGS (1965), Ballance (1970), Beteem et al., (1971), Ballance (1972), and Ballance and Dinwiddie (1972). From likely scenarios, the groundwater travel times and seafloor arrival locations were determined for historical assumptions of hydraulic conductivity and recharge. Data at Milrow were not investigated due to limited data collection (Unsworth, 2007) of the magnetotelluric measurements in 2004.

The groundwater system and groundwater travel times on Amchitka Island have been investigated in earlier models (U.S. Army Corps of Engineers and USGS, 1965; Ballance, 1970; Fenske, 1972; Wheatcraft, 1995; Hassan et al., 2002; Hassan and Chapman, 2006). Ballance (1970) estimated the groundwater travel time at Cannikin from measured hydraulic conductivities in the emplacement hole. Fenske (1972) used Darcy's law, age dating water, and infiltration parameter to estimate the groundwater travel time at the detonation sites. Wheatcraft (1995) used a finite element program and modeled the Long Shot site as an isotropic subsurface and with the groundwater divide at half-island. Further investigation by Hassan et al., (2002) was done for the three

detonation sites, where finite element and stochastic modeling approaches were used. The modeled sections were established from the upper boundary condition and the location of the topographic divide and were assigned an assumed homogeneous but anisotropic subsurface (ratio 1:10), with a spatial variability for the detonation cavity and chimney. Hassan et al., (2002) also used a mean effective porosity of  $5 \times 10^{-4}$  which, compared to the MT results is up to four orders of magnitude less than determined by MT.

In contrast to other models, here the whole cross section of the island from the Bering Sea to the Pacific Ocean was used. The full effect of the topography has therefore not been considered before nor has using the groundwater table as a boundary constraint. Moreover, this is also the first time MT data had been used as an added tool to determine the groundwater travel time on Amchitka Island. Finally, unique to this study is determining the saltwater concentration for the TZ as determined by MT. A deterministic model was chosen due to the greater control of investigating each simulation to make sure that the result yields a possible scenario. For example, when calibrating to hydraulic head measurements, even though the simulated hydraulic head fits the measured data at the emplacement hole, it does not mean that it gives a realistic result at other locations on the island. Also, even though it matches the hydraulic head measurements at deeper depths it does not mean that it will yield a probable groundwater table. Hassan et al. (2002) used a stochastic approach and some of their calibration to the hydraulic head yielded non-realistic freshwater tables that, at Cannikin, are 15 – 20 m above the ground surface (estimated from graph). A groundwater table that is higher than the ground surface will result in a deeper freshwater lens and thus shorter groundwater travel times. Due to the random selection of parameters in a stochastic approach it is also difficult to investigate how each parameter affects the shape of the transition zone.

This model is being developed for further usage by University of Alaska and the State of Alaska as part of the Amchitka long-term stewardship effort. The

National Academy of Science has recognized that multiple assessments are necessary for successful long-term stewardship. Multiple assessments generated by different groups provide stakeholders with multiple views upon which to base their confidence level in decisions being made about a site that will impact them. The resulting models will enable improved estimation of radionuclide transport rates and location for further offshore measurements as a part of a long-term monitoring program for Long Shot and Cannikin by using additional information about the subsurface as provided by magnetotellurics.

### Chapter 3 Amchitka Island

Amchitka is one of the Rat Islands in the seismically very active western part of the Aleutian chain (Merritt, 1973). The arc lies along a zone of convergence between the Pacific Ocean floor and the Bering Sea floor (Merritt and Fuller, 1977) and is one of the largest and most active subduction zones in the world (Myers, 1994). Amchitka Island is 2 to 7 km wide, 65 km long, and has an area of approximately 30,000 ha (Figure 3.1). The island is roughly boot shaped that most likely originates from faulting (Merritt and Fuller, 1977). Main great earthquakes occur along the contact zone between the subducting and overriding plate (Ryan and Scholl, 1993). Along the Aleutian arc the great earthquakes occur at the Rat and Andreanof blocks where stress is concentrated along mechanically strong segments. Numerous faults and fractures cross the island with an east-northeast trend. Most of the land surface has a rich growth of alpine-zone mosses and grasses. The elevations on the island range from sea level to 350 m with an estimated average elevation of 85 m. The characteristic of the eastern third of the island, where the detonations occurred, is a rolling country with many ponds that have little or no surface water outlet. Reported mean annual precipitation for February 1943 through June 1948, and from October 1967 through June 1972 was 828 and 953 mm respectively (Merritt and Fuller, 1977). U.S. Geological Survey (USGS) investigated the geologic, hydrologic, and tectonic environment of Amchitka Island at possible detonation sites prior to the detonations from 1964 to 1972 (Merritt and Fuller, 1977).

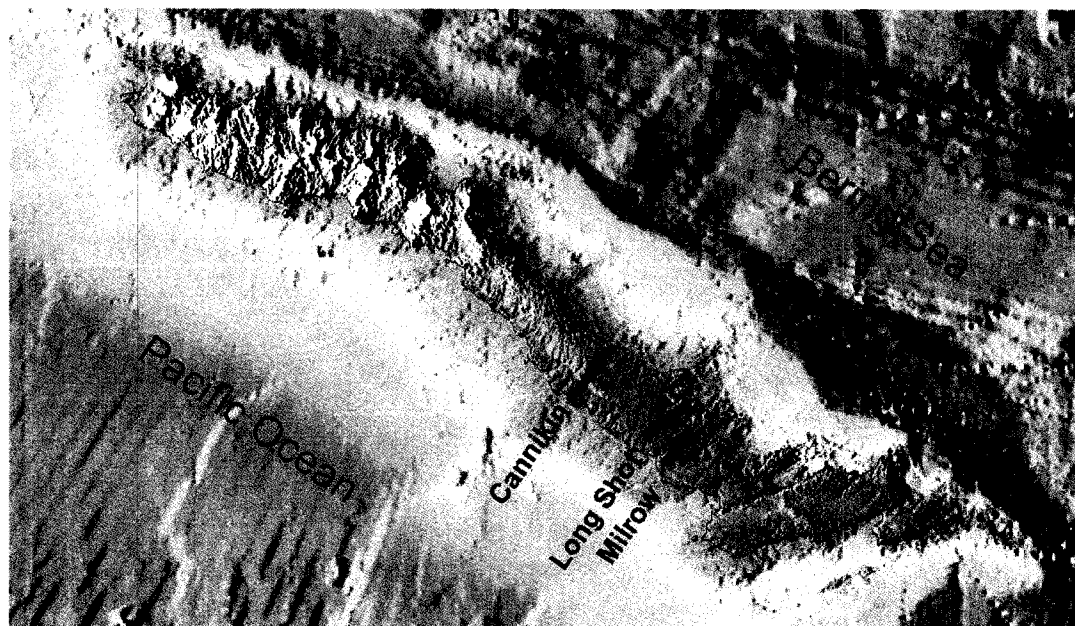


**Figure 3.1** Amchitka Island and the MT profiles shown as filled circles. Triangles show the location of the detonations (Unsworth et al., 2005).

### 3.1. Geology

USGS performed extensive studies on the geology and hydrology of Amchitka Island prior to the underground detonations from 1964 to 1972. Amchitka Island is a part of the Aleutian Island arc that extends from the Gulf of Alaska across the north Pacific to Kamchatka with a parallel ridge rising to the north (Merritt and Fuller, 1977). The western part of this ridge is the Aleutian Islands and the eastern part is the mountainous Alaska Peninsula. A zone of convergence exists along the Aleutian arc, although some of the tectonic features within the islands are of probable tensional origin. Faulting, differential uplift, marine, stream, and glacial erosion, which are predominant forces in the Aleutians, have disturbed Amchitka Island (U.S. Army Corps of Engineers and USGS, 1965). The island has a strongly developed joint and fault system. Submarine topography of the north side of the island displays southeast-trending linear scarps, ridges and troughs paralleling the island whereas the south side of the island shows northeast-trending scarps, ridges, and troughs that lie normal to the trend of the

island. The faulting and jointing of the island may be reflected by these northeast-trends.

The bedrock of Amchitka Island is primarily Tertiary submarine and subaerially deposited volcanoclastic rocks with subordinate lava flows and intrusive units (U.S. Corps of Engineers and USGS, 1965). The rock of Amchitka Island is divided into four major stratigraphic units: (1) older breccias and hornfels, (2) the pillow lavas and breccias of Kirilof Point, (3) the Banjo Point Formation, and (4) the Chitka Point Formation (Carr and Quinlivan, 1969).

Most of the anisotropic character of the site can be accounted for between 200 and 400 mbsl, suggesting that below a depth of 400 mbsl the island can be considered homogeneous and isotropic.

### **3.1.1. Geology at the Long Shot site**

The Long Shot site is underlain by 1,220 m of Banjo Point formation (Gard and Hale, 1964). Fractures and/or fault zones bound tertiary volcanic tuffs and breccias on the northwest, southeast, and southwest sides (U.S. Army Corps of Engineers and USGS, 1965). At ground zero (GZ), the rocks are altered pyroclastic rocks of andesitic and basaltic composition. The trend of the lineations is generally transverse to the island (N 55°E to N 60°E) near the Long Shot site (Gard and Hale, 1964).

Starting in 1964, the U.S. Corps of Engineers performed exploratory drilling for the Long Shot detonation. Vertical and directional holes EH-1, EH-3, EH-5 (emplacement hole), EH-5a, EH-6, and EH-6a were successfully cored and logged (U.S. Army Corps of Engineers and USGS, 1965). The cores obtained from the exploratory drilling and from outcrop rocks are of volcanic material with a composition of basaltic andesite (U.S. Corps of Engineers and USGS, 1965). Breccias and tuffs are the primary rock types. Pyroclastic and intrusive rocks are less representative. One notable stratigraphic feature in this region of the island is the two layers of andesite encountered in EH-3, EH-5, EH-5a, and EH-6a between depths of 678 and 771 mbsl. The "main andesite" is about 76 m thick

overlaid by a 4.6 m thick layer, referred to as the "first andesite". A layer of tuff and siltstone is embedded in between the andesite sills. The horizontal extent of this layer is unknown but if extensive, this layer of enhanced hydraulic conductivity could result in a shorter groundwater travel time into the marine environment. Long Shot was detonated within one of the main sills.

### **3.1.2. Geology at the Cannikin site**

At the Cannikin site, boreholes UA-1 and UA-1-HTH-1 were drilled to a depth of 1,461 and 1,004 mbsl respectively (Ballance, 1970; Ballance and Dinwiddie, 1972). UA-1-HTH-1 was located approximately 1 km north of the emplacement hole. UAe-1 was drilled about 90 m southwest of UA-1 to a depth of 2,070 mbsl (Ballance, 1972). The Banjo Point Formation and the Amchitka Formation are penetrated at the Cannikin site with the Amchitka Formation divided into pillow lavas and breccias of Kirilof Point and older breccias (Lee and Gard, 1971). The older breccias and hornfels are fine- to coarse-grained sedimentary breccias with approximately 10 to 20 percent interbedded sandstone, siltstone and claystone containing volcanic debris (Carr and Quinlivan, 1969). Merritt and Fuller (1977) estimated the fracture porosity to range between  $1.9 \times 10^{-3}$  and  $6.3 \times 10^{-2}$  % at the Cannikin site.

When compared to overlying and underlying aquifers there is a low hydraulic conductivity zone at a depth of 200 to 400 mbsl (Fenske, 1972). In the lithologic log there is a 21-m zone of sandstone at approximately 197 mbsl and a 12-m zone of siltstone at a depth of 368 mbsl, which have a low porosity and most likely a low hydraulic conductivity.

### **3.2. Hydrology**

A hydrologic network was established on Amchitka Island in 1967 and continued through August 1974. The hydrologic studies were prompted by the potential of using Amchitka Island as a location for high-yield nuclear weapons testing. Surface water gauging stations and groundwater observation wells were installed

at potential sites for possible high-yield emplacement holes. Groundwater investigations performed during this investigation included water level monitoring in test wells and other holes. The program included detailed testing of deep exploratory holes at actual and potential test sites across the island. The investigation also integrated a surface study of hydrologic features such as springs, terrestrial seeps, and perennial lakes and streams.

The lower plateaus of Amchitka Island are composed of small drainage basins and hundreds of small lakes and ponds (Gonzalez, 1977) with bottom sediments of low permeability materials (Merritt and Fuller, 1977). Precipitation temporarily stored in the lakes and mantle of tundra and peat moves directly to the stream channels or laterally to the stream courses, and thereafter discharges into the ocean (U.S. Army Corps of Engineers and USGS, 1965). The upper few meters to a few hundred meters beneath the surface of Amchitka Island consist of permeable materials such as tundra, soil, peat, and fractured and weathered volcanic rocks (Merritt and Fuller, 1977). In shallow observation wells, a rapid response in water levels could be seen during precipitation events. This response indicates a high infiltration rate in the top few meters of the subsurface. A clay zone is present at the base of the tundra and peat in some areas across the island, which retards the recharge to the bedrock (U.S. Army Corps of Engineers and USGS, 1965). These two observations lead to the conclusion that a large fraction of precipitation infiltrates and flows through shallow aquifers and discharges to surface bodies. Gonzalez (1977) and Merritt and Fuller (1977) performed a comparison between precipitation and runoff altitude relationships and concluded that most precipitation results in surface water runoff. At several test holes, the water level was within few meters of the land surface, which implies that the sediment of the lowland parts of the island is saturated essentially to land surface. Gonzalez (1977) and Merritt and Fuller (1977) also suggest that the water table is at or very near surface over most of Amchitka

Island. The hydraulic conductivity on Amchitka has been estimated to range over three orders of magnitude  $1.2 \times 10^{-9}$  to  $1.2 \times 10^{-6}$  m/s (Hassan et al., 2002).

### **3.2.1. Hydrology at the Long Shot site**

The Long Shot explosion was detonated at a depth of 654 mbsl and within the Banjo Point Formation. Based on swab tests in hole EH-5 and pumping tests in EH-1 and EH-5, Gard and Hale (1964) estimated an overall hydraulic conductivity of the aquifer system ranging between  $1.0 \times 10^{-7}$  and  $3.5 \times 10^{-7}$  m/s. Estimated and measured values of recharge and hydraulic conductivities are listed in Table 3.1. The andesite sills encountered between 678 to 771 mbsl contain cooling joints. When compared with the bulk of the bedrock, the sills are of moderate hydraulic conductivity and, thus affect the overall groundwater flow. The hydraulic conductivity of the fractured andesite sill units is one to two orders of magnitude greater than the host rock formation,  $4.7 \times 10^{-8}$  to  $4.7 \times 10^{-7}$  m/s, which is slightly greater than the hydraulic conductivity of the Banjo Point bedrock (U.S. Corps of Engineers and USGS, 1965). The permeability of the Banjo Point formation above the sills is approximately  $4.7 \times 10^{-9}$  m/s. A bulk hydraulic conductivity of the Banjo Point formation is approximately  $3.5 \times 10^{-8}$  m/s (Hazleton-Nuclear Science Corporation, 1964). However, the Banjo Point formation may have an overall greater hydraulic conductivity than indicated from swab and pump tests because conditioned drilling fluids were used to reduce circulation losses and existing mud-filled fractures were not reopened (U.S. Army Corps of Engineers and USGS, 1965). A higher than reported permeability of the formation was also indicated by increased water losses out of the borehole, as well as a greater number of reported fractures in EH-3, which was directionally drilled across the principal fracture grain. In summary, the most permeable of the Banjo Point formation is within fracture zones, followed by a moderate permeability in the sills and the bulk of the formation is of low permeability. Considering the thickness of the sills in comparison to fractured zones, the sills are more transmissive and, thus constitute a major pathway for groundwater flow.

Principal recharge to the system at the Long Shot site is most likely along fracture zones.

Gard and Hale (1964) computed a recharge rate to range between 4 and 12 % ( $9.7 \times 10^{-5}$  to  $2.9 \times 10^{-4}$  m/day) at Long Shot presuming an annual precipitation of 889 mm. This rate was based on flow-net model, head distribution, and estimated hydraulic conductivity for Long Shot. Hassan et al., (2002) estimated the recharge to  $9.3 \times 10^{-5}$  m/day from the temperature profile at Milrow (UAe-2).

**Table 3.1** Recharge and hydraulic conductivities at Long Shot (LS), Cannikin, and Amchitka as reported by Hassan et al.,<sup>(1)</sup> (2002), Gard and Hale<sup>(2)</sup> (1964), Fenske<sup>(3)</sup> (1972), Hazleton-Nuclear Science Corporation (1964)<sup>(4)</sup> and U.S. Army Corps of Engineers and USGS<sup>(5)</sup> (1965).

Recharge	(m/day)
LS Temperature profile <sup>(1)</sup>	$9.3 \times 10^{-5}$
LS 4 % <sup>(2)</sup>	$9.7 \times 10^{-5}$
LS 12 % <sup>(2)</sup>	$2.9 \times 10^{-4}$
DRI LS calibration <sup>(1)</sup>	$2.2 \times 10^{-5}$ to $3.86 \times 10^{-4}$
DRI Cannikin calibration <sup>(1)</sup>	$2.2 \times 10^{-5}$ to $5.2 \times 10^{-4}$
Cannikin Temperature profile <sup>(1)</sup>	$1.2 \times 10^{-5}$
Cannikin UAe-1 <sup>(3)</sup>	$2.2 \times 10^{-4}$
Hydraulic conductivity	(m/s)
Banjo Point formation <sup>(4)</sup>	$3.5 \times 10^{-8}$
Above andesite sills <sup>(5)</sup>	$4.7 \times 10^{-8}$ to $4.7 \times 10^{-9}$
Fractured andesite sill units <sup>(5)</sup>	$4.7 \times 10^{-8}$ to $4.7 \times 10^{-7}$
Long Shot aquifer <sup>(2)</sup>	$1.0 \times 10^{-7}$ to $3.5 \times 10^{-7}$
Cannikin aquifer <sup>(3)</sup>	$2.9 \times 10^{-7}$ to $3.8 \times 10^{-7}$
Amchitka <sup>(1)</sup>	$1.2 \times 10^{-9}$ to $1.2 \times 10^{-6}$

### 3.2.2. Hydrology at the Cannikin site

Cannikin site is located in the White Alice Creek drainage basin (Gonzalez, 1977). The basin drains into the Bering Sea and is approximately 2 km<sup>2</sup> in area. A layer of turf and underlying peat covers the land surface and only 2 % of the basin is covered with lakes. The average altitude at the Cannikin site is 50 m with a range from 15 to 85 m (Gonzalez et al., 1974). Based on cumulative precipitation and runoff comparisons, the precipitation at the Cannikin site is most likely in excess of 1.1 m (Gonzalez, 1977). The recharge at Cannikin was estimated from the temperature profile at UAe-2 to  $1.2 \times 10^{-5}$  m/day (Hassan et al., 2002) and by Fenske (1972) to  $2.2 \times 10^{-4}$  m/day. Hydraulic conductivities

were estimated from hydrotest data at the Cannikin site to range between  $2.9 \times 10^{-7}$  and  $3.8 \times 10^{-7}$  m/s (Fenske, 1972).

### 3.2.3. Location of the freshwater – saltwater transition zone

Beneath oceanic islands, a lens of moving freshwater overlies denser saline water. In the ideal case of a homogeneous and isotropic island, the freshwater body assumes a lenticular (lens-like) shape bounded at its base by a concave-upward surface with the thickest part under the middle of the island (Figure 3.2). The infiltrating water flows laterally and thereafter upward, exiting in seepage zones along the shoreline (Figure 3.3). At the transition zone between the freshwater and saltwater, the saltwater is not static but flows in a cycle from the seafloor to the zone of diffusion and back to the sea (Cooper et al., 1964).

Several methods have been formulated to estimate the freshwater interface with saltwater in coastal and island aquifers. A simplified method is by assuming freshwater and saltwater to be immiscible and that the liquids are static (Cooper et al., 1964). The freshwater – saltwater interface,  $z$ , can be estimated by using the Ghyben-Herzberg relationship:

$$z = \frac{\rho_f}{\rho_s - \rho_f} h \approx 40h \quad 3.1$$

where  $\rho_f$  ( $\text{g/cm}^3$ ) is the freshwater density,  $\rho_s$  ( $\text{g/cm}^3$ ) is the saltwater density, and  $h$  is the head in the fresh water. The freshwater – saltwater TZ is at a depth of approximately 40 times the elevation of the water table above sea level (Figure 3.2). However, in actuality a sharp interface between the two fluids does not exist as assumed in the Ghyben-Herzberg model. Instead, there is a mixing or transition zone through the action of ocean tides, seasonal fluctuations of the water table, diffusion in response to salinity, density gradient of saltwater, and temperature gradients. The assumption of hydrostatic fluids in the Ghyben-

Herzberg model eliminates discharge of the freshwater, but the actual lens extends out under the sea floor and provides a discharge area for the fresh groundwater. In addition, there is a head loss due to friction from the fresh groundwater that seeps through the rocks. The assumptions that make up this relationship result in an overestimation of the depth to the freshwater – saltwater transition zone by the Ghyben-Herzberg model.

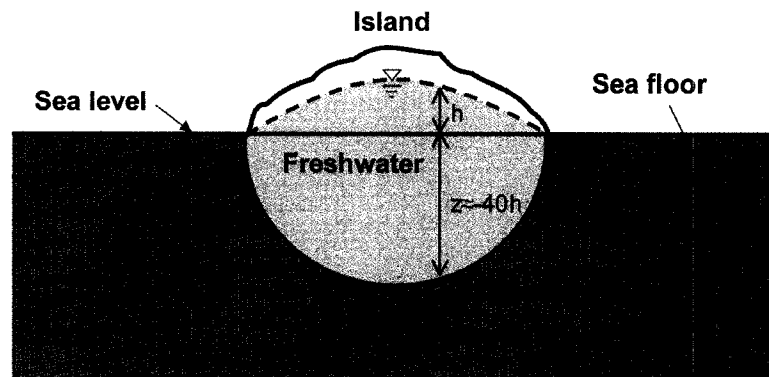


**Figure 3.2** Illustration of island hydrology showing the freshwater lens for a homogeneous subsurface. The thickness of the freshwater lens ( $z$ ) is approximately forty times the elevation of the groundwater table from the sea level ( $h$ ).

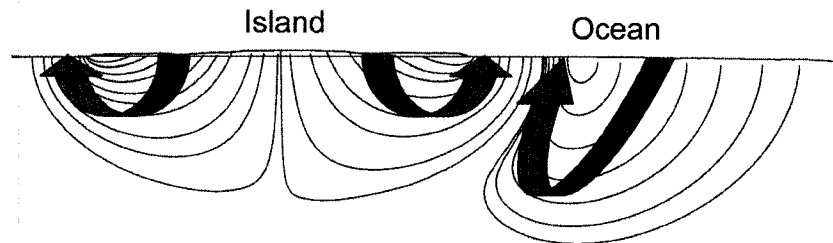


**Figure 3.3** Flow pattern (solid lines) for a homogeneous and isotropic subsurface. The general direction of flow is illustrated with dark gray arrows.

On Amchitka, the groundwater is most likely flowing from approximately the central part of the island towards the coast as is consistent with island groundwater hydrology (U.S. Army Corps of Engineers and USGS, 1965). According to hydraulic tests and temperature surveys, the hydraulic head decreases with depth and the overall direction of groundwater flow beneath most of Amchitka is downward (Gonzalez, 1977).

Several methods have been used to determine the freshwater saltwater – transition zone at Amchitka Island. The Ghyben-Herzberg relationship results in an interface depth of 1,720 mbsl at Long Shot when considering the ground surface elevation to be 43 m (U.S. Corps of Engineers and USGS, 1965). At the Cannikin site the elevation is 63 m resulting in an interface depth at 2,520 mbsl.

Another method to locate the freshwater – saltwater transition zone is the potential method (Fenske, 1972). By using piezometer wells at different depths throughout the system, the potential distributions in the lens can be found. The interface is at a depth of the inflection point (in the TZ) of the environmental head (measured hydraulic head in an aquifer with non-uniform density) curve. From potential data at Long Shot (EH-1 and EH-5) and Cannikin (UAe-1 and UA-1-HTH-1), Fenske (1972) estimated this point to be 1,120 mbsl at the Long Shot and Cannikin sites. It should be noted that these estimates are based on potential data that are subject to error at both sites.

Chemical analysis of groundwater samples taken at various depths provides another means of determining the depth to the interface. An increase in salinity with depth in exploratory holes could generally be seen from water swabbed at intervals isolated by straddle packers (Beteem et al., 1971). Analyzing multiple groundwater samples for total dissolved-solids (TDS) results in a TDS distribution from which the depth to the interface can be inferred. Figure 3.4 shows TDS concentration measurements from EH-5 (Long Shot), UAe-1 (Cannikin) and UAe-2 (Milrow). At the Long Shot site (EH-5), the water contained between 300 and 500 ppm chloride at a depth of 671 to 792 mbsl (Fenske, 1972). This result implies a freshwater – saltwater interface close to this depth. The salinity in UAe-1 is approximately a tenth of that predicted. It could be that the freshwater is from a time when the sea level was lower or that drilling fluid contaminated the rocks (Fenske, 1972). A lower salinity than predicted is not detected in UAe-2, making the contamination of rocks by drilling fluids the most likely explanation. In contrast, Merritt and Fuller (1977) reported that data is correct and that the

freshwater lens extends to at least 1,750 meters below sea level (mbsl) at the Cannikin site.

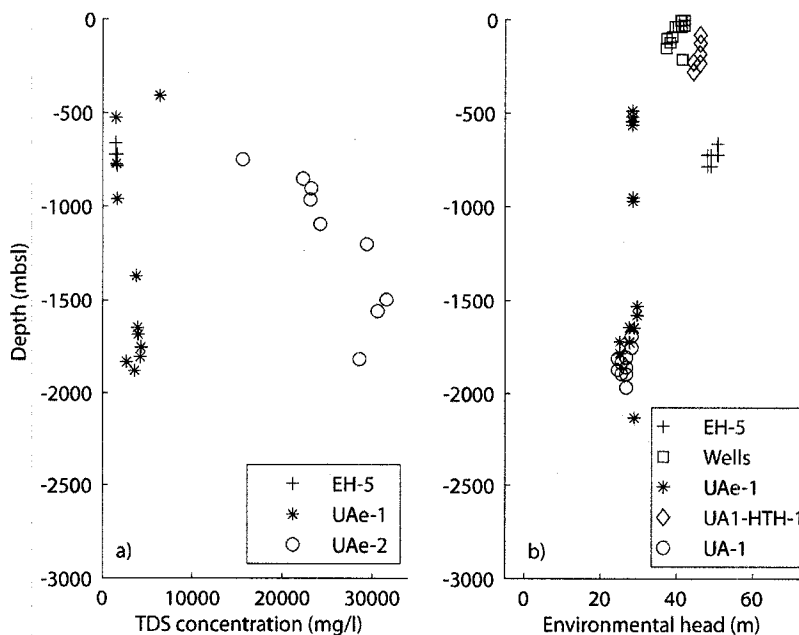


**Figure 3.4** a) Total dissolved salinity (TDS) measurements at Long Shot (EH-5), Cannikin (UAe-1) and Milrow (UAe-2) (Beteem et al., 1971; U.S. Corps of Engineers and USGS, 1965). b) Environmental head measurements at Long Shot (EH-5), Cannikin (UAe-1, UA1-HTH-1, UA-1), and shallow wells (U.S. Corps of Engineers and USGS, 1965; Ballance, 1972; Ballance and Dinwiddie, 1972; Ballance, 1970).

In 2004, magnetotelluric measurements were performed in order to locate the freshwater – saltwater TZ depth (Unsworth et al., 2007). It was concluded that the zone of increasing salinity is approximately between 600 and 1,700 m at the Long Shot site (Figure 3.5). Due to non-uniqueness of the data analysis (data error, insufficiency, and data sparseness), the top and base of the transition zone could be in the range 500 to 1,000 m and 1,500 to 2,000 m respectively. At Cannikin, the freshwater – saltwater transition zone was measured between 1,100 and 2,300 mbsl, with uncertainties ranging from 1,000 to 1,200 mbsl and 2,000 to 2,700 mbsl for the top and bottom boundary respectively (Unsworth, 2007). The location of the TZ at Cannikin is considered deeper than what has been found in previous studies. This would result in shorter groundwater travel times when the location of the TZ as determined by MT is used. It is interesting

how well the bottom of the TZ as measured by MT corresponds to the TZ as estimated by using the Ghyben-Herzberg definition (1,720 mbsl at Long Shot and 2,520 mbsl at Cannikin).

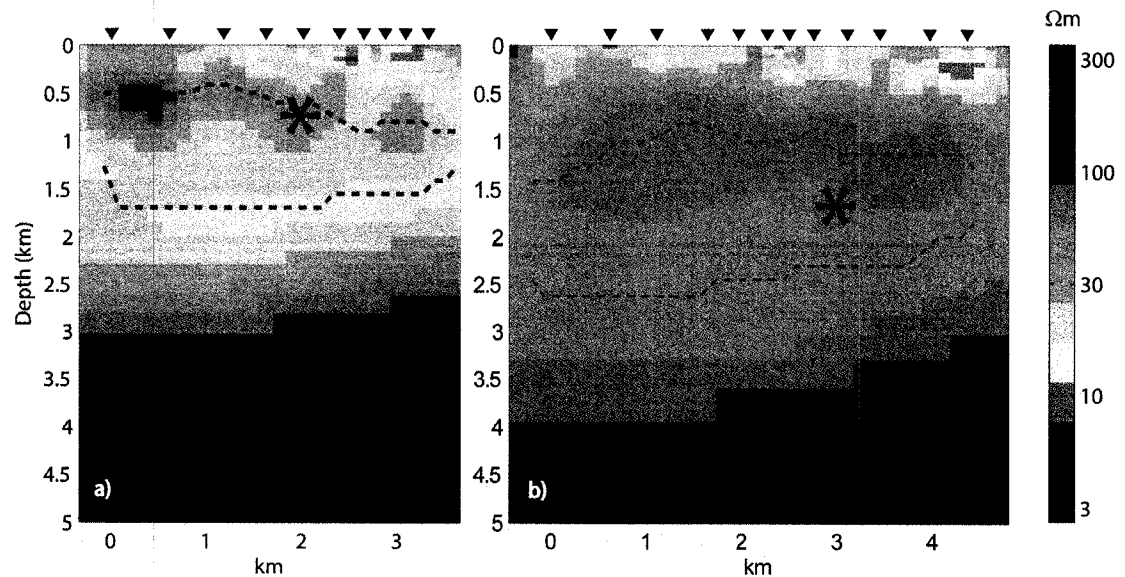


**Figure 3.5** Electrical resistivity models of the a) Long Shot and b) Cannikin profile derived from magnetotelluric (MT) data (Unsworth, 2007). The triangles show locations of MT measurement stations and asterisks show the nuclear explosion locations. Dashed lines illustrate the TZ and are associated with a downward decrease in resistivity caused by an increase in groundwater salinity (Unsworth et al., 2007).

## Chapter 4 Underground Nuclear detonations

In an underground nuclear detonation, the material surrounding the nuclear device vaporizes and a shock wave is created from the expanded vapor (Allen et al., 1997). The shock wave vaporizes and melts more rock creating a region of high heat and pressure. A roughly spherical cavity is created from the driving force of the high-pressure gases and the momentum imparted by the shock wave. Gases are held within the cavity by residual compressive stresses. The shock wave force deforms the rock inelastically, causing fracturing beyond the cavity region. When the shock wave reaches the ground surface, a dome-like expansion or uplift can be seen. At the bottom of the cavity, melted rock collects and solidifies as a puddle of glass containing most of the radioactive material. Eventually, the cavity walls collapse and the overlying rock falls downward as rubble, forming a cylindrical shaped column above the cavity referred to as the rubble chimney. International Advisory Committee (IAEA) (1998a) estimates the rubble chimney porosity at underground nuclear detonations to range between 19 and 21 %. Owing to the initial creation of a chimney from the cavity upwards and the subsequent collapse of overburden material into this chimney, the porosity of the chimney zone is most likely substantially greater than the surrounding fractured rock. The formation of a rubble chimney most likely results in an increase of hydraulic conductivity (Garber, 1971). In granite rocks, a two to three orders of magnitude increase in hydraulic conductivity of the rubble chimney compared to the surrounding rock has been seen (Boardman and Skrove, 1966).

During initial cooling of the cavity, the radionuclides are incorporated into the melt glass and deposited on the rubble (Kersting, 1996). The partitioning between the melt glass and rubble depends on the radionuclide. As an example, IAEA (1998a) reported a partitioning between the melt glass and rubble chimney for  $^{233}\text{U}$  and  $^{236}\text{U}$  to 90 and 10 % respectively. Plutonium isotopes partitions were

also reported to 98 and 2 % between the melt glass and rubble chimney, respectively. Radionuclides are also deposited along fractured surface both within and outside the cavity but their initial maximum distribution is unknown (Kersting, 1996). At the Nevada Test Site (NTS) radionuclides have been documented throughout the rubble at a minimum distance of five cavity radii vertically for the most volatile elements. Dissolution (leaching) rates between glass, debris, and water determine whether radionuclides are transported with the groundwater. Smith and Bourcier (1998) performed a dissolution rate model and reported that the release of radionuclides from the melt glass at Amchitka is over a period of more than one million years.

The following processes control the concentration and transport of radionuclides to the groundwater once leached from the melt glass or rubble: precipitation, aqueous complexation, sorption, and colloid formation (Kersting, 1996). Radionuclides can either sorb to or form colloidal particles and depending on their size they can move either slower or faster than the groundwater (Silva and Nitsche, 1995). An enhanced relative velocity will occur when repelled from the host rock if the colloids have the same charge as the rock.

At the Nevada Test Site (NTS), 828 underground nuclear detonations were conducted between 1951 and 1992 at depths between 500 and 1,200 mbgs (DOE, 2000; Hu et al., 2003). The primarily geologic media where these detonations occurred were tuffs, rhyolites, and tuffaceous alluvium (Hu et al., 2003). In the Pacific there has been 106 numbers of nuclear tests (DOE, 2000). France conducted 193 nuclear experiments above and beneath the atolls of Mururoa and Fangataufa (IAEA,1998b).

#### **4.1.1. Effects from the Long Shot explosion**

A few seconds after the Long Shot explosion, 30-m high plumes of water and soil were ejected into the air (McKeown et al., 1967). The fill around bridge abutments settled about 0.2 m at a distance of approximately 1,100 m from the surface ground zero (SGZ). Regions of fractured ground, mostly in

unconsolidated areas were found as far as 2,300 m from ground zero. Cracks were up to 8 cm wide and up to 120 m long and maximum vertical displacement were 50 cm approximately 700 m from SGZ. No apparent effects on the hydrologic regime were detected from the Long Shot detonation. Tritium was detected in water of sump ponds used for drilling mud and in associated drainage ditches near the SGZ several weeks subsequent the Long Shot detonation (Castagnola, 1969; EPA, 1998). Samples from several shallow wells close to SGZ, taken in 1971, indicate maximum tritium contamination at depths between 60 and 90 mbgs. Periodical sampling show tritium concentrations decreasing faster than expected if only radioactive decay was taking place, indicating that dilution is also occurring (EPA,1998).

#### **4.1.2. Effects from the Cannikin explosion**

At Cannikin, a near-vertical rubble chimney was formed extending from the explosion cavity to the land surface, as a result of the collapse of the cavity 38 hr after the explosion (Merritt and Fuller, 1977). The height and porosity of the rubble chimney and the cavity radius at Cannikin are not known. Prior to the Cannikin event, Fenske (1972) estimated porosity to 0 % at the bottom and 14 % at the top of the rubble chimney with an average of 7 %. From the rate of rise of water level in the chimney Claassen (1978) estimated the rubble chimney porosity to range from approximately 10 % near the bottom, to 4 % near the top of the chimney. IAEA (1998a) defines the void fraction in rubble chimneys between 24 and 29 % resulting in rubble chimney porosity between 19 and 22 %. Claassen (1978) estimated the cavity radius at Cannikin to 133 m from a relationship that takes the energy yield, overburden density and the depth of detonation into account.

Often the ground surface above a cavity subsides, which was the case following the Cannikin detonation. Cannikin has resulted in the most dramatic collapse sink at an underground nuclear explosion based on U.S experience (Allen et al., 1997). A surface depression was created offset from SGZ, centered

about 360 m southeast of SGZ creating a non-vertical rubble chimney. About 460 m southeast was the location of the deepest part of the triangular collapse sink (Gonzalez et al., 1974). Infill of the surface depression with surface water from White Alice Creek started approximately 11 months after the detonation (Merritt and Fuller, 1977). Approximately 13 months after the detonation the largest lake on the Island, Cannikin Lake (Figure 4.1), was created. The lake has a length of about 660 m, width of 200 m, maximum depth of 9 m, approximate volume of  $4 \times 10^5 \text{ m}^3$ , water surface area of 12.1 ha, and shoreline length of approximately 2 km (Gonzalez et al., 1974).



**Figure 4.1** Cannikin Lake that was created from the Cannikin explosion (Photo courtesy of Martyn Unsworth).

Cannikin is located in the White Alice Creek basin where nearly all surface drainage was intercepted by the collapse sink (Claassen, 1978). A hydraulic sink was created from the chimney resulting in infill of the chimney by groundwater (Merritt and Fuller, 1977). Almost no flow could be seen in White Alice Creek until the infill of Cannikin Lake was completed almost a year after the detonation (Merritt 1973). After the infill of Cannikin Lake the flow in White Alice Creek was about 80 percent of preshot volume (Merritt, 1973). At some turf lake beds the water drained through fractures created from the Cannikin event (USGS, 1972). Four of seven largest lakes located 900 m east of SGZ drained through fractures that cut the lakebeds.

In general, the uplifts around Cannikin SGZ were irregular (Merritt 1973). Some structures in the Cannikin GZ area indicated an upward displacement of approximately 8 m (USGS, 1972). Along the Bering coast, an uplift of approximately 1 m could be seen (Merritt, 1973). Permanent uplifts of up to 5 m

could be seen 850 m to the northeast and 1,200 m to the south of GZ. Two major faults, one located 760 m southeast of the Cannikin GZ and the Teal Creek fault located 1,070 northwest of GZ, and two northwest trending fractures, less than 200 m northeast of GZ, can be seen in the vicinity of Cannikin (USGS, 1972). A displacement of about a meter occurred on the Teal Creek fault (Merritt, 1973).

Measurements taken in 1972 from 72 locations on the island showed no measurable increase in radioactivity as a result of the Cannikin event (Schroder and Ballance, 1973). A terrestrial and freshwater radiological sampling program on Amchitka Island was conducted in 1997 with additional radiological sampling in 1998 by a federal, state, tribal and non-governmental team (Dasher et al., 2002). Measurements of  $^3\text{H}$  in surface waters and  $^{240}\text{Pu}/^{239}\text{Pu}$  ratios in various sample media provided no evidence for leakage of  $^{241}\text{Am}$  or other radionuclides into the terrestrial or freshwater environment. Since volatilized radionuclides were not discharged to the surface during the explosion, a process called venting, radioactivity resulting from this process was not expected to be found on the surface. In addition, the explosion cavity is located at such a great depth that any seeps in the basin are expected to be free of radioactivity from the Cannikin test.

An extensive biological investigation of Amchitka Island was performed in 2004 (Powers et al., 2005). No evidence of migration of radioactivity from the nuclear explosions was found in the marine environment during this investigation.

## Chapter 5 Previous groundwater models

### 5.1. Long Shot

The first finite-element modeling of the groundwater system on Amchitka Island was performed by Wheatcraft (1995). The finite element program SUTRA (Voss, 1984) was used and the subsurface properties were assumed isotropic and homogeneous. The recharge was assumed to have a value of  $2.7 \times 10^{-4}$  m/day and a homogenous hydraulic conductivity of  $4.6 \times 10^{-7}$  m/s. This resulted in a depth to the mid-point of the transition zone at 1,200 m. In the study, Wheatcraft investigated three different longitudinal dispersivities (33.3 m, 66.7 m and 133 m). Transverse dispersivities were chosen as a tenth of the longitudinal dispersivities, and the effective porosity value was not documented. Wheatcraft (1995) concluded that the groundwater travel time was 900 years from the Long Shot explosion cavity to the Bering Sea.

Further modeling by Hassan et al., (2002) used the finite element program FEFLOW (Diersch, 2002). The island was modeled with homogeneous but anisotropic hydraulic conductivity for the subsurface and with a spatial variability for the detonation cavity and chimney. Hassan et al., (2002) analyzed data regarding hydraulic conductivity and recharge for the island and used these to constrain the simulations. Their calibration resulted in a hydraulic conductivity of  $1.8 \times 10^{-7}$  m/s and a recharge of  $1.0 \times 10^{-4}$  m/day (Hassan et al., 2002). This resulted in a mean depth of the 50 % seawater concentration out of the 240 realizations at 1,200 mbsl. An anisotropy ratio of 1:10 was used in their calibrated model but they also investigated the influence of an anisotropy ratio of 1:30. Longitudinal and transverse dispersivities of 100 and 10 m respectively were used. To estimate the groundwater travel time, random distributions of the hydraulic conductivity, recharge, and effective porosity were used with ranges that were based upon site-specific and island-specific data analysis;  $2.7 \times 10^{-8}$  to  $5.1 \times 10^{-7}$  m/s for the hydraulic conductivity;  $2.2 \times 10^{-5}$  to  $3.9 \times 10^{-4}$  m/d for

recharge;  $1.0 \times 10^{-4}$  and  $5.2 \times 10^{-3}$  for porosity. Almost 100 % of their 240 realizations showed a mass breakthrough within 2,200 years. Most of the realizations show a first arrival time less than 300 years with 55 realizations within 10 years. Only 45 realizations have a last arrival time beyond 2,200 years.

## 5.2. Cannikin

Several estimates of the travel time from the Cannikin cavity to the seafloor have been conducted in the past (Ballance, 1970; Fenske, 1972; Hassan et al., 2002; Hassan and Chapman, 2006). The studies range from a flow net model to a rigorous stochastic model. Fenske (1972) used Darcy's law, age dating water, and infiltrating parameter and determined the groundwater travel time from the edge of the rubble chimney to the seafloor to range between 3,300 and 4,400 years. Prior to the detonation, hydraulic tests were performed in drillhole UA-1 at the depth of the emplacement chamber (approximately 1,500 to 1,900 mbsl) (Ballance, 1970). Hydraulic conductivities from the tests were used and Ballance (1970) estimated the groundwater travel time from this section to the ocean to range from more than hundred years to more than a million years.

Hassan et al., (2002) performed stochastic modeling of the three nuclear detonations on Amchitka Island and their purpose was to provide information needed to conduct a human health risk assessment of potential hazard from the underground nuclear explosions on Amchitka Island. Monte Carlo simulations generated 260 realizations with a range of homogenous hydraulic conductivity between  $2.5 \times 10^{-8}$  to  $5.1 \times 10^{-7}$  m/s and a range of homogenous recharge between  $2.2 \times 10^{-5}$  to  $5.2 \times 10^{-4}$  m/day. The range of homogenous porosity values used was  $1.0 \times 10^{-5}$  to  $5.2 \times 10^{-3}$ . A hydraulic conductivity to recharge ratio of  $1.1 \times 10^{-2}$  was reported. Longitudinal and transverse dispersivities of 100 and 10 m respectively were used and an anisotropy of 1:10 was applied. Within the simulation time of 2,200 years approximately 85 of the 260 realizations did not show any mass breakthrough and only 5 realizations have above 90 % breakthrough. The plume discharges at a distance approximately 1,700 to 3,700

m from shore. Hassan et al., (2002) also looked at the impacts of Cannikin Lake in an isothermal, 3-D, density-dependent flow and mass transport model. They concluded that the lake had minimal impact on the results compared to other sources of uncertainty in their model. They also studied the effect of the rubble chimney using a rubble chimney porosity of 7 %. It was shown that the rubble chimney had a great influence on the groundwater travel time and the transition zone was moved closer to the surface. Hassan and Chapman (2006) refined their model using the effective porosity and transition zone defined by Unsworth et al., (2007). They concluded that there would be no radionuclide breakthrough to the marine environment within their modeling timeframe of 2,000 years. It is unclear how they implemented the location of the freshwater saltwater transition zone seeing as the saltwater concentrations for the TZ was not defined in the MT study.

## Chapter 6 Methods

In the present study, the groundwater flow pattern was modeled with the density dependent mass and heat transport model finite element program FEFLOW as an equivalent continuum with dual porosity (Diersch, 2002). This modeling effort included bathymetry as collected by Johnson and Stewart (2005) and topography data obtained from Shuttle Radar Topography Mission (SRTM, 2005; SRTM, 2006). The topography data was noisy and was therefore interpolated, which may result in some discrepancies from real topography. Interpolated topography is shown in Figure 6.1. The entire cross section from the North Pacific coast to the Bering Sea coast was modeled. Earlier conceptual models (Fenske, 1972; and Wheatcraft, 1995;) assumed and modeled the groundwater divide in the middle of the island. The modeled sections by Hassan et al., (2002) were established from the upper boundary condition and the location of the topographic divide.

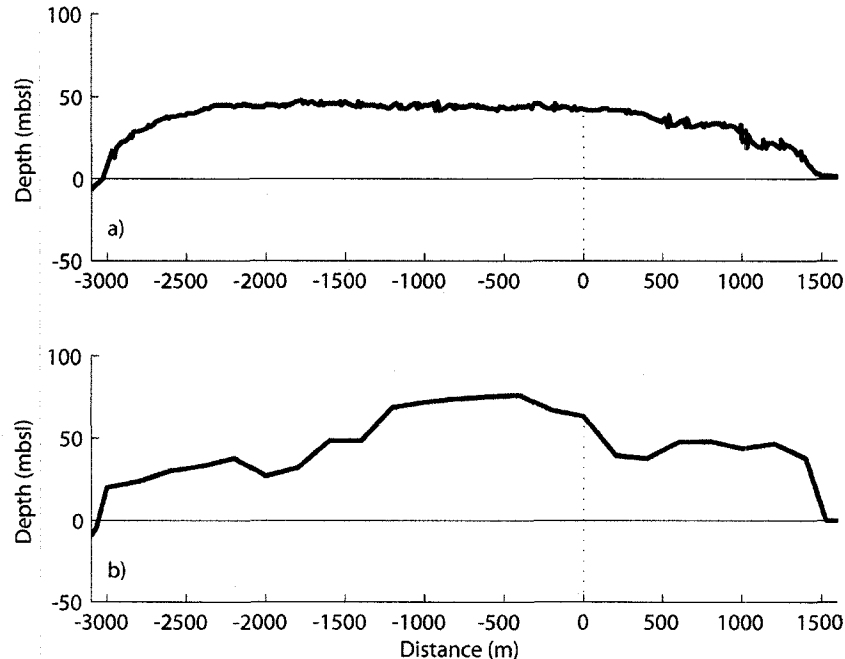


**Figure 6.1** Topography at a) Long Shot and b) Cannikin as obtained from SRTM. Dashed line shows the location of the emplacement hole.

The sites were modeled in two dimensions with a cross section perpendicular to the long axis of the island and profiles (see Figure 6.2) coincident with the location where magnetotelluric (MT) data were collected (Unsworth et al., 2007). A sketch of the modeled cross section is shown in Figure 6.3. Lateral boundaries were established at a sufficient distance from the subsea discharge zones to result in a cross section width of 16 km. The highest surface elevation at the Long Shot and Cannikin profile were 47 and 75 m above sea level respectively, and the lower no-flow boundary condition was placed at 6,000 mbsl. The finite element mesh was generated automatically in FEFLOW with 105,500 and 117,000 triangular elements respectively at Long Shot and Cannikin. In a similar study, several different sized meshes were used in a stability test in order to confirm its size and coarseness. A refined mesh provided the same result but with a shorter simulation time giving confidence in using this sized mesh.

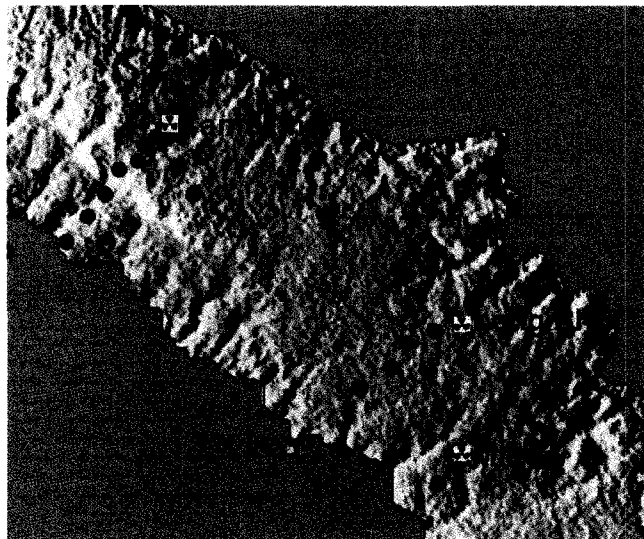


**Figure 6.2** Location of the MT measurement stations (Unsworth et al., 2007).

The ocean was modeled as a hydrostatic pressure boundary condition and the island was assigned a constant hydraulic head boundary condition. The location of the freshwater – saltwater transition zone is directly related to the location of the water table, recharge and subsurface characteristics. On Amchitka Island, the groundwater table is within a few meters of the ground surface

(Gonzalez, 1977; Merritt and Fuller, 1977). When looking at the location of the groundwater table, the shortest groundwater travel time is for a scenario that has a groundwater table close to the ground surface. In this study, the groundwater table was set to one meter below the ground surface at both sites, which is more conservative compared to a scenario that has a deeper groundwater table. A conservative scenario will hereafter be referred to as the scenario that results in the shortest groundwater travel time. Using a fixed hydraulic head as a boundary condition at the ground surface sets the water table at a certain depth below ground surface. At steady state, the net flux (flux in – flux out) and, thus, recharge into the ground surface can be determined. Recharge will vary throughout the ground surface due to the difference in elevation and it will also change depending on the subsurface characteristics.

MT defines the TZ as a domain of decreasing bulk resistivity with depth (Unsworth et al., 2007). The top of TZ is defined at the depth where the resistivity begins to decrease and the bottom of the TZ is defined at the depth where the salinity has reached the seawater value and cannot increase anymore, which is where the bulk resistivity begins to increase again with depth owing to a decrease in porosity. At Long Shot, the TZ is defined at 600 to 1,700 mbsl with an uncertainty range of 500 to 1,000 mbsl for the top and 1,500 to 2,000 mbsl for the bottom. The transition zone is located deeper at Cannikin, 1,100 to 2,300 mbsl, with an uncertainty range of 1,000 to 1,200 mbsl for the top and 2,000 to 2,700 mbsl for the bottom (Unsworth, 2007). It is not possible to determine the salinity concentrations for the top and bottom of the TZ from the magnetotelluric measurements and therefore the model cannot be calibrated to a certain range of salinity concentrations. The calibration process included comparing simulated shapes of the freshwater – saltwater TZ to the measured TZ, identifying saltwater concentration distributions throughout the TZ, comparing simulated hydraulic heads to measured hydraulic heads and comparing simulated salinity measurements to measured salinities. FEFLOW generates freshwater hydraulic

heads, which cannot be compared to measured hydraulic heads in an aquifer with non-uniform density. Luszczynski (1961) defined the environmental head ( $H_{in}$ ) as the measured head in a non-uniform aquifer, which can be derived from the freshwater hydraulic head ( $H_{if}$ ) as:

$$H_{in} = H_{if} + Z_r - Z_i + \frac{\rho_a}{\rho_f} (Z_i - Z_r) \quad 6.1$$

where

$i$  = any point in groundwater of variable density.

$Z_r$  = elevation of reference point from which the average density of water to  $i$  is determined and above which water is fresh; elevation measured positively upward.

$Z_i$  = elevation of  $i$ , measured positively upward

$\rho_a$  = average density of water between  $Z_r$  and  $i$ , as defined by

$$\frac{1}{Z_r - Z_i} \int_{Z_i}^{Z_r} \rho dz$$

$\rho_f$  = is the density of the freshwater.

In the remaining text, environmental head will be referred to as hydraulic head.

The shape of the TZ as determined by MT was compared to simulated TZ for several different scenarios. Changing the hydraulic conductivity of the subsurface does not change the shape of the TZ when the hydraulic head at the ground surface is fixed unless heterogeneities are included. The shape of the TZ changes with dispersivities and anisotropy of the subsurface. Several scenarios were simulated with a hydraulic conductivity of  $10^{-6}$  m/s (about the highest hydraulic conductivity estimated an Amchitka Island) and different dispersivities and anisotropies. The range of saltwater concentrations for the TZ could be determined from these scenarios and vary depending on the subsurface characteristics such as anisotropy and dispersivities.

Once the calibration process was completed, additional simulations were carried out for scenarios that fit the measured data. For these scenarios, several simulations were run where hydraulic conductivity was varied (and thus recharge) and corresponded to some of the measured and estimated values as listed in Table 3.1. Only some of the measured and estimated values were simulated due to the long simulation time when a low hydraulic conductivity is applied to the subsurface. From simulated scenarios, the groundwater travel time was determined and this was used to derive empirical relationships between recharge and travel times, and hydraulic conductivities and groundwater travel times. These relationships were then used to calculate travel times for remaining estimated and measured values that were not simulated at the different sites (see Table 3.1).

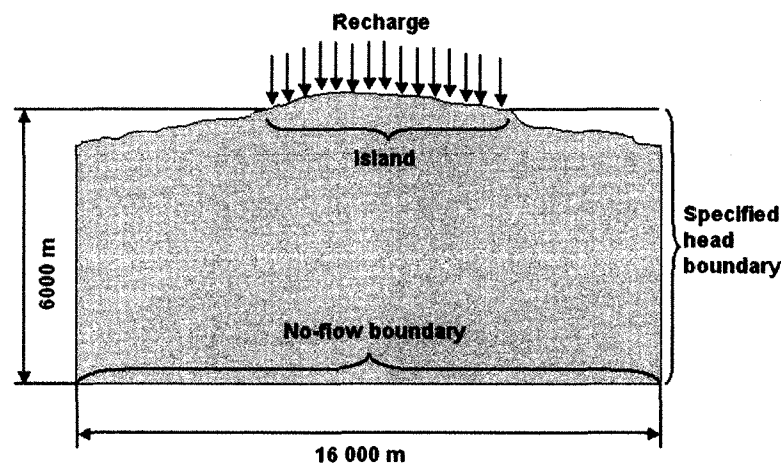


**Figure 6.3** Schematic cross-section with geometry and boundary conditions of the island.

### 6.1. Model parameters

In all simulations, a seawater salinity of 33,000 mg/l was applied as measured in 2004 (Johnson, 2005). The recharge was assigned a saltwater concentration of 0 mg/l which is lower than actual saltwater concentration. Freshwater and saltwater densities were 1,000 and 1,026 kg/m<sup>3</sup> respectively (Fetter, 1988; Johnson, 2005). Unsworth et al., (2007) reported porosities for the Long Shot site with values

decreasing exponentially from 0.45 at the surface to 0.003 at 6,000 mbsl. At Cannikin the porosity decreased from 0.36 at the ground surface to 0.004 at a depth of 6,000 mbsl (see Figure 6.4). These porosities were derived from electrical resistivity values using Archie's law (Archie, 1942) and salinity data at the Milrow site (Unsworth et al., 2007). These porosity depth variations were assumed throughout the cross section in this modeling effort.

Longitudinal and transverse dispersivities are not known for this aquifer. Anderson (1979) and Knox et al., (1993) suggest a longitudinal to transverse ratio in most aquifers can be found to be between 10 and 100, and 10 to 30 times, respectively. Several different longitudinal dispersivities were investigated to see how they effect the shape of the transition zone at the Long Shot and Cannikin sites. A longitudinal dispersivity ten times the transverse dispersivity was applied in this modeling effort. Wheatcraft (1995) and Hassan et al., (2002) also used this longitudinal to transverse ratio in their modeling efforts of Amchitka Island. Dispersion in this study is associated to the saline water (macro-dispersivity) and not to the dispersion of radionuclides (local dispersivity).

The ratio of horizontal to vertical hydraulic conductivity ( $K_x/K_z$ ) can range from less than 10 to more than 100 in layered soils or rocks (Fitts, 2002). Groundwater travel times increase with increasing anisotropy in layered soils and rocks due to  $K_x > K_z$ . From hydraulic head measurements, Fenske (1972) suggests that the island can be treated as isotropic and homogeneous and that most anisotropy ( $K_x > K_z$ ) can be accounted for between 200 and 400 mbsl. A conservative assumption (one that gives the shortest groundwater travel time) for a homogeneous subsurface would be that the subsurface is isotropic. These simulations included investigating isotropy and an anisotropy ratio ( $K_z/K_x$ ) of 1:2 and 1:10.

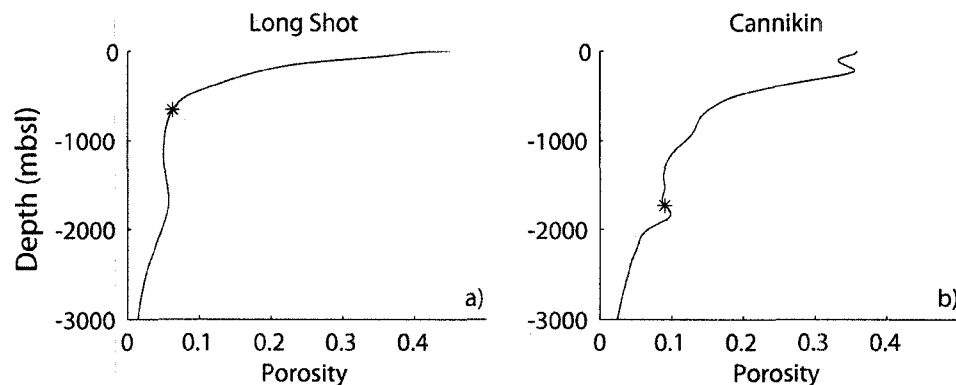


**Figure 6.4** Effective porosity distributions as determined by magnetotellurics at a) Long Shot and b) Cannikin (Unsworth et al., 2007). Asterisks illustrate the depth of the nuclear detonations.

### 6.1.1. Long Shot groundwater modeling parameters

In addition to the homogeneous simulations at Long Shot, the andesite sill with its enhanced hydraulic conductivity was included as a subsurface characteristic. Because a hydraulic conductivity is only known for these sills as a whole (U.S. Army Corps of Engineers and USGS, 1965), one layer of sill with a thickness of 100 m from a depth of 670 to 770 mbsl was modeled. The lateral extent and width of this layer are not known. Both the width of the andesite sill layer and the lateral location were therefore adjusted and the simulated shape of the transition zone was compared to the shape of the TZ as determined by MT. The hydraulic conductivity for the andesite sills is one to two orders of magnitude higher than surrounding rocks (U.S. Army Corps of Engineers and USGS, 1965). In order to model a conservative andesite sill scenario, the hydraulic conductivity of the subsurface was chosen to the high value estimated by Gard and Hale (1964) for the Long Shot aquifer ( $3.5 \times 10^{-7}$  m/s) and the hydraulic conductivity of the sill was chosen to a magnitude higher than the surrounding rock.

### 6.1.2. Cannikin groundwater modeling parameters

Owing to the creation of a chimney from the cavity upwards and the subsequent collapse of overburden material into this chimney, the porosity of the chimney zone is most likely substantially greater than the surrounding fractured rock.

Fenske (1972) estimated rubble chimney porosity values for Cannikin from no additional porosity at the bottom to 14 % at the top of the chimney with an average porosity of 7 %. From the rate of rise of water level in the chimney, Claassen (1978) calculated the rubble chimney porosity to approximately 10 % near the bottom and 4 % at the top. IAEA (1998a) estimates the rubble chimney porosity at underground nuclear detonation to range between 19 and 21 %. These values are smaller than porosities estimated at shallow depths by MT (Unsworth et al., 2007). The porosity of the rubble chimney should be greater than the surrounding rock. Either the estimation of the rubble chimney porosity is incorrect or the effective porosity determined by MT is incorrect. An increase of the rubble chimney porosity will only increase the groundwater travel time so the effect of higher rubble chimney porosity will not be investigated. At the location of the cavity and assumed rubble chimney at Cannikin, Unsworth et al., (2007) reported a reduced resistivity. This feature could not be resolved with confidence due to sparse measurement stations. If a higher porosity was detected at an assumed cavity and rubble chimney, the porosity used for the cross section is somewhat overestimated, which could result in longer travel times. It is difficult to say how much this influences the groundwater travel times. Effective porosities as determined by MT compare well with effective porosities reported by Spitz and Moreno (1996) for generic volcanic tuff and basalt. This comparison may not mean much because these estimations of the effective porosities were not performed on Amchitka.

Some simulations included Cannikin Lake to determine its effect on groundwater travel time. The MT profile at Cannikin was not run across the lake, making this scenario somewhat artificial. The topography and possibly the porosity would differ somewhat for a profile running across the lake. Without additional information about the subsurface, it is difficult to determine how much this would influence the resulting groundwater travel time. A lake was added to the ground surface by increasing the hydraulic head to a maximum of 10 m,

which is equivalent to the maximum depth of the lake. This is illustrated in Figure 6.5. Due to the topography, the width of the modeled lake is a little shorter (450 m) than Cannikin Lake (600 m).

It is unknown if Cannikin Lake is connected to the rubble chimney and the explosion cavity. The fact that there was almost no flow in White Alice Creek after the explosion until the infill of the subsidence (Cannikin Lake) suggests interconnection between the shot cavity and Cannikin Lake. The hydraulic conductivity of the rubble chimney is higher than the surrounding rock and will thus decrease the groundwater travel time. To see this affect on the lake scenario, a hydraulic conductivity of one order of magnitude higher than surrounding rock was added to the model. Claassen (1978) estimated the cavity radius to 133 m and in view of the finite element mesh; an approximate cavity radius of 150 m was applied for these simulations. For high yield tests, the French Liaison Office estimates the height of the rubble chimney to be eight times the cavity radius (IAEA, 1998a). Applying this rule to Cannikin would result in a rubble chimney height of approximately 1,200 m for a radius of 150 m. For a conservative scenario, the rubble chimney with an enhanced hydraulic conductivity was estimated to start at a depth of 1,900 mbsl and end at the surface. Including heterogeneities other than the rubble chimney in the subsurface cannot be justified at the Cannikin site with today's knowledge.

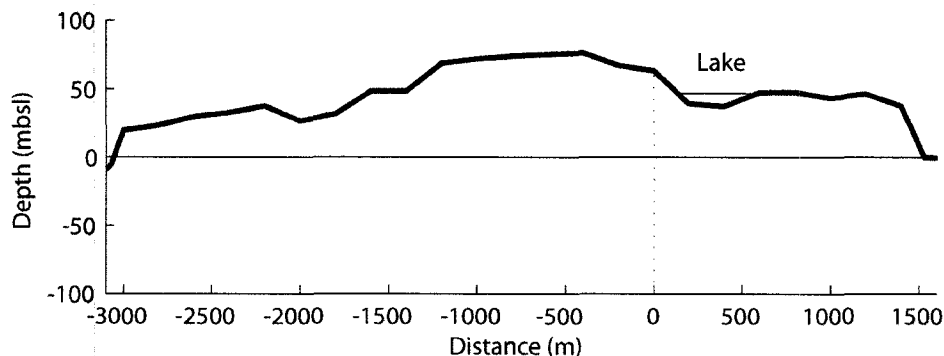


**Figure 6.5** Illustration of topography and Cannikin Lake. The dotted line shows the location of the emplacement hole.

## Chapter 7 Results

Several scenarios were simulated to investigate how subsurface characteristics, dispersivity, and anisotropy influence the shape of the transition zone. At Long Shot, the andesite sill layer with its enhanced hydraulic conductivity and its influence on the shape of the transition zone were also investigated. At Cannikin, an enhanced hydraulic conductivity was added for the assumed rubble chimney to see its influence on the shape of TZ compared to MT. Cannikin Lake was also added to the model to see how this changed the shape of the TZ. Likely scenarios were established by looking at the saltwater concentration distribution for the transition zones, and by comparing simulated hydraulic heads and saltwater concentrations to measured values. Once this comparison was completed, additional simulations were performed to establish groundwater travel times and seafloor locations for historical assumptions of hydraulic conductivities and recharge.

### 7.1. Long Shot

#### 7.1.1. Simulated and measured shapes of TZ

For a homogeneous subsurface, twelve scenarios were simulated. Three scenarios did not include anisotropy but they each had different longitudinal dispersivities; 50 m, 100 m, and 200 m. The transverse dispersivities were assigned a tenth of the longitudinal dispersivities. Anisotropy ratios, 1:2 and 1:10, were investigated in six additional scenarios. Each anisotropy ratio was simulated with longitudinal dispersivities of 50 m, 100 m, and 200 m. The shape of the transition zone of these simulations can be seen in Figure 7.3. MT reported an uncertainty range for the top and bottom of the TZ. At the emplacement hole, these uncertainty ranges resulted in saltwater concentrations at each depth (500 and 1,000 mbsl for the top and 1,500 and 2,000 mbsl for the bottom) that were used for the remaining simulated TZ and this was illustrated in gray.

In general, the shape of the simulated TZ compares fairly well to the measured TZ for all scenarios; although the bottom of the TZ compares better than the top. There is a suppression of the top TZ to the east of the island and there is an upturn on the bottom TZ to the west of the island that could not be matched successfully.

### **7.1.2. Saltwater concentration distribution throughout the TZ**

The saltwater concentration distribution for the transition zones varies depending on the subsurface characteristics. Table 7.1 lists the saltwater concentration distributions for locations throughout the transition zone as estimated by simulations. At Long Shot, there are a great variety of saltwater concentration distributions for the different scenarios. The top TZ shows an increase in range of saltwater concentration with an increase in anisotropy, and the bottom shows a decrease. Looking at the isotropic scenarios (1 – 3), there is a wide range of saltwater concentration for the bottom TZ. This is also seen for the top TZ for scenarios 7 – 9 that have an anisotropy ratio of 1:10.

### **7.1.3. Simulated and measured saltwater concentrations**

A comparison of the measured and simulated saltwater concentrations is shown in Figure 7.1a. The scenario with anisotropy ratio of 1:10 compares the best with the measured values. Applying different dispersivities to the subsurface affect the transition zone with a sharper transition zone for a small dispersivity compared to a large dispersivity (Figure 7.1b).

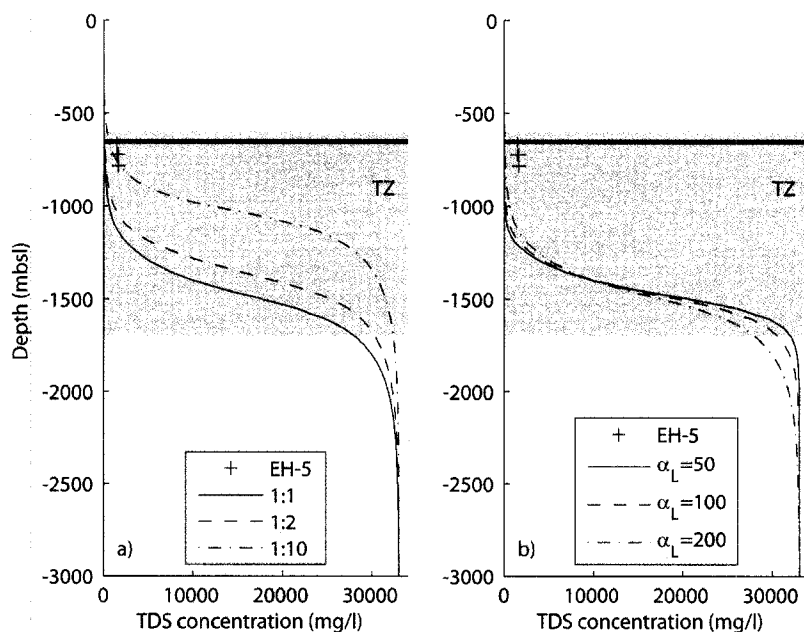


**Figure 7.1** Simulated and measured saltwater concentrations for Long Shot scenarios (U.S. Corps of Engineers and USGS, 1965). a) Scenarios 3, 6, 9 with isotropic subsurface properties (solid line), anisotropy ratio 1:2 (dashed line), and anisotropy ratio 1:10 (dashed dotted line). b) Represents scenarios 1, 2, and 3 where the effect of the dispersivity on saltwater concentration is shown for the isotropic scenarios. Solid line has a dispersivity of 50 m, dashed line has a dispersivity of 100 m, and dashed dotted line has a dispersivity of 200 m. The gray field shows the transition zone as determined by MT and the thick line is the depth at which Long Shot was detonated.

#### 7.1.4. Simulated and measured environmental heads

A comparison of the measured and simulated environmental heads is shown in Figure 7.2. The simulated values compare well with the shallow measurements for all scenarios. The subsurface with an anisotropy ratio of 1:10 compares well with measurements from EH-5.

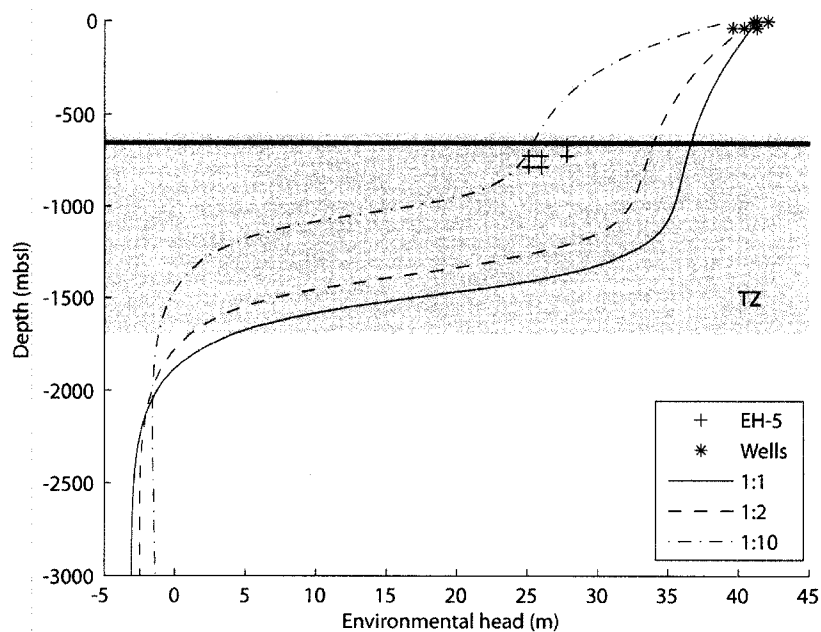


**Figure 7.2** Simulated and measured environmental head measurements at Long Shot (U.S. Corps of Engineers and USGS, 1965). Measured heads are from EH-5 (plus) and shallow wells (star) at the Long Shot test site. Simulated scenarios are isotropic (solid line), anisotropy 1:2 (dashed line) and anisotropy 1:10 (dash dotted line). Thick solid line illustrates the depth of the Long Shot detonation.

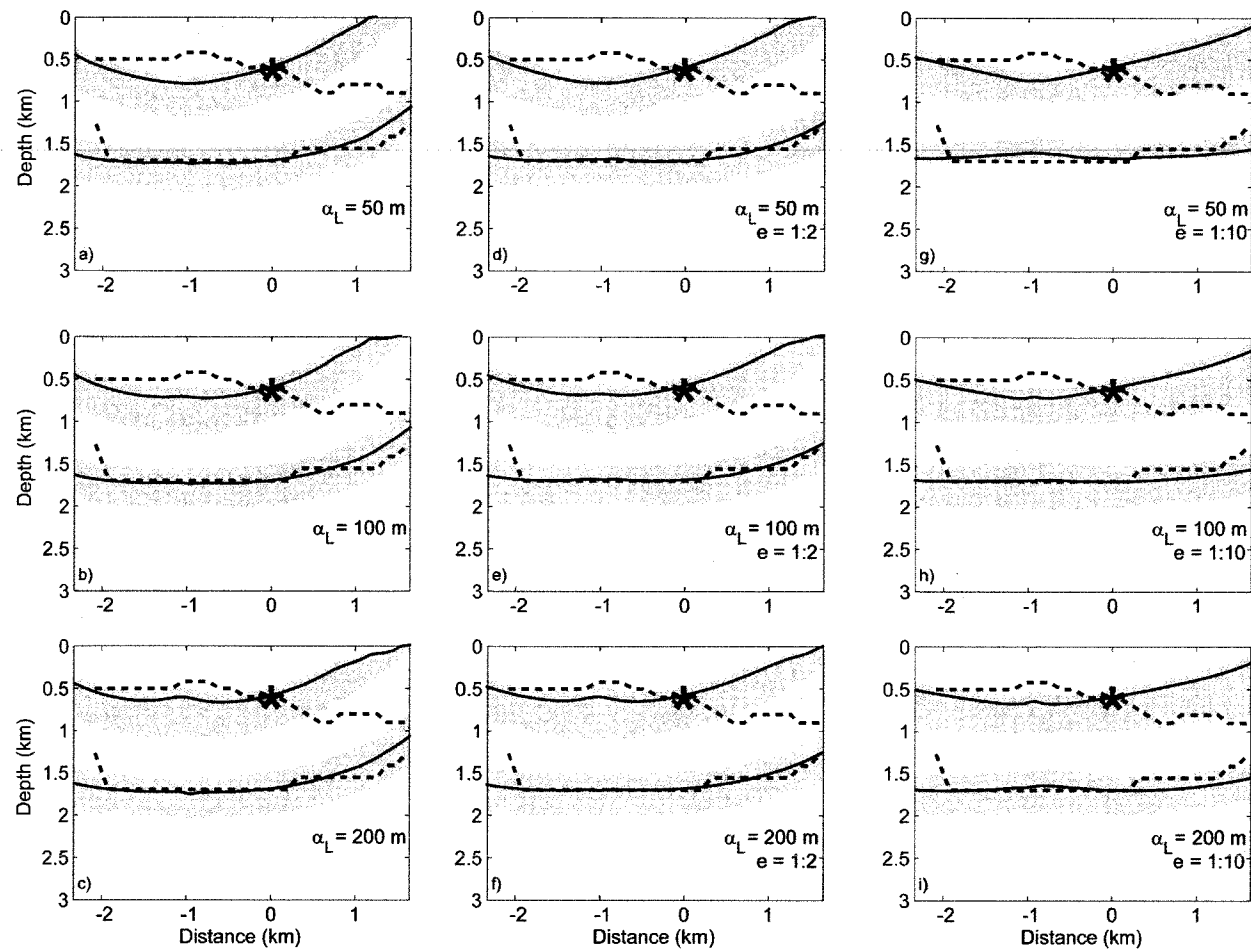


**Figure 7.3** Shapes of the TZ (solid line) at Long Shot for isotropic and anisotropic (e) simulations with different longitudinal dispersivities ( $\alpha_L$ ). The TZ uncertainty range as determined by MT is shown in gray. Dashed line is the TZ as estimated by MT (Unsworth et al., 2007).

**Table 7.1** Saltwater concentration distributions throughout the TZ for Long Shot (1 – 9) and Cannikin (10 – 18). Top and bottom of the TZ are highlighted in light gray and dark gray summarizes range of saltwater concentration. Uncertainty range for the top is 500 to 1,000 mbsl (Long Shot) and 1,000 to 1,200 mbsl (Cannikin) and for the bottom is 1,500 to 2,000 mbsl (Long Shot) and 2,000 to 2,700 mbsl (Cannikin).

Anisotropy	1			1:2			1:10		
Scenario	1	2	3	4	5	6	7	8	9
$\alpha_L$ (m)	50	100	200	50	100	200	50	100	200
	(mg/l)								
410 mbsl	0	0	17	0	1	21	1	13	87
500 mbsl	0	1	28	0	2	37	6	36	175
600 mbsl	0	3	49	0	6	71	34	118	389
710 mbsl	1	9	94	2	21	147	212	449	971
1000 mbsl	57	187	603	247	525	1,152	12,333	12,079	11,938
1500 mbsl	20,843	19,557	17,705	30,097	28,153	25,396	32,978	32,728	31,505
1700 mbsl	32,036	30,595	28,032	32,815	32,114	30,312	32,998	32,948	32,373
2000 mbsl	32,981	32,789	31,813	32,997	32,920	32,296	33,000	32,997	32,839
Scenario	10	11	12	13	14	15	16	17	18
$\alpha_L$ (m)	100	200	320	100	200	320	100	200	320
	(mg/l)								
980 mbsl	0	8	86	0	28	181	445	1,424	2,401
1000 mbsl	0	9	93	0	32	199	590	1,709	2,755
1100 mbsl	0	18	150	1	74	344	6,496	6,920	7,609
1200 mbsl	0	38	240	5	173	601	24,651	20,118	17,774
1880 mbsl	27,237	21,601	18,325	32,635	30,658	28,130	32,994	32,768	31,868
2000 mbsl	31,794	29,117	25,969	32,896	31,781	29,901	32,998	32,876	32,226
2300 mbsl	32,832	32,266	30,801	32,995	32,727	31,803	33,000	32,974	32,704
2700 mbsl	32,980	32,901	32,371	33,000	32,964	32,653	33,000	32,997	32,919

### 7.1.5. Seafloor arrival locations

Locating the seepage zones at the seafloor is important for successful sampling. Figure 7.4 illustrates the travel paths of particles that originate at 710 mbsl (bottom of the cavity) and 410 mbsl (five cavity radii into the rubble chimney) and arrive at the seafloor. In general, the seafloor arrival locations are farther offshore with an increase in anisotropy and maximum distances of approximately 1 km.

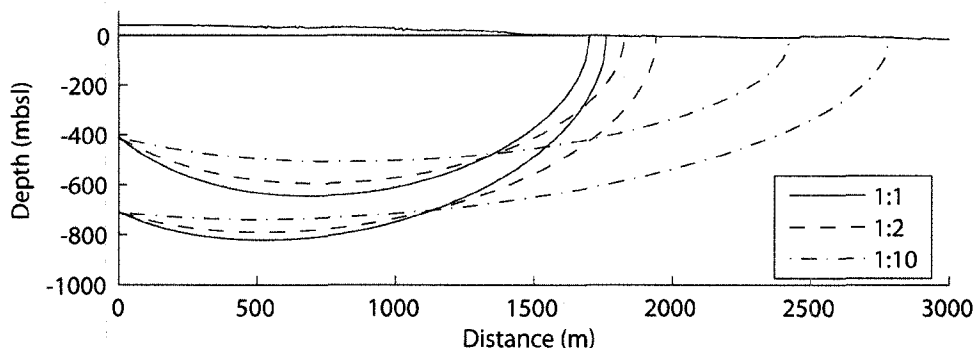


**Figure 7.4** Travel paths at Long Shot for different anisotropy with particles originating at the bottom of the cavity (710 mbsl) and at five cavity radii up into the rubble chimney (410 mbsl). Isotropy is illustrated with a solid line, an anisotropy ratio of 1:2 is illustrated with a dotted line and an anisotropy ratio of 1:10 is illustrated with a dotted-dashed line.

### 7.1.6. Groundwater travel times

Excluding possible subsurface characteristics (isotropic, anisotropy ratio of 1:2, and 1:10) could not be done when comparing simulated and measured shapes of the transition zone. There is a wide range of simulated saltwater concentration for the top and bottom TZ for an anisotropic ratio of 1:10 and an isotropic scenario. In comparison, the simulated concentration range is narrower for an anisotropy ratio of 1:2. Since this simulated ratio best fits the MT results the hydraulic conductivity of the fractured rock most likely has an anisotropic ratio of 1:2. This being said, the TDS and head measurements compared the best to simulated TDS and heads for a subsurface with an anisotropy ratio of 1:10. Shallow head measurements fit all scenarios well.

When comparing the groundwater travel times for an isotropic subsurface, an anisotropy ratio of 1:2 and 1:10, the shortest groundwater travel time will be for

an isotropic subsurface. Due to that the above comparisons all yielded different results on what simulated subsurface characteristics compares the best to measured data and that an anisotropy ratio of 1:10 yields significantly longer groundwater travel times than an isotropic subsurface, additional simulations using estimated and measured hydraulic conductivities to acquire groundwater travel times were only simulated for an isotropic subsurface and an anisotropy ratio of 1:2. These scenarios were all simulated with the groundwater table fixed at one meter below ground surface and using assumed or estimated values for hydraulic conductivity (see Table 3.1).

Using a hydraulic conductivity of  $10^{-6}$  m/s (scenarios 1 – 9) resulted a recharge that can be considered high compared to estimated recharge. This hydraulic conductivity was chosen due to shorter simulation times compared to when lower hydraulic conductivities are assigned to the subsurface. Even though the recharge is too high, it is still possible to distinguish how the dispersivity affects the groundwater travel time in relative terms. In order to decide what dispersivity to be used when determining the groundwater travel times for previously assumed values of hydraulic conductivity, the groundwater travel time for these scenarios (1 – 9) were thus investigated. The difference in groundwater travel time between longitudinal dispersivities at Long Shot is minimal (see Figure 7.5a). Because of the minimal difference in groundwater travel time between dispersivities and because the simulated shape of the TZ with a longitudinal dispersivity of 200 m matched the shape of the TZ as determined by MT the best a longitudinal dispersivity of 200 m was thus chosen for the additional simulations (Figure 7.3c).

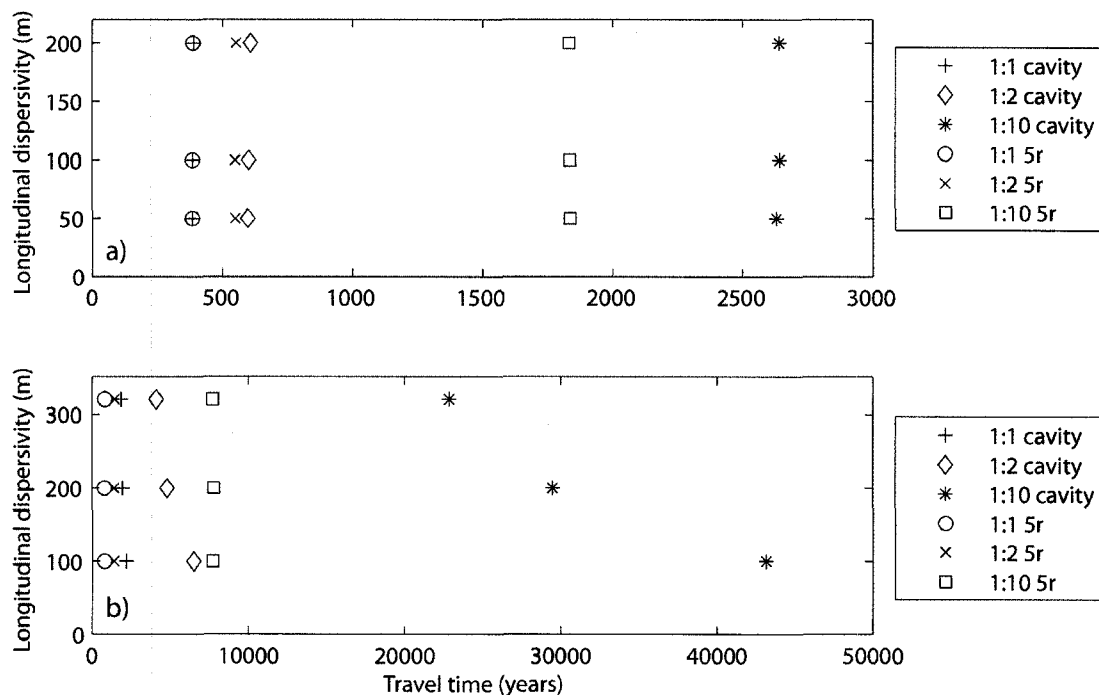


**Figure 7.5** Comparison between longitudinal dispersivities and its affect on travel time for isotropic and anisotropic scenarios (scenarios 1 – 18 in Table 7.1) at a) Long Shot and b) Cannikin. The groundwater travel times are from the bottom of the cavity and from five cavity radii up into the rubble chimney (5r) to the seafloor. The hydraulic conductivities used in these scenarios are  $10^{-6}$  m/s, which resulted in a recharge that is most likely higher than probable at Amchitka Island. The scenario without anisotropy is illustrated with a plus and circle, the scenario with an anisotropy ratio of 1:2 with a diamond and a cross, and the scenario with an anisotropy ratio of 1:10 with a star and square.

### *Isotropic Subsurface*

Several simulations were performed for an isotropic subsurface and by applying different hydraulic conductivities. This resulted in a power relationship that can be seen in Figure 7.6. There is no apparent difference between the groundwater travel times from the bottom of the cavity and at five cavity radii into the rubble chimney. The power relations for the groundwater travel time from the bottom of the cavity ( $t_{\text{cavity}}$  in years) and from five cavity radii up into the rubble chimney ( $t_{5r}$  in years) were derived from fitted lines in Figure 7.6 and the empirical equations are expressed as:

$$\begin{aligned}
 t_{cavity} &= e^{\left(\frac{0.05994 - \ln R}{1.00085}\right)} & t_{cavity} &= e^{\left(\frac{7.84087 - \ln K}{1.00079}\right)} \\
 t_{5r} &= e^{\left(\frac{0.05099 - \ln R}{1.00097}\right)} & t_{5r} &= e^{\left(\frac{7.84273 - \ln K}{0.99910}\right)}
 \end{aligned}
 \tag{7.1 - 7.4}$$

where R is the recharge in units of m/day and K is the hydraulic conductivity in units of m/s. The groundwater travel times were calculated using equations 7.1 – 7.4 and estimated and measured values of recharge and hydraulic conductivities. The average of  $t_{cavity}$  and  $t_{5r}$  are listed in Table 7.2 and were calculated from equations 7.1 – 7.2 and 7.3 – 7.4 respectively.

The shortest groundwater travel time (300 years) is for the simulation that used the highest hydraulic conductivity (Hassan et al., 2002) reported at Amchitka. This scenario resulted in a recharge greater than measured precipitation. A high resulting recharge can also be seen for a subsurface with a hydraulic conductivity of  $4.7 \times 10^{-7}$  m/s. These two scenarios are thus not very likely, making the shortest groundwater travel time for the isotropic simulation approximately 1,100 years. This scenario with a hydraulic conductivity as estimated by Fenske (1972) can still be considered to have a high recharge when compared with estimated values of recharge. The longest groundwater travel time for an isotropic scenario is  $3.3 \times 10^5$  years.

**Table 7.2** Calculated travel times from the bottom of the cavity to the seafloor ( $t_{cavity}$ ) and from five cavity radii above the detonation to the seafloor ( $t_{5r}$ ) for a homogeneous subsurface and for a subsurface with an anisotropic ratio ( $e$ ) of 1:2 at Long Shot (LS) and Cannikin. Recharge ( $R$ ), and hydraulic conductivities ( $K$ ) in bold are values as reported by Hassan et al.,<sup>(1)</sup> (2002), U.S. Army Corps of Engineers and USGS<sup>(2)</sup> (1965), Gard and Hale<sup>(3)</sup> (1964), Fenske<sup>(4)</sup> (1972) and other values are calculated from a recharge hydraulic conductivity ratio and Equations 7.1 – 7.16. High or low it means that a range was given for these aquifers and refers to the high or low value of the range.

Anisotropic ratio	1				1:2			
Long Shot	R (m/year)	K (m/s)	$t_{cavity}$ (years)	$t_{5r}$ (years)	R (m/year)	K (m/s)	$t_{cavity}$ (years)	$t_{5r}$ (years)
Amchitka <sup>(1)</sup> high	1.140	<b><math>1.16 \times 10^{-6}</math></b>	300	300	0.831	<b><math>1.16 \times 10^{-6}</math></b>	500	500
Fractured andesite sill <sup>(2)</sup>	0.463	<b><math>4.70 \times 10^{-7}</math></b>	800	800	0.338	<b><math>4.70 \times 10^{-7}</math></b>	1,300	1,200
LS Aquifer <sup>(3)</sup> high	0.345	<b><math>3.50 \times 10^{-7}</math></b>	1,100	1,100	0.251	<b><math>3.50 \times 10^{-7}</math></b>	1,700	1,600
LS Aquifer <sup>(3)</sup> low	0.108	<b><math>1.10 \times 10^{-7}</math></b>	3,600	3,600	0.079	<b><math>1.10 \times 10^{-7}</math></b>	5,500	5,000
Above andesite sills <sup>(2)</sup> high	0.046	<b><math>4.70 \times 10^{-8}</math></b>	8,300	8,300	0.034	<b><math>4.70 \times 10^{-8}</math></b>	12,800	11,600
Banjo Point Formation <sup>(2)</sup>	0.034	<b><math>3.50 \times 10^{-8}</math></b>	11,200	11,200	0.025	<b><math>3.50 \times 10^{-8}</math></b>	17,100	15,600
Above andesite sills <sup>(2)</sup> low	0.005	<b><math>4.70 \times 10^{-9}</math></b>	82,900	83,200	0.003	<b><math>4.70 \times 10^{-9}</math></b>	$1.3 \times 10^5$	$1.2 \times 10^5$
Amchitka <sup>(1)</sup> low	0.001	<b><math>1.16 \times 10^{-9}</math></b>	$3.3 \times 10^5$	$3.3 \times 10^5$	0.001	<b><math>1.16 \times 10^{-9}</math></b>	$5.1 \times 10^5$	$4.7 \times 10^5$
12% Recharge <sup>(3)</sup>	<b>0.108</b>	$1.09 \times 10^{-7}$	3,600	3,600	<b>0.108</b>	$1.50 \times 10^{-7}$	4,000	3,700
4% Recharge <sup>(3)</sup>	<b>0.036</b>	$3.65 \times 10^{-8}$	10,700	10,700	<b>0.036</b>	$5.01 \times 10^{-8}$	12,000	10,900
LS T profile <sup>(1)</sup>	<b>0.034</b>	$3.44 \times 10^{-8}$	11,300	11,400	<b>0.034</b>	$4.72 \times 10^{-8}$	12,700	11,600
Anisotropic ratio	1				1:2			
Cannikin	R (m/year)	K (m/s)	$t_{cavity}$ (years)	$t_{5r}$ (years)	R (m/year)	K (m/s)	$t_{cavity}$ (years)	$t_{5r}$ (years)
Amchitka <sup>(1)</sup> high	0.675	<b><math>1.16 \times 10^{-6}</math></b>	1,700	700	0.547	<b><math>1.16 \times 10^{-6}</math></b>	4,200	1,200
Cannikin Aquifer <sup>(4)</sup> high	0.222	<b><math>3.80 \times 10^{-7}</math></b>	5,200	2,100	0.180	<b><math>3.80 \times 10^{-7}</math></b>	12,600	3,700
Cannikin Aquifer <sup>(4)</sup> low	0.169	<b><math>2.90 \times 10^{-7}</math></b>	6,800	2,800	0.137	<b><math>2.90 \times 10^{-7}</math></b>	16,500	4,900
Banjo Point Formation <sup>(2)</sup>	0.020	<b><math>3.50 \times 10^{-8}</math></b>	56,400	22,900	0.017	<b><math>3.50 \times 10^{-8}</math></b>	$1.3 \times 10^5$	40,500
Amchitka <sup>(1)</sup> low	0.001	<b><math>1.16 \times 10^{-9}</math></b>	$1.7 \times 10^5$	$6.9 \times 10^5$	0.001	<b><math>1.16 \times 10^{-9}</math></b>	$4.0 \times 10^5$	$1.2 \times 10^5$
Cannikin UAe-1 <sup>(4)</sup>	<b>0.080</b>	$1.38 \times 10^{-7}$	14,300	5,800	<b>0.080</b>	$1.70 \times 10^{-7}$	28,000	8,300
Cannikin T profile <sup>(1)</sup>	<b>0.004</b>	$7.51 \times 10^{-9}$	$2.6 \times 10^5$	$1.1 \times 10^5$	<b>0.004</b>	$9.26 \times 10^{-9}$	$5.0 \times 10^5$	$1.5 \times 10^5$

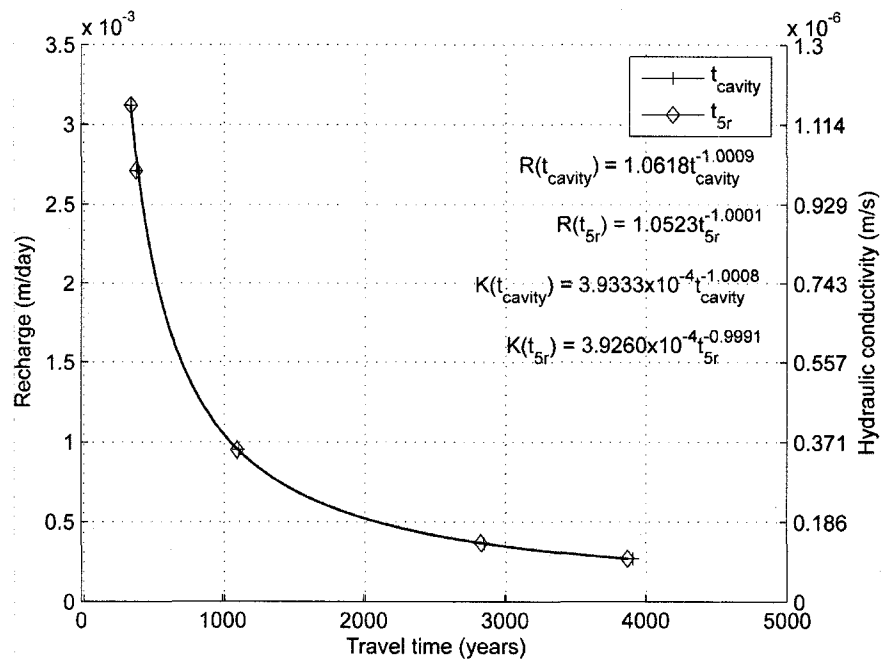


**Figure 7.6** Recharge and hydraulic conductivity plotted versus groundwater travel times with fitted lines for an isotropic subsurface at Long Shot. Particles originate at the bottom of the cavity ( $t_{\text{cavity}}$ ) and from five cavity radii up into the rubble chimney ( $t_{5r}$ ) and travel to the seafloor. Longitudinal dispersivity for these simulations is 200 m. The plus symbol illustrates  $t_{\text{cavity}}$  and the diamond illustrates  $t_{5r}$  to the seafloor.

*Subsurface anisotropy ratio of 1:2*

Simulations were performed using estimated and measured values of hydraulic conductivities and an anisotropy ratio of 1:2. The results can be seen in Figure 7.7 for groundwater travel times from the bottom of the cavity ( $t_{cavity}$  in years) and from five cavity radii up into the chimney ( $t_{5r}$  in years) to the seafloor arrival locations. Empirical equations for  $t_{cavity}$  and  $t_{5r}$  are

$$\begin{aligned}
 t_{cavity} &= e^{\left(\frac{0.21299 - \ln R}{1.00503}\right)} & t_{cavity} &= e^{\left(\frac{7.37882 + \ln K}{1.00403}\right)} \\
 t_{5r} &= e^{\left(\frac{0.11504 - \ln R}{1.00466}\right)} & t_{5r} &= e^{\left(\frac{7.47667 + \ln K}{1.00366}\right)}
 \end{aligned}
 \tag{7.5 - 7.8}$$

as derived from the fitted lines in Figure 7.7 where R is recharge in units of m/day and K is hydraulic conductivity in units of m/s. The groundwater travel times were calculated using equations 7.5 – 7.8 and estimated and measured values of recharge and hydraulic conductivities. The average of  $t_{cavity}$  and  $t_{5r}$  are listed in Table 7.2 and were calculated from equations 7.5 – 7.6 and 7.7 – 7.8 respectively.

The shortest groundwater travel time for a subsurface with an anisotropy ratio of 1:2 and a hydraulic conductivity of  $1.16 \times 10^{-6}$  m/s is 500 years. The resulting recharge is considered high. Applying the fractured andesite sill (Fenske, 1972) results in a more reasonable recharge, though still high, the groundwater travel time from the bottom of the cavity is approximately 1,300 years. For a particle that originates at five cavity radii up into the chimney the travel time is slightly less (1,200 years). The maximum groundwater travel time is  $5.1 \times 10^5$  years.

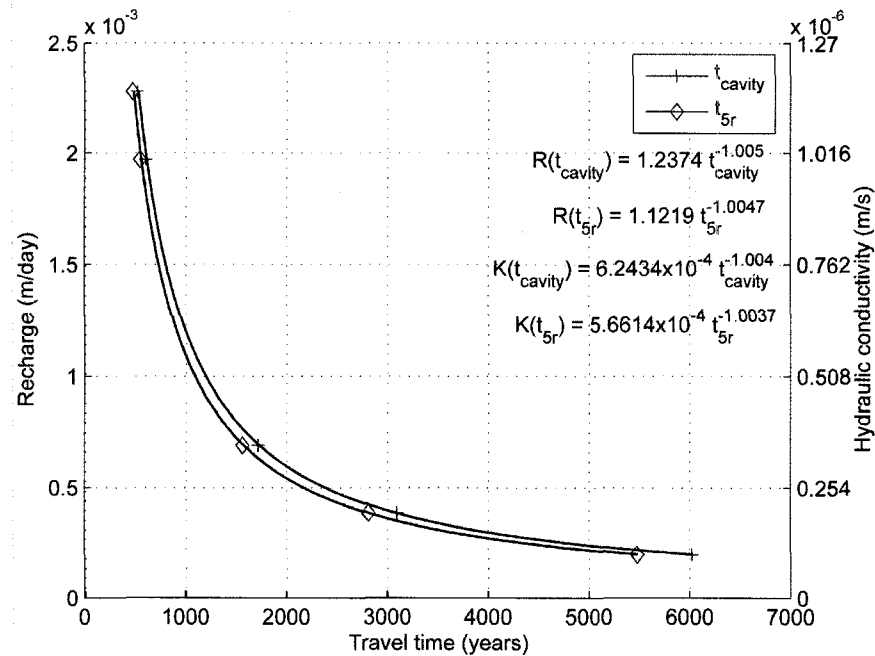


**Figure 7.7** Recharge and hydraulic conductivity plotted versus groundwater travel times with fitted lines for a subsurface with an anisotropy ratio of 1:2 at Long Shot. Particles originate at the bottom of the cavity ( $t_{cavity}$ ) and from five cavity radii up into the rubble chimney ( $t_{5r}$ ) and travel to the seafloor. Longitudinal dispersivity for these simulations is 200 m. The plus symbol illustrates  $t_{cavity}$  and the diamond illustrates  $t_{5r}$  to the seafloor.

### 7.1.7. Andesite sill layer

Simulations were performed to investigate how the andesite sill layer influences the groundwater travel time. From the isotropic and anisotropic simulations it was seen that a hydraulic conductivity of  $10^{-6}$  m/s yielded recharges that were considered high when compared to previously estimated recharge values a hydraulic conductivity of  $3.5 \times 10^{-7}$  m/s (as estimated for the Long Shot aquifer by Fenske, 1972) was thus assigned to the surrounding rocks and one order of magnitude higher ( $3.5 \times 10^{-6}$  m/s) was assigned to the andesite sill layer. The andesite sill layer was assigned depths of 670 to 770 mbsl. The lateral extent of this layer is not known, thus several scenarios were simulated with total widths of 3 km to 8 km. Several vertical locations were also investigated. It was shown in the isotropic and anisotropic scenarios that the groundwater travel time was not

influenced by the difference in dispersivity. A longitudinal dispersivity of 200 m was used so that the andesite sill scenarios could be compared with the isotropic and anisotropic scenarios. The shapes of the transition zone for these scenarios are illustrated in Figure 7.8. It can be seen in this figure that the andesite sill layer predominantly affects the shape of the top of the transition zone. The andesite sill layer does not affect the bottom of the transition zone significantly. When the layer is extended to more than 3 km east and west of the Long Shot detonation, the shape of the transition zone seems unaffected (see Figure 7.8c and d). Anisotropy seems to push down the top of the transition zone on the east side of the island (f). This effect is also seen (not to the same extent) when the andesite sill layer starts at the Long Shot test site and extends to 3 km east.

It was investigated how the groundwater travel times is affected by the total width of the andesite sill layer. This is illustrated in Figure 7.9. It should be noted that these simulations resulted in a recharge that can be considered high when compared to previously estimated recharge (0.35 to 0.38 m/year). The shortest groundwater travel time for the andesite sill layer simulations is approximately 500 years for the particle that originates at the bottom of the cavity, which is only 45 % of  $t_{\text{cavity}}$  for a subsurface without an andesite sill layer. The decrease in groundwater travel time from the bottom of the cavity is thus more than 50 %. Even though the recharge can be considered high, these numbers can be looked at as relative numbers where it is shown how the groundwater travel time decreases significantly when an andesite sill layer is included. It should also be noted that there is a difference between  $t_{\text{cavity}}$  and  $t_{5r}$  that was not seen for the isotropic subsurface. This is most likely due to the difference in travel paths (Figure 7.10). The most distant seafloor arrival location is approximately 200 m offshore.

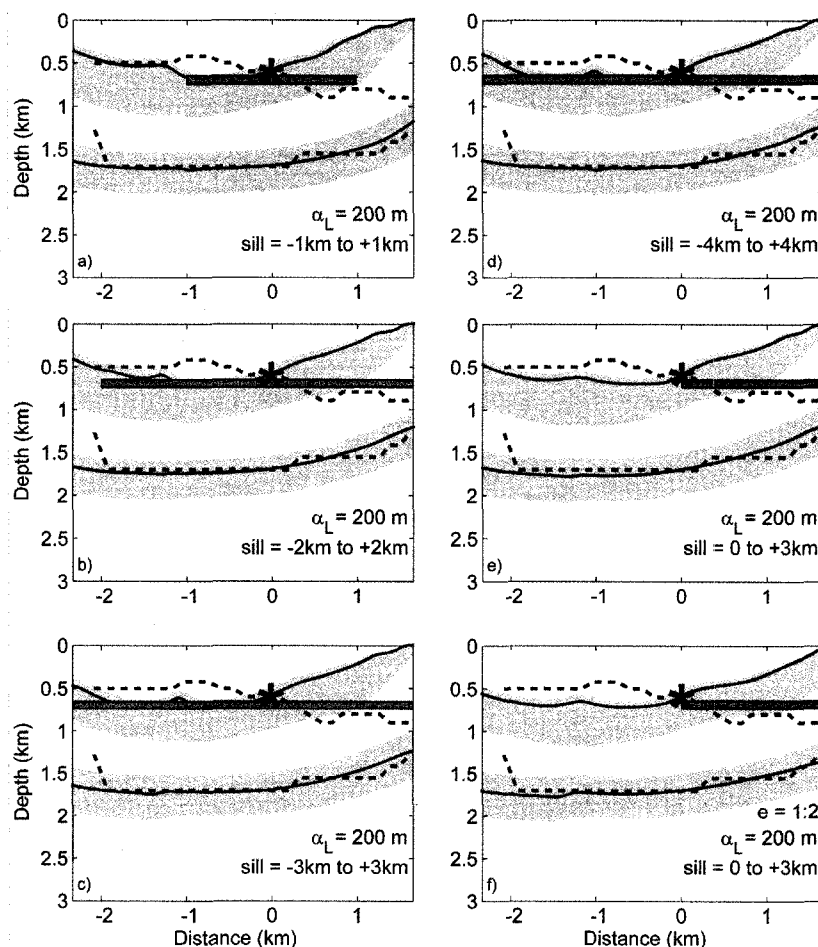


**Figure 7.8** Shape of transition zones for the andesite sill scenarios with a longitudinal dispersivity ( $\alpha_L$ ) of 200 m. Symbols are the same as Figure 7.3. The vertical location and width of the andesite sill layer (dark gray field) was changed in each scenario. Locations of the sills and lateral extensions in each scenario was: a) 1 km west to 1 km east, b) 2 km west to 2 km east, c) 3 km west to 3 km east, d) 4 km west to 4 km east, e) 0 to 3 km east, and f) 0 to 3 km east of the emplacement hole. An anisotropy ratio (e) of 1:2 was included in f).

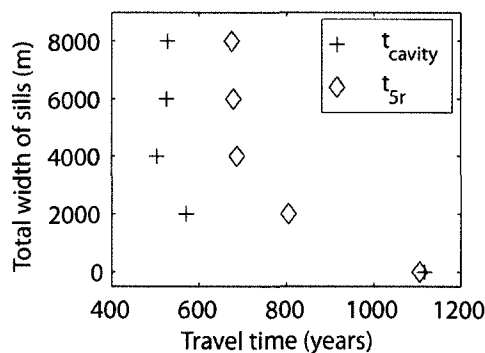


**Figure 7.9** Total width of sills plotted versus groundwater travel times for the andesite sill layer simulations at Long Shot. A plus illustrates the groundwater travel time from the bottom of the cavity ( $t_{cavity}$ ) and diamond illustrates the groundwater travel time from five cavity radii up into the rubble chimney ( $t_{5r}$ ) to the seafloor.

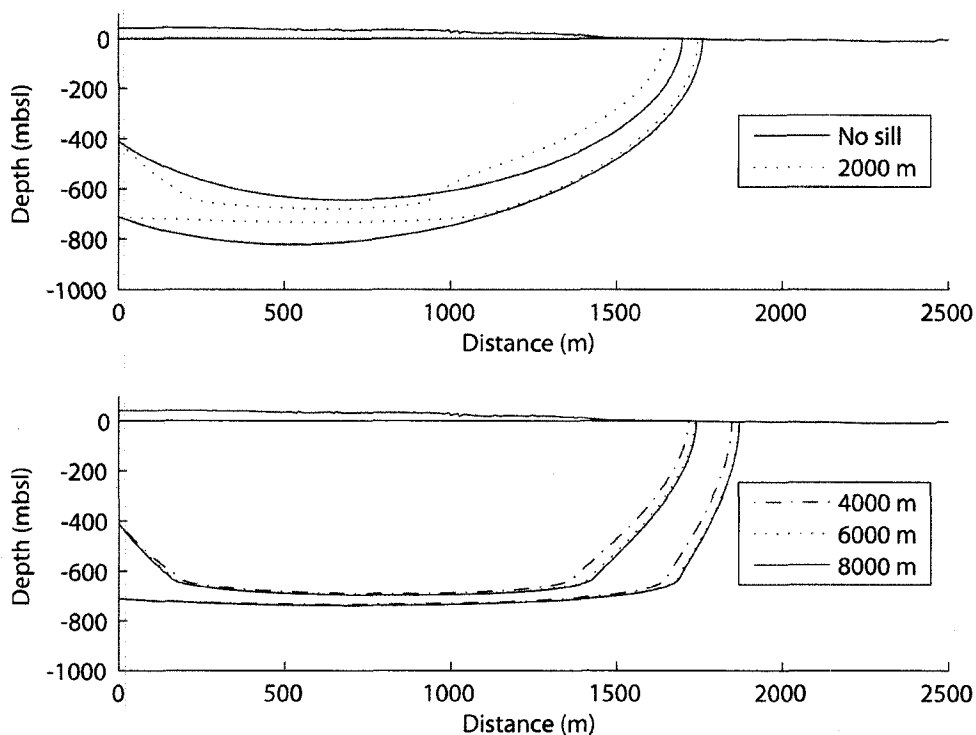


**Figure 7.10** Travel paths and seafloor arrival locations for different andesite sill lengths at Long Shot. Particles originate at the bottom of the cavity (710 mbsl) and at five cavity radii up into the chimney (410 mbsl). The top graph (a) shows the travel paths for an isotropic subsurface (no sill) and the dashed line shows the travel paths for a simulation that has an andesite sill located between 1 km west and east of the emplacement hole (total width of 2 km). The bottom graph (b) shows the travel paths for simulations with an andesite sill of a total width of 4000 m (dashed dot), 6,000 m (dashed), and 8,000 m (solid line). show sill location, a and b darker lines

## **7.2. Cannikin**

### **7.2.1. Simulated and measured shapes of TZ**

In total, twelve simulations were performed investigating the effect that anisotropy and dispersivity have on the shape of the transition zone at Cannikin. An isotropic subsurface was studied in three simulations each with different dispersivity (100 m, 200 m, and 320 m). A larger dispersivity was chosen at Cannikin compared to at Long Shot due to the wider transition zone measured by MT at Cannikin. Simulations with an anisotropy ratio of 1:2 and 1:10 were also studied. The resulting shape of these transition zones can be seen in Figure 7.11. Note that the differences in saltwater concentration are small at the top and bottom of Figure 7.11a and g respectively, resulting in difficulties plotting these uncertainty zones.

In general, the simulated bottom of the transition zone fits the shape of the TZ as determined by MT better than the top of the transition zone. It appears that, at Cannikin, the dispersivity does not have an influence on the shape of the transition zone. This could be due to heterogeneities or the low resolution of the MT data at the boundaries of the island.

### **7.2.2. Saltwater concentration distributions throughout the TZ**

At Cannikin the saltwater concentration distributions vary between simulated scenarios (Table 7.1). The widest range of saltwater concentration is seen for the top of the transition zone (total range of 15 000 – 24 000 mg/l depending on the dispersivity) where an anisotropy ratio of 1:10 is applied to the subsurface (scenarios 16 – 18). This effect was also seen at Long Shot.

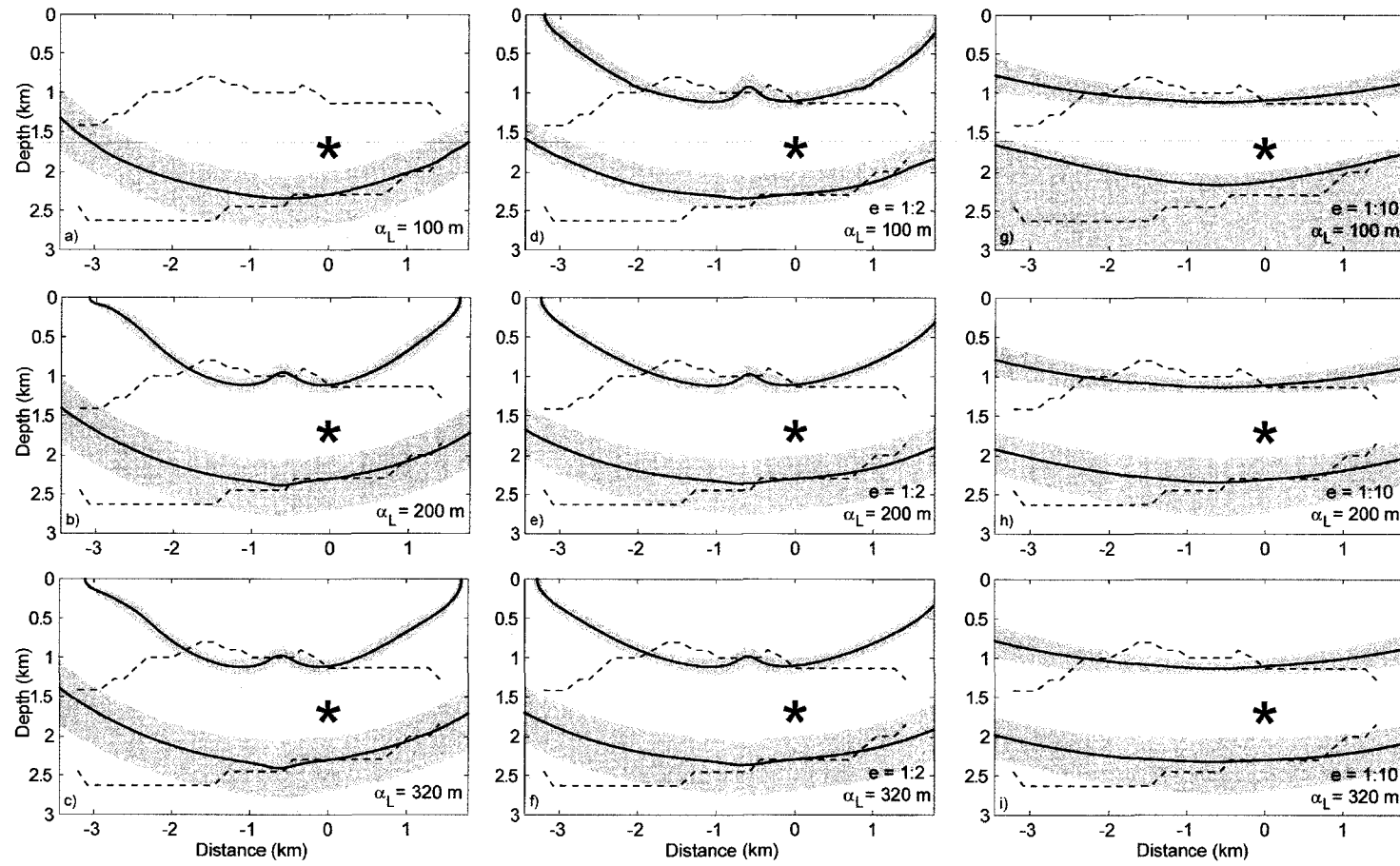


**Figure 7.11** Shapes of the TZ (solid line) for isotropic and anisotropic (e) simulations with different longitudinal dispersivities ( $\alpha_L$ ) at Cannikin (asterisk). The gray field shows the uncertainty range and dashed line is the TZ as estimated by MT (Unsworth et al., 2007). a) shows no top TZ due to the small difference in saltwater concentrations, this is also the reason for the continuous gray field in g).

### 7.2.3. Simulated and measured saltwater concentrations

The simulated saltwater concentrations were compared to the measured saltwater concentrations in Figure 7.12a. With the limited data available, the simulated isotropic scenario compares the best to the measured TDS. Figure 7.12b shows the effect dispersivity has on the shape of the saltwater concentration with a sharper transition between freshwater and saltwater for smaller dispersivities.

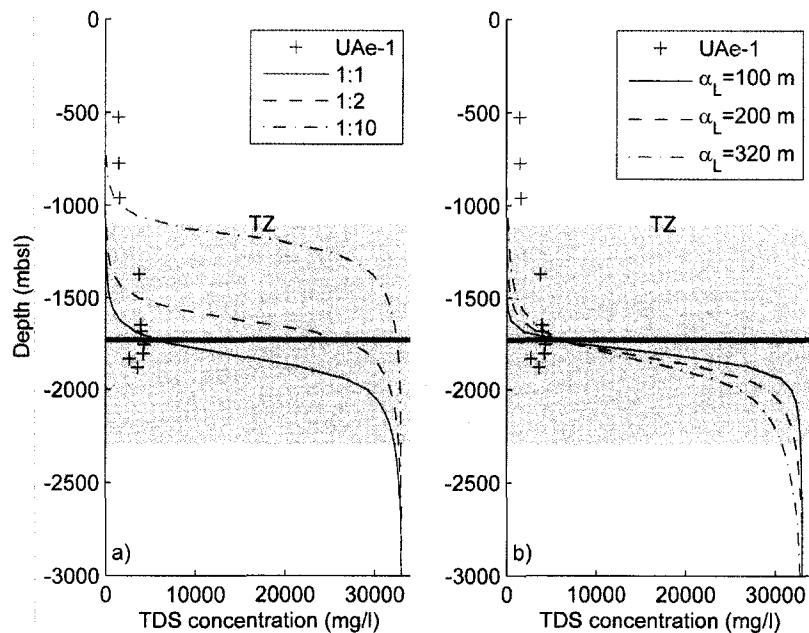


**Figure 7.12** Measured and simulated saltwater concentrations for Cannikin scenarios. a) Represents scenarios 11, 14, 17 with an isotropic subsurface (solid line), anisotropy ratio 1:2 (dashed line), and anisotropy ratio 1:10 (dashed dotted line). b) Represents isotropic scenarios (10, 11, and 12) where the effect of the dispersivity on saltwater concentration is shown. Solid line has a dispersivity of 100 m, dashed line has a dispersivity of 200 m, and dashed dotted line has a dispersivity of 320 m. The gray field shows the range of transition zone and the thick line shows the depth at which Cannikin was detonated.

### 7.2.4. Simulated and measured environmental heads

Measured heads from UA1-HTH-1 compare well for a subsurface with an anisotropy ratio of 1:10 (Figure 7.13). For an anisotropy ratio of 1:2 and the isotropic scenario, these head measurements do not match simulated heads.

Deeper simulated environmental heads compare well with measured heads for the scenario that has an anisotropy ratio of 1:2 and the isotropic scenario. Measurements from UAe-1 at a depth of 500 mbsl could not be matched with any scenario.

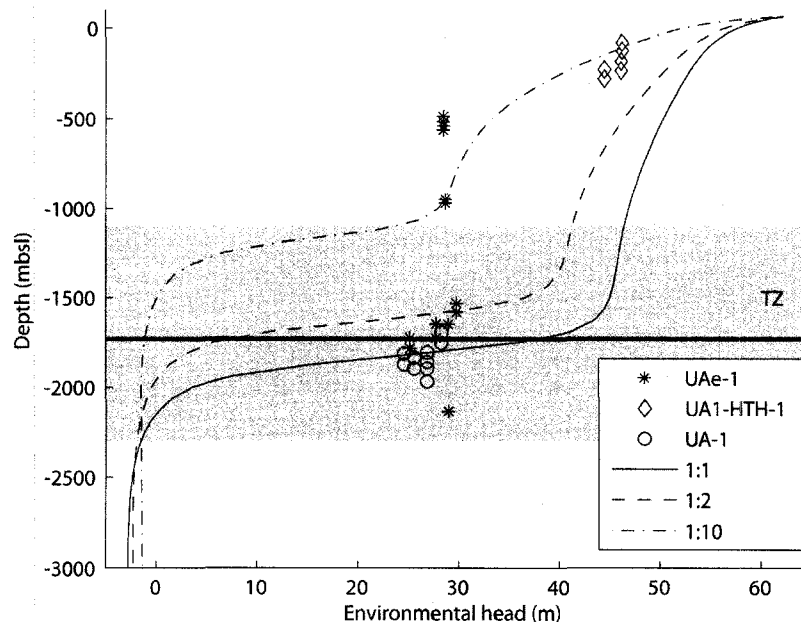


**Figure 7.13** Simulated and measured environmental head measurements at Cannikin. Measured heads are from UAe-1 (plus), UA1-HTH-1 (diamond) and UA-1 (circle). Simulated scenarios (11, 14, 17) with an isotropic subsurface (solid line), anisotropy 1:2 (dashed line) and anisotropy ratio 1:10 (dash dotted line). Thick solid line illustrates the depth of the Cannikin detonation.

### 7.2.5. Seafloor arrival locations

Seafloor arrival locations were investigated for an isotropic subsurface and for scenarios with an anisotropy ratio of 1:2 and 1:10. The travel paths and arrival locations for the isotropic and anisotropic scenarios are illustrated in Figure 7.14. For an isotropic subsurface the particle arrival locations are 750 m and 550 m offshore, for a particle that originates at the bottom of the cavity (1,880 mbsl) and for a particle that originates five cavity radii up into the chimney (980 mbsl) respectively. An anisotropy ratio of 1:2 increased the distance from shore with approximately 350 meters. When the subsurface has an anisotropy of 1:2 the particle that originates at a depth of 1,880 mbsl arrives at the seafloor

approximately 1,100 m offshore and the particle that originates at 980 mbsl arrives at sea about 200 m closer to shore. The seafloor arrival locations for a subsurface with an anisotropy ratio of 1:10 is approximately 2,100 m offshore for the particle that originates at 1,880 mbsl and for the particle that originates at 980 mbsl the seafloor arrival location is about 2,000 m offshore.

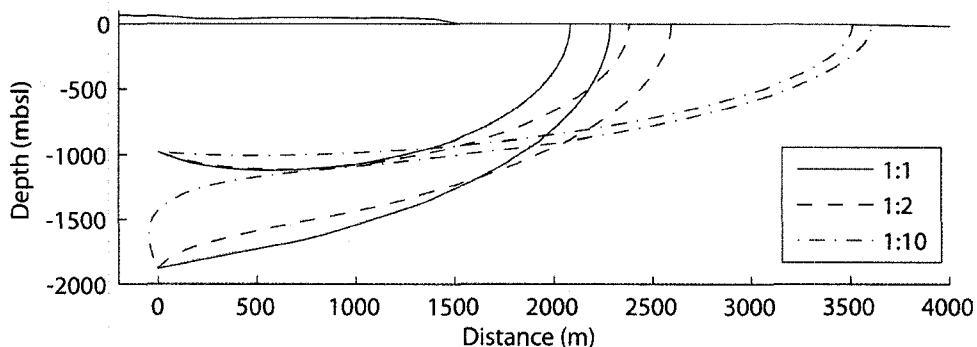


**Figure 7.14** Travel paths at Cannikin for particles originating at the bottom of the cavity (1,880 mbsl) and at five cavity radii up into the rubble chimney (980 mbsl). Isotropic is illustrated with a solid line, an anisotropy ratio of 1:2 is illustrated with a dotted line and an anisotropy ratio of 1:10 is illustrated with a dotted-dashed line.

### 7.2.6. Groundwater travel times

The shape of the transition zones as compared to the TZ measured by MT implies that the subsurface is anisotropic. Comparisons between measured and simulated saltwater concentrations entail an isotropic subsurface. Measured and simulated hydraulic heads at depths of approximately 500 mbsl indicates an anisotropy ratio of 1:10 whereas at deeper depths it is implied that the subsurface is isotropic or has an anisotropic ratio of 1:2. From the ranges of saltwater concentrations for the transition zone, the subsurface is most likely isotropic or has an anisotropy ratio of 1:2. Fenske (1972) reported that the island could be considered homogeneous and isotropic below a depth of 400 mbsl. Most data in this study implies an isotropic subsurface or an anisotropy ratio of 1:2. The groundwater travel time decreases with a decrease in anisotropy, thus a subsurface with an anisotropy ratio of 1:10 was excluded when determining the groundwater travel time for estimated and measured hydraulic conductivities.

It could not be determined from above comparisons which dispersivity results in a most likely scenario. The difference in groundwater travel time for scenarios with different dispersivities and anisotropy (scenarios 10 – 18, Table 7.1) can be seen in Figure 7.5b). At Long Shot no difference in groundwater travel time for different dispersivities could be seen (Figure 7.5a) whereas at Cannikin there is a significant difference in groundwater travel time with an increase in dispersivity. These groundwater travel times are from simulations that were assigned a hydraulic conductivity of  $10^{-6}$  m/s, which resulted in recharges that can be considered high when, compared to estimated recharges. These groundwater travel times should be looked at as relative numbers and not true groundwater travel times. Compared to Long Shot, there is a great difference in groundwater travel time for different dispersivities, especially with an increase in anisotropy for the particle originating at the bottom of the cavity (at a depth of 1,880 mbsl).

For the isotropic scenario, a dispersivity of 320 m results in the shortest groundwater travel time, but this scenario has a wide range of saltwater concentration, (6,000 mg/l) resulting in a dispersivity of 200 m. This dispersivity was used in the following simulations where estimated and measured hydraulic conductivities and the effect on groundwater travel time were investigated.

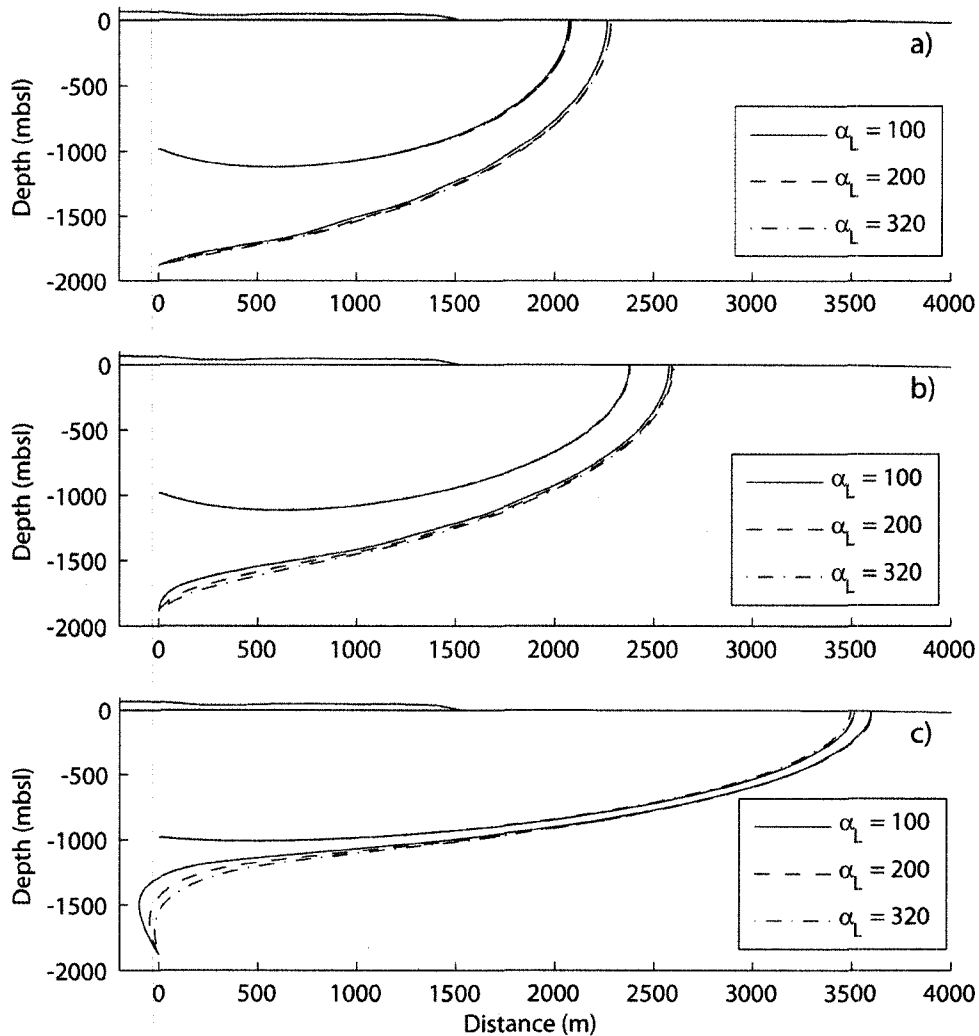


**Figure 7.15** Groundwater travel paths at Cannikin for different dispersivities (100 m, 200 m, and 320 m) and subsurface: a) isotropic, b) anisotropy ratio of 1:2 and c) anisotropy ratio of 1:10.

#### *Isotropic subsurface*

Results from simulations using an isotropic subsurface with some of the hydraulic conductivities as listed in Table 3.1 are shown in Figure 7.16. The groundwater travel times from the bottom of the cavity ( $t_{\text{cavity}}$  in years) and from five cavity radii up into the chimney ( $t_{5r}$  in years) to the seafloor can be derived from fitted lines in Figure 7.16. The empirical equations for an isotropic subsurface is

$$\begin{aligned}
 t_{cavity} &= e^{\left(\frac{1.12088 - \ln R}{0.99736}\right)} & t_{cavity} &= e^{\left(\frac{6.23534 + \ln K}{0.99924}\right)} \\
 t_{5r} &= e^{\left(\frac{0.24716 - \ln R}{0.99980}\right)} & t_{5r} &= e^{\left(\frac{7.11070 + \ln K}{1.00169}\right)}
 \end{aligned}
 \tag{7.9 - 7.12}$$

where R is the recharge in units of m/day and K is the hydraulic conductivity in units of m/s. Groundwater travel times were calculated for remaining estimated and measured values of recharge and hydraulic conductivity as listed in Table 3.1 using equations 7.9 – 7.12. The average of  $t_{cavity}$  and  $t_{5r}$  are listed in Table 7.2 and were calculated from equations 7.9 – 7.10 and 7.11 – 7.12 respectively. Groundwater travel times for an isotropic scenario range from 700 to  $1.7 \times 10^6$  years. The hydraulic conductivity that yields a groundwater travel time of 700 years is most likely not a possible scenario due to the resulting high recharge. It should be noted that the shortest groundwater travel time is more likely to be 2,100 years because it results in a more probable recharge.

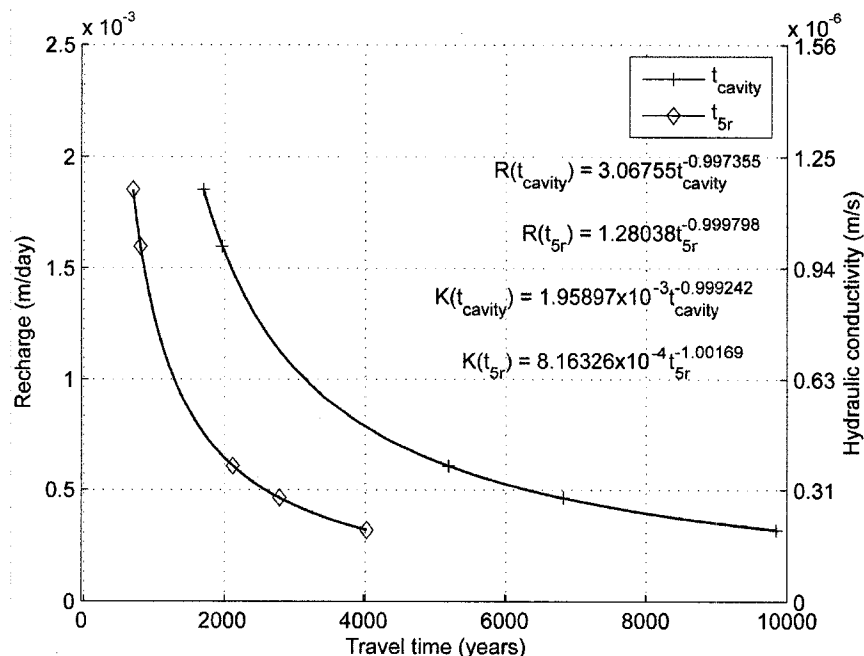


**Figure 7.16** Recharge and hydraulic conductivity plotted versus groundwater travel times with fitted lines for an isotropic subsurface at Cannikin. Particles originate at the bottom of the cavity ( $t_{cavity}$ ) and from five cavity radii up into the rubble chimney ( $t_{5r}$ ) and travels to the seafloor. Longitudinal dispersivity for these simulations is 200 m. The plus illustrates  $t_{cavity}$  and the diamond illustrates  $t_{5r}$  to the seafloor.

### Anisotropy 1:2

Simulations with an anisotropy ratio of 1:2 were performed using some of the assumed and estimated values of hydraulic conductivity at Cannikin as listed in Table 3.1. This resulted in power relations between groundwater travel times and recharge and hydraulic conductivity (Figure 7.17). The groundwater travel times from the bottom of the cavity ( $t_{cavity}$  in years) and from five cavity radii up into the rubble chimney ( $t_{5r}$  in years) to the seafloor are derived from the fitted lines in Figure 7.17. The empirical equations are expressed as

$$t_{cavity} = e^{\left(\frac{1.88443 - \ln R}{1.00652}\right)} \quad t_{cavity} = e^{\left(\frac{5.27368 + \ln K}{1.00715}\right)} \quad (7.13 - 7.16)$$

$$t_{5r} = e^{\left(\frac{0.60792 - \ln R}{1.00015}\right)} \quad t_{5r} = e^{\left(\frac{6.55094 + \ln K}{1.00078}\right)}$$

where  $R$  is the recharge in the units of m/day and  $K$  is the hydraulic conductivity in the units of m/s. The groundwater travel times for remaining hydraulic conductivities and recharge in Table 3.1 were calculated using equations 7.13 – 7.16. The average of  $t_{\text{cavity}}$  and  $t_{5r}$  are listed in Table 7.2 and were calculated from equations 7.13 – 7.14 and 7.15 – 7.16 respectively. For an anisotropic subsurface of 1:2 the groundwater travel times range from 1,200 to  $4.0 \times 10^6$  years. More likely the shortest groundwater travel time is 3,700 years (from a depth of 410 mbsl) due to the more reasonable recharge.

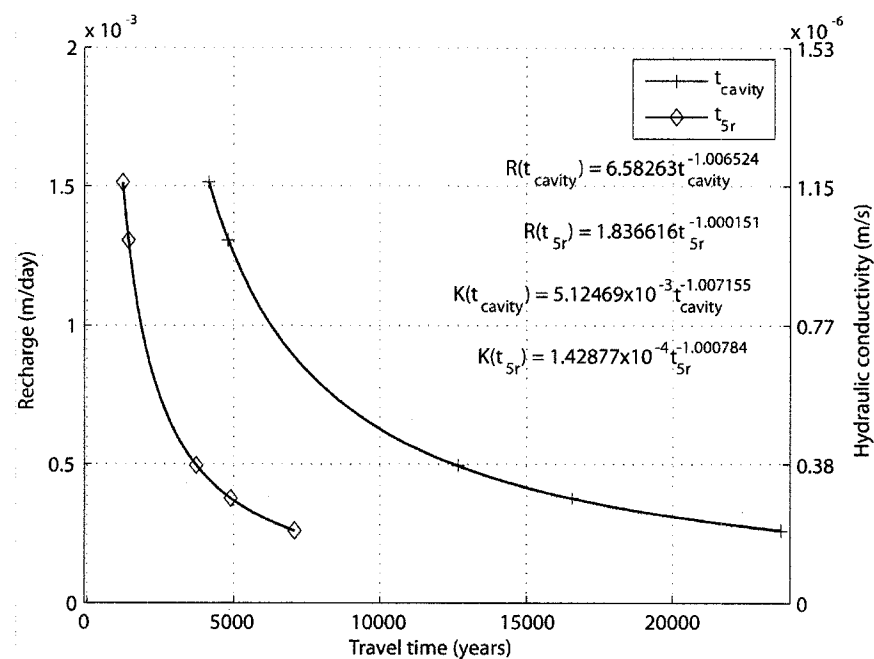


**Figure 7.17** Recharge and hydraulic conductivity plotted versus groundwater travel times with fitted lines for a subsurface with an anisotropy ratio of 1:2 at Cannikin. Particles originate at the bottom of the cavity ( $t_{\text{cavity}}$ ) and from five cavity radii up into the rubble chimney ( $t_{5r}$ ) and travels to the seafloor. Longitudinal dispersivity for these simulations is 200 m. The plus illustrates  $t_{\text{cavity}}$  and the diamond illustrates  $t_{5r}$  to the seafloor.

### 7.2.7. Cannikin Lake and Rubble Chimney

Including Cannikin Lake to the model (see Figure 6.5) did not result in a different shape of the transition zone (Figure 7.18a) compared to the scenario without a

lake (Figure 7.11b). It was also investigated how an enhanced hydraulic conductivity at an assumed rubble chimney and the lake would effect the shape of the transition zone and the groundwater travel time. The shape of the transition zone changes somewhat (Figure 7.18b).

The difference in groundwater travel time when adding Cannikin Lake to the simulation decreases the groundwater travel time with only a few percent. It was also investigated how an enhanced hydraulic conductivity at an assumed rubble chimney affects the seafloor arrival location and the groundwater travel time. The simulation with an isotropic subsurface and a hydraulic conductivity of  $3.8 \times 10^{-7}$  m/s resulted in a recharge that can be considered high but likely accurate (Table 7.2). This hydraulic conductivity was therefore used in this simulation. Boardman and Skrove (1966) suggest that at underground nuclear explosions, the hydraulic conductivity can be orders of magnitude higher in the rubble chimney compared to surrounding rock. An order of magnitude higher hydraulic conductivity was applied to the assumed rubble chimney. The rubble chimney was assumed from a depth of 1,880 mbsl and extended to the surface with a radius of 150 m. When an enhanced hydraulic conductivity is assigned for the assumed rubble chimney, the particles arrive at the seafloor approximately 70 m farther out from shore compared to when the rubble chimney is not included in the model. The groundwater travel time decreased approximately 25 % and 10 % for  $t_{cavity}$  (from 5,200 to 3,900 years) and  $t_{5r}$  (from 2,100 to 1,900 years) respectively when compared to the scenario without an enhanced hydraulic conductivity at the rubble chimney. The recharge increased with 250 % (from 0.222 to 0.533 m/year) and resulted in a recharge that is most likely too high when compared to assumed recharge. The saltwater distribution for the TZ also changed when a higher hydraulic conductivity was assigned the assumed rubble chimney. The saltwater concentration range for the top TZ did not change significantly but the range for the bottom TZ did (from 29,100 – 32,900 mg/l to 6,300 – 32,700 mg/l).

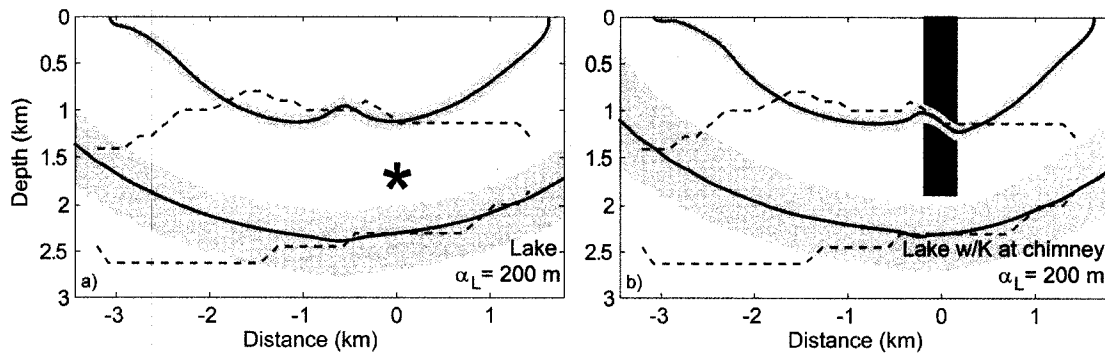


**Figure 7.18** Shape of transition zones for a) an isotropic subsurface with a longitudinal dispersivity ( $\alpha_L$ ) of 200 m and Cannikin Lake, and b) one simulation where in addition to Cannikin Lake a hydraulic conductivity (K) with an order of magnitude higher than surrounding rock was applied to the assumed rubble chimney (dark gray). The transition zone as measured by MT is marked with a dashed line and the simulated TZ is illustrated as a solid line with uncertainty range as marked with a light gray field.

### 7.3. Saltwater concentration distribution for the TZ

For future modeling efforts, it is important to determine the saltwater concentration for the TZ. In order to establish the saltwater concentrations for the transition zone, a comparison of the saltwater distribution is made for scenarios 4 – 6 (Long Shot) and scenarios 10 – 15 (Cannikin) in Table 7.1. Other scenarios (1 – 3, 7 – 9, and 16 – 18) were excluded due the wide range of saltwater concentration for the top or bottom of the TZ. The saltwater concentration for the top TZ (at a depth of 600 mbsl at Long Shot and a depth of 1,100 mbsl at Cannikin) is between 0 and 300 mg/l with an uncertainty range of 0 to 1,200 mg/l. and the bottom TZ (at a depth of 1,700 mbsl at Long Shot and 2,300 mbsl at Cannikin) is between 30,300 and 33,000 mg/l with an MT uncertainty range of 25,400 to 33,000 mg/l. The bottom range of uncertainty may be considered wide. If the largest dispersivities are excluded and only scenarios 4, 10, and 13 are considered the top TZ is at 0 – 1 mg/l with an uncertainty range of 0 – 200 mg/l. The bottom TZ has a saltwater concentration of 32,800 to 33,000 mg/l with an uncertainty range between 30,100 to 33,000 mg/l.

#### 7.4. Groundwater table constraint

Calibrating simulated hydraulic heads to hydraulic head measurements have been used in earlier studies by Hassan et al. (2002). If the groundwater table is not fixed to the surface and if the ground surface is not an idealized lenticular lens, the resulting simulated groundwater table may exceed the elevation of ground surface and yield results that are not reasonable. How much is the groundwater travel time influenced if the groundwater table is only calibrated at the emplacement hole? To answer this, several simulations were carried out using a hydraulic conductivity of  $10^{-6}$  m/s and changing the recharge (no fixed hydraulic head). With a fixed hydraulic conductivity several scenarios with different recharge values were simulated until a groundwater table at the emplacement hole was one meter below the ground surface.

At Long Shot, a recharge of  $7.9 \times 10^{-4}$  m/day and a hydraulic conductivity of  $10^{-6}$  m/s resulted in a groundwater table approximately one meter below ground surface at the emplacement hole (Figure 7.19a). Using these values for recharge and hydraulic conductivity and not fixing the groundwater table resulted in a  $t_{\text{cavity}}$  that is 35 % longer than when the groundwater table is fixed to one meter below the ground surface throughout the ground surface of the island.

At Cannikin, for a groundwater table to be located approximately one meter below the ground surface (Figure 7.19b), with a hydraulic conductivity of  $10^{-6}$  m/s resulted in a recharge of  $1.6 \times 10^{-3}$  m/day. The groundwater travel time is shorter for a scenario where the groundwater table is approximately one meter below ground surface at the emplacement hole compared to a scenario where the groundwater table is fixed at one meter below the surface throughout the island; 20 % less for  $t_{\text{cavity}}$  and 5 % less for  $t_{5r}$ .

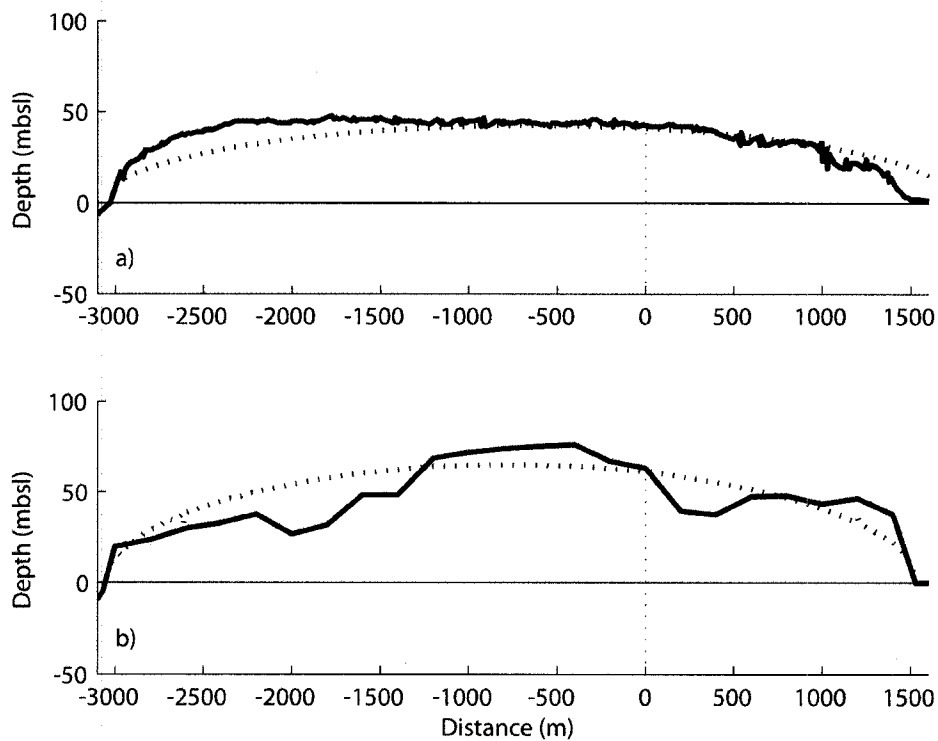


**Figure 7.19** Topography (thick line) and groundwater table (thick dashed line) at a) Long Shot and b) Cannikin when the hydraulic head is not fixed at one meter below the ground surface. The dotted line shows the location of the emplacement hole.

## Chapter 8 Discussions

### 8.1. Long Shot

#### 8.1.1. Shapes of the transition zone

The general simulated shape of the transition zone compare well with the measured TZ. With an increase in anisotropy the TZ results in a more horizontal profile. The suppression of the top east side of the TZ and the upturn of the bottom west side of the TZ could not be matched successfully. Unknown anisotropies could result in the suppression of the top of the TZ. The suppression of the top of the TZ and upturn of the bottom could also be caused by heterogeneities in the subsurface that are unknown and cannot be included in the model at this time. But more likely, it is due to the lower resolution of MT data at edge of array, which are the boundaries of the island (Unsworth, 2007). The suppression is then an artifact, explaining the difficulties in fitting the simulated data to measured data. Unsworth et al., (2007) also reported lateral variations in the resistivity, which could be the result of heterogeneities, but due to the non-uniform station spacing this could not be confirmed.

Scenarios with a longitudinal dispersivity of 200 m fit better to the measured TZ than smaller dispersivities for all scenarios. This relatively better fit may not be so much the influence from the longitudinal dispersivity but it is more likely a result of the value selected for transverse dispersivity as well, which is four times greater ( $\alpha_T = 20$  m compared to  $\alpha_T = 5$  m). Scenarios cannot be excluded by looking at the shape of the TZ as compared to MT. If a comparison is being made between simulated and measured shape of transition zones, it appears from these results that it is important to include the dispersivity in the modeling.

#### 8.1.2. Saltwater concentration distribution of the TZ

There is a great difference in the range of saltwater concentration for the transition zone when comparing simulated scenarios (Table 7.1). The bottom of

the TZ for an isotropic subsurface (scenarios 1 – 3) has a wide range of saltwater concentration (from 12,000 to 14,000 mg/l depending on the dispersivity) whereas the top of the transition zone for a subsurface with an anisotropy ratio of 1:10 (scenarios 7 – 9) has a wide range of saltwater concentration (approximately 12,000 mg/l). Assuming that the subsurface is anisotropic with a ratio of 1:10, it could be that it is more difficult to detect the actual saltwater concentration at shallow depths and that is why there is such a wide range of saltwater distribution. Or vice versa, assuming isotropic properties, it could be that it is more difficult to detect differences in saltwater concentrations at deeper depths. Or do we have a combination of anisotropy and isotropy? Perhaps the subsurface is anisotropic at deeper depths and not at shallower. The more likely alternative is that these scenarios (1 – 3 and 7 – 9) are not probable simulations of the subsurface at Long Shot. The saltwater concentration distribution for scenarios with anisotropy of 1:2 seems to represent a more reasonable range.

### **8.1.3. Comparing measured and simulated saltwater concentrations**

TDS was only measured successfully at two intervals in EH-5 (U.S. Army Corps of Engineers and USGS, 1965). These measurements do not extend into the transition zone. Only a very limited comparison between the simulated and measured saltwater concentration values is thus possible. The simulated scenario with a subsurface that has an anisotropy ratio of 1:10 compares the best to the measured TDS implying that the subsurface has an anisotropy ratio of 1:10. It should be remembered that these measurements are prior to the detonations. The displacement at Long Shot was 50 cm, which must likely have had some affect on have the subsurface structure. However, there are only measurements from two-straddle pack intervals, thus no conclusion on the possible subsurface structure should be drawn from these comparisons.

Different dispersivities and their affect on the shape of the saltwater concentration were also simulated. As expected, a sharper transition between freshwater and saltwater for smaller dispersivities are seen. Pohlmann et al.,

(2002) also reports that the dispersivity has an impact on saltwater concentrations.

#### **8.1.4. Comparing measured and simulated environmental heads**

All scenarios show a good fit with the shallow well measurements whereas a subsurface with an anisotropy ratio of 1:10 compares better with measurements from EH-5 than a subsurface with an anisotropy ratio of 1:2 or an isotropic subsurface. An anisotropy ratio that is slightly less than 1:10 (maybe 1:8) would compare even better with the measurements from EH-5. This suggests that, when comparing the simulated environmental heads, to measured heads, the subsurface has an anisotropy ratio of 1:10 or slightly less. Hassan et al., (2002) also showed a good comparison with the shallow wells and EH-5 for an anisotropy of 1:10. It should be noted that the hydraulic head measurements are at depths that do not extend into the transition zone and these measurements were also acquired prior to the detonations, so these may not be representative of the actual subsurface.

#### **8.1.5. Seafloor arrival locations**

At Long Shot, the seafloor arrival is less than 100 m from shore for both a particle that originates at the bottom of the cavity and for a particle that originates at five cavity radii up into the chimney. For an anisotropy ratio of 1:2 the seafloor, arrival locations for the particle originating at the bottom of the cavity and at five cavity radii up into the chimney are 100 to 200 meters offshore. Maximum distance of seafloor arrival locations according to this study is approximately 1 km offshore and can be seen for the particle that originates at the bottom of the cavity where an anisotropy ratio of 1:10 is applied to the subsurface. It can be seen that the seafloor arrival locations vary greatly depending on the subsurface characteristics. The seafloor arrival location is almost ten times further offshore for an anisotropy ratio of 1:10 compared to an isotropic subsurface. According to these results, monitoring should be performed from the shoreline and up to 1 km

offshore. It should be remembered that 1 km is based on a subsurface with an anisotropic ratio of 1:10, which has shown not to be a likely scenario. Sampling should therefore be taken at a higher frequency closer to shore.

#### **8.1.6. Groundwater travel times**

When comparing the simulated shapes of transition zone with the measured location of the TZ, likely scenarios modeled in this study could not be excluded. The ranges of saltwater concentration distributions imply that an anisotropy ratio of 1:2 is the most likely scenario. When compared to simulated results, the saltwater concentration fit the best with the scenario that had an anisotropy ratio of 1:10. All scenarios compared well to shallow head measurements while the scenario with an anisotropy ratio of 1:10 compared the best to measurements from EH-5. From these comparisons it is not possible to exclude any of the simulated scenarios. Due to the great range of saltwater concentration for the transition zone in the scenarios with an anisotropy ratio of 1:10 and that groundwater travel time increases with increasing anisotropy, it was justifiable to exclude investigating groundwater travel times for a subsurface anisotropy ratio of 1:10. It should also be noted that Fenske (1972) reported that the island could be considered homogeneous and isotropic below a depth of 400 mbsl validating the exclusion of an anisotropy ratio of 1:10.

It is unknown how far up into the chimney radionuclides are distributed at the time of detonation. Radionuclides have been measured at other sites at least five cavity radii up into the chimney (Kersting, 1996). For this study, it was decided that groundwater travel times from the bottom of the cavity and from five cavity radii up into the chimney should be investigated. Before additional simulations could be performed, it was necessary to investigate how the longitudinal dispersivity affects the groundwater travel time (Figure 7.5a). The simulations shown in Figure 7.5a used a hydraulic conductivity of  $10^{-6}$  m/s and resulted in recharge values higher than probable at Amchitka Island. Even if the groundwater travel times can be considered too short in view of the unrealistically

high recharge, the numbers and therefore the difference between scenarios can be looked at as relative numbers showing the significance of certain parameters. At Long Shot, the longitudinal dispersivity does not influence the groundwater travel time but we can see that there is a significant difference in groundwater travel time when comparing  $t_{\text{cavity}}$  and  $t_{5r}$  for an anisotropy ratio of 1:10. For the isotropic subsurface, no difference between  $t_{\text{cavity}}$  and  $t_{5r}$  can be seen. The difference in saltwater concentrations between 410 mbsl and 710 mbsl for the different scenarios is small (100 to 1,000 mg/l, see Table 7.1) and most likely does not influence the groundwater travel time significantly. The large difference between  $t_{\text{cavity}}$  and  $t_{5r}$  for a subsurface with an anisotropy ratio of 1:10 is due to the longer travel path for the particle that originates at 710 mbsl compared to 410 mbsl (see Figure 7.4). This shows the importance in looking at groundwater travel times from five cavity radii up into the chimney when the subsurface is anisotropic.

Additional simulations applying estimated and measured hydraulic conductivities were performed using a longitudinal dispersivity of 200 m. At low hydraulic conductivities (or recharge), small changes result in a great increase in groundwater travel time, whereas at high hydraulic conductivities (or recharge) small changes result in small increases of groundwater travel time. The groundwater travel time is very sensitive to changes in recharge and hydraulic conductivity, making it even more critical to determine the actual recharge and/or hydraulic conductivity.

The difference between  $t_{\text{cavity}}$  and  $t_{5r}$  in the anisotropic scenario, which could not be seen in the isotropic scenario, is due to the longer travel path and lower hydraulic conductivity ( $K_z < K_x$ ) in the anisotropic scenario compared to the isotropic scenario (Figure 7.4).

It should be noted that the effective porosity as determined by MT and also used in this study is up to three orders of magnitude less than the effective porosity used in the study by Hassan et al., (2002). What if the effective porosity

is one order of magnitude less than measured by MT? For such a case, the groundwater travel time would be close to 100 years. The effective porosities for generic volcanic tuff and basalt range between approximately 7 and 35 percent and between 3 and 25 percent (estimated from graphs), respectively (Spitz and Moreno, 1996), which falls within the range as determined by MT. This is for generic tuff and basalt; it would be helpful if the effective porosity as determined by MT could be confirmed due to its sensitivity when looking at the groundwater travel time. Also, what if there are numerous layers with an enhanced hydraulic conductivity? This could decrease the groundwater travel time significantly. These are all important aspects that need to be investigated in further studies.

#### **8.1.7. Andesite sill layer**

It can be seen that the andesite sill layer influences the shape of the transition zone but not to the extent where the shape of the transition zone compares better to the measured than when the andesite sill layer is not included. This suggests that there are additional unknown heterogeneities that influence the shape of the transition zone.

The resulting simulated recharge is considered high when compared to estimated values, 0.35 to 0.38 m/year depending on the extent of the andesite sill layer. There is a significant decrease in groundwater travel time when an andesite sill layer is included in the model. Only an isotropic subsurface was investigated. If an andesite sill layer is applied to the scenario that has a subsurface with an anisotropy ratio of 1:2, the groundwater travel time would be longer than 500 years. This shows the importance of including the andesite sill layer in further modeling efforts. When the andesite sill layer exceeds a total width of 4,000 m, the groundwater travel time is constant. Even if the andesite sill layer extends more than 2,000 m east and west of Long Shot, the groundwater travel time does not increase. Note that  $t_{5r}$  is greater than  $t_{cavity}$ , which is due to the longer travel path when the andesite sill layer is included (Figure 7.10). The groundwater travel time is very sensitive to total width of andesite sill layer as

long as the extent of the sill from the emplacement hole is less than the width of the island. The seafloor arrival locations do not change significantly once the total width of the andesite sill layer is wider than 4,000 m, i.e. on the east side of the emplacement hole the andesite sill extends to 2,000 m. When the andesite sill layer extends further than the island, the seawater influences the groundwater flow pattern more than the enhanced layer of hydraulic conductivity.

The particles arrive further offshore when an andesite sill layer is included compared to a scenario without the andesite sill due to that the andesite sill provides a horizontal pathway for the particles. The particle does not flow horizontally and follow the total width of the andesite sill layer; it starts flowing towards the seafloor at approximately 1,700 m from the emplacement hole. The seafloor arrival locations are about 150 m offshore for the andesite sill layer scenarios that have a total width wider than 4 km. Including an andesite sill to the subsurface does not affect the seafloor arrival locations considerably but the andesite sill layer has a significant influence on the groundwater travel time.

## **8.2. Cannikin**

### **8.2.1. Shapes of the transition zone**

At Cannikin there is no apparent difference of the shape of the transition zone between different dispersivities. At Long Shot the shape of the TZ between different dispersivities was not large but some changes could be seen (Figure 7.3). It is not apparent why there is no difference between dispersivities at Cannikin, but most likely this is due to the deeper transition zone at Cannikin compared to at Long Shot. The flattening of the transition zone with an increase in anisotropy as seen at Long Shot can also be seen at Cannikin.

The andesite sill layer at Long Shot influenced the shape of the transition zone. It is possible that there are heterogeneities in the subsurface that causes the dips on the east and west side of the island, and the upturn of bottom TZ on the west side of the island. More likely, in view of the fact that the dip and the

upturn on the west also were also seen at Long Shot, the low resolution of the MT data at the boundaries of the island (Unsworth, 2007) effect the measured MT and thus result in difficulties fitting the simulated data to the suppression on the east and west side of the island. Mapping features on the east boundary of the island is important because these features, if they have an enhanced hydraulic conductivity, could affect the groundwater travel time significantly as was shown at Long Shot. The simulated shapes of the anisotropic subsurface transition zone seems to fit the measured better (the flattening feature) but it should be remembered that the data from the boundaries of the island has a low resolution, so this flattening feature could be an artifact presented by the MT measurements.

### **8.2.2. Saltwater concentration distribution for the TZ**

There is a wide range of the saltwater concentration for the top of the transition zone where the subsurface has an anisotropic ratio of 1:10 (Table 7.1). This same feature was seen at Long Shot. The wide range of saltwater concentration that was simulated for the top TZ at Long Shot for the isotropic scenarios (1 – 3) could not be seen for the isotropic scenarios (10 – 12) at Cannikin. This strengthens the argument that the subsurface most likely does not have an anisotropic ratio of 1:10. At Cannikin, the subsurface is thus most likely isotropic or has an anisotropic ratio of 1:2. The saltwater concentrations for all remaining scenarios (10 – 15) but the isotropic scenario with a dispersivity of 320 m (scenario 12) have a range less than 4,000 mg/l making it impossible to distinguish the most likely scenario.

### **8.2.3. Comparing measured and simulated saltwater concentration**

There have been different opinions on whether the saltwater concentrations at UAe-1 are reliable. Fenske (1972) suggested that the saltwater concentration at Cannikin is too low whereas Merritt and Fuller (1977) suggest that the measurements are correct. According to these results, the simulated isotropic

scenario compares well to the measured saltwater concentrations suggesting that the saltwater measurements are correct.

As expected and as seen at Long Shot, a sharper transition between freshwater and saltwater for smaller dispersivities is seen. Pohlmann et al., (2002) also reported this effect.

#### **8.2.4. Comparing measured and simulated environmental heads**

No simulation showed a good fit to both shallow and deeper head measurements. Shallow head measurements imply that the subsurface has an anisotropy ratio of 1:10 whereas deeper head measurements imply that the subsurface has an anisotropy of 1:2 or is isotropic. Hassan et al., (2002) used an anisotropy ratio of 1:10 and they also experienced difficulties matching simulated heads to both shallow and deep head measurements in the same simulation. Difficulties matching both shallow and deep head measurements are most likely due to a combination of poor hydraulic head measurements and unknown heterogeneities in the subsurface. There is almost no decrease in hydraulic head between measurements at depths of approximately 500 and 1,500 mbsl at UAe-1. A greater decrease in hydraulic head would be expected when there is a vertical flow implying that these measurements cannot be trusted. At the time of hydraulic testing at UAe-1 there were problems with the drilling and testing, which could explain why it is difficult simulating a scenario where the data matches measured UAe-1 heads at depths of approximately 500 mbsl. It should be noted that the shallow head measurements are from a well (UA1-HTH-1) that is located approximately 1 km north of SGZ and outside the White Alice Creek basin, which could explain why the simulated (isotropic and anisotropy of 1:2) do not compare with this measured head. Due to discrepancies in the UAe-1 head measurements and that UA1-HTH-1 is located approximately 1 km from the emplacement hole it is implied that the subsurface is isotropic or that the subsurface has an anisotropy ratio of 1:2.

### **8.2.5. Seafloor arrival locations**

There is a difference of approximately 1,500 m for the seafloor arrival locations when comparing the results from an isotropic subsurface and an anisotropic subsurface with a ratio of 1:10. There is only a 200 m difference of seafloor arrival locations when comparing the particle that originates at the bottom of the cavity and at five cavity radii into the chimney for an isotropic subsurface and an anisotropy ratio of 1:2. This difference is only 100 m for a subsurface with an anisotropy ratio of 1:10. Note the great difference in travel paths from the bottom of the cavity (1,880 mbsl in Figure 7.14) for an isotropic subsurface and for a subsurface with an anisotropy ratio of 1:10. This is due to the great difference in saltwater concentration at this depth, which is approximately 22,000 mg/l for the isotropic subsurface and approximately 33,000 mg/l for a subsurface with an anisotropy ratio of 1:10. The longer travel path for the subsurface with an anisotropy ratio of 1:10 will result in a groundwater travel time significantly longer than for an isotropic subsurface. This illustrates the importance of establishing the saltwater concentration throughout the depth of the emplacement hole when the seafloor arrival location and groundwater travel times are investigated. According to these simulations sampling should be performed from approximately 500 m off shore to 2 km off shore. More frequent sampling should be performed closer to shore due to that a distance of 2 km is based on a subsurface with an anisotropy ratio of 1:10, which is a less likely scenario.

### **8.2.6. Groundwater travel times**

Even though the simulated shapes of the transition zone imply an anisotropic subsurface it should be remembered that the flattening of the transition zone that makes the comparison of the measured and simulated transition zone compare better to an anisotropic subsurface are most likely due to the low resolution of the MT measurements at the boundaries of the island. The range of the saltwater concentration imply an isotropic subsurface or a subsurface with an anisotropy ratio of 1:2. Saltwater concentration comparisons between measured and

simulated imply an isotropic subsurface. Measured and simulated hydraulic heads at depths of approximately 500 mbsl imply an anisotropy ratio of 1:10. These measurements are from a well that is located approximately 1 km from the emplacement hole and outside the drainage basin. Measurements from deeper depths imply that the subsurface is isotropic or has an anisotropic ratio of 1:2. Fenske (1972) reported that the island could be considered homogeneous below a depth of 400 mbsl. This all implies that subsurface has an anisotropy ratio of less than 1:10. The groundwater travel time decreases with a decrease in anisotropy; a subsurface with an anisotropy ratio of 1:10 was thus excluded when the groundwater travel time was determined for estimated and measured hydraulic conductivities.

To decide which dispersivity that were to be used in additional simulations, the groundwater travel times were investigated for the simulations having a hydraulic conductivity of  $10^{-6}$  m/s (scenarios 10 – 18). Compared to Long Shot, the groundwater travel time shows a significant difference when applying different dispersivities (Figure 7.5), especially with an increase in anisotropy for the particle originating at the bottom of the cavity (at a depth of 1,880 mbsl). The greatest difference in groundwater travel time (with the same anisotropy but different dispersivity) is seen for a subsurface with a ratio of 1:10 where  $t_{\text{cavity}}$  for a scenario with dispersivity of 100 m is almost twice as long (190 %) when compared to a scenario with dispersivity of 320 m (Figure 7.5b). When the subsurface has an anisotropy ratio of 1:2 the difference is smaller; 60 % longer for a scenario with a dispersivity of 320 m compared to 100 m. For an isotropic subsurface the groundwater travel time is 20 % longer for  $\alpha_L = 100$  m compared to  $\alpha_L = 320$  m. These differences cannot be seen when looking at the particles originating at a shallower depth (980 mbsl). The groundwater travel times from a depth of 980 mbsl are approximately the same for scenarios having the same anisotropy (Figure 7.5b).

Why is there no difference in groundwater travel time between dispersivities (that have the same anisotropy) when looking at particles originating at a depth of 980 mbsl? This can be explained by looking at the travel paths for particles that originates at a depth of 980 mbsl. When looking at an isotropic subsurface (Figure 7.15a) the travel paths are the same for all dispersivities. This can also be seen for a subsurface that has an anisotropy ratio of 1:2 (Figure 7.15b) and 1:10 (Figure 7.15c). In addition, a factor that influences the groundwater travel time is the saltwater concentration. At a depth of 980 mbsl the difference of saltwater concentration between dispersivities with the same anisotropy is small and the actual saltwater concentration is low; less than 2,000 mg/l with maximum saltwater concentration of 2,400 mg/l (see Table 7.1 at a depth of 980 mbsl for scenarios 10 – 18). This small difference and the fact that the saltwater concentration is only 2,400 mg/l results in almost no difference in groundwater travel time.

Why is the difference in groundwater travel time between different dispersivities smaller in the isotropic scenarios compared to the anisotropic scenarios at a depth of 1,880 mbsl? The travel paths for an isotropic subsurface are approximately the same for different dispersivities scenarios at a depth of 1,880 mbsl (Figure 7.15a). At a depth of 1,880 mbsl there is a greater difference in saltwater concentration, approximately 9,000 mg/l, between the isotropic scenarios (10 and 12), compared to 1,100 mg/l for the subsurface with an anisotropy ratio of 1:10 (scenarios 16 and 18). Just because there is a great difference in saltwater concentrations does not mean that there will be a great difference in groundwater travel time as illustrated at a depth of 1,880 mbsl for an isotropic subsurface (scenarios 10 and 12). For the subsurface with an anisotropy ratio of 1:10 there is a great difference in groundwater travel time even though the difference in saltwater concentration between the two scenarios (16 and 18) is small (1,100 mg/l). This is partly due to the fact that the groundwater travel path is longer for  $\alpha_L = 100$  m than for  $\alpha_L = 320$  m (Figure

7.15c). The great difference in groundwater travel time is most likely due to the fact that the saltwater concentration is 32,994 mg/l in scenario 16 ( $\alpha_L = 100$  m) compared to 31,868 mg/l in scenario 18 ( $\alpha_L = 320$  m). The greatest differences in groundwater travel times when looking at the same subsurface but different dispersivities (scenarios 10 – 18) are seen when the saltwater concentrations are greater than 32,000 mg/l (scenario 13, 16, and 17). According to this study, when the saltwater concentration is greater than 32,000 mg/l, there is a significant decrease in groundwater velocity and thus a significant increase in groundwater travel time. This would mean that all particles that originate at a depth with saltwater concentrations greater than 32,000 mg/l would have a long groundwater travel time.

Pohlmann et al., (2002) showed that the dispersivity has a minor impact on simulated saltwater concentrations. This study shows that even though there is a limited difference in saltwater concentrations there can be a great difference in groundwater travel time as shown in Figure 7.5b.

Note that the same sensitivity to probable recharge and hydraulic conductivities is seen here as was seen at Long Shot (Figure 7.6 and Figure 7.7). Observe that the groundwater travel times five cavity radii up into the chimney is only approximately 40 % of the groundwater travel time from the bottom of the cavity. The maximum distance of initial radionuclide distribution from the cavity is unknown but volatile radionuclides have been detected at distances of five cavity radii up into the chimney at other underground detonations. Most volatile radionuclides have a short half-life so it can be argued if this distance is too far up into the chimney to be investigated. But then again, the maximum distance of initial radionuclide distribution is unknown and IAEA (1998a) reported that 10 % of  $^{233}\text{U}$  and  $^{236}\text{U}$  and 2 % of plutonium isotopes could be distributed in the rubble chimney. These results show the importance of looking at groundwater travel times for other locations throughout the chimney. The shortest groundwater travel time,  $t_{5r} = 700$  years, is for an isotropic subsurface with a hydraulic conductivity

equal to the maximum hydraulic conductivity reported for Amchitka Island. This resulted in a recharge that can be considered high, it is about two thirds of the total precipitation on Amchitka. A more likely recharge can be seen for a hydraulic conductivity of  $3.8 \times 10^{-7}$  m/s as reported by Fenske (1972), where  $t_{\text{cavity}}$  and  $t_{5r}$  is 5,200 and 2,100 years respectively.

At the location of the cavity and assumed chimney a reduced resistivity was reported which could be due to an enhanced porosity at this location (Unsworth et al., 2007). The effective porosity as reported by Unsworth et al., (2007) was used for the whole cross section. If the reduced resistivity is due to effect of the cavity and chimney, the effective porosity used in this study is too high at these depths. This would result in calculated groundwater travel times that are too long. It is difficult to determine how much this affects the groundwater travel time but most likely not to a great extent.

#### **8.2.7. Cannikin Lake and Rubble Chimney**

A greater difference of the groundwater travel time than just a few percent when adding the lake to the simulation was expected. Hassan et al., (2002) also showed that Cannikin Lake had minimal impact on the groundwater travel time. The saltwater concentration distribution for the bottom TZ only changes about 800 mg/l when Cannikin Lake is added. At a depth of 1,880 mbsl the saltwater concentration decreases by 3,000 mg/l (from 21,600 to 18,600 mg/l) when the lake is added to the simulation. It has been shown, in this study, that the groundwater travel time increases significantly once the saltwater concentration is greater than 32,000 mg/l. The difference in groundwater travel time for a lake and no lake scenario would be greater if the saltwater concentration at the investigated depth (1,880 mbsl) in the no lake scenarios was greater than 32,000 mg/l. Assume that the saltwater concentration is greater than 32,000 mg/l at a depth of 1,880 mbsl, and that a lake was added to this scenario, the lake would suppress the saltwater with approximately 3,000 mg/l resulting in a saltwater concentration of 29,000 mg/l. This would most likely decrease the groundwater

travel time significantly and the lake would thus have a significant influence on the groundwater travel time.

The recharge when a rubble chimney is added to the lake scenario is too high and the bottom range of the saltwater concentration is too wide. Including a rubble chimney that extends to the surface with an order of magnitude higher hydraulic conductivity than the surrounding rock is therefore not a probable scenario. Assuming a rubble chimney that does not extend to the surface with a uniform hydraulic conductivity or assuming other hydraulic conductivities may change the saltwater concentration and thus result in a more probable scenario. This shows the importance of looking at the saltwater concentration distribution of the TZ when applying heterogeneities of the subsurface. Even if a higher porosity for the rubble chimney were added to the model, this would not change the range of saltwater concentration.

### **8.3. Determining saltwater concentrations for the transition zones**

From the MT measurements performed in 2004, the saltwater concentration could not be determined. The saltwater concentration affects the groundwater travel time significantly making it important to establish the saltwater concentrations for the transition zones so that future modeling efforts of Amchitka Island can be calibrated to the TZ location as determined by MT. This range could also possibly be used in other studies when MT has been used to determine the freshwater – saltwater transition zone. It has been shown that MT can determine a likely range of saltwater concentration for the transition zone.

### **8.4. Groundwater table constraint**

There is a significant difference in groundwater travel time when comparing a scenario with a fixed groundwater table (one mbgs) throughout the island to a scenario where the groundwater table is calibrated to approximately one meter at the emplacement hole. At Long Shot, the difference in groundwater travel time is most likely due to the smaller recharge used in the scenario where the

groundwater table was not fixed compared to the scenario where the groundwater table was fixed. A smaller recharge will result in a higher transition zone, a higher saltwater concentration at the depth of the cavity, and result in longer groundwater travel times.

A greater recharge compared to Long Shot is needed due to the higher elevation at Cannikin compared to Long Shot. This will also result in a deeper transition zone at Cannikin than at Long Shot.

This shows that at Long Shot, the groundwater travel time will be underestimated by 35 % if the groundwater table is not fixed to one meter below the surface. In contrast, at Cannikin the groundwater travel time will result in longer travel times for a scenario where the groundwater table is not fixed to a meter below the surface. As mentioned earlier, topography used in this study were obtained from SRTM and it had to be interpolated due to noise. This comparison shows the importance in using real topography as the island boundary. Due to the fact that the transition zone is directly related to the topography it would be useful to apply real topography to the island boundary.

This study has shown the importance in fixing the groundwater table at the ground surface throughout the ground surface instead of only calibrating the model to shallow head measurement at the emplacement hole. If the simulated hydraulic heads are calibrated to shallow hydraulic head measurements (if groundwater table is close to the surface) the simulated groundwater table may be extended above the ground surface, which would be unrealistic.

#### **8.5. Groundwater travel times compared to earlier studies**

The groundwater travel times to the marine environment from the underground nuclear detonations on Amchitka Island has been estimated in several studies (Ballance, 1970; Fenske, 1972; Wheatcraft, 1995; Hassan et al., 2002; Hassan and Chapman, 2006). Compared to earlier studies this study has used freshwater – saltwater transition zone locations and effective porosities as determined by magnetotelluric measurements in 2004 to determine the

groundwater travel times and seafloor arrival locations at Long Shot and Cannikin. A different modeling approach was applied in this study where the whole island with its actual topography has been used. In addition, the groundwater table has been fixed to the surface instead of calibrating the model by changing the recharge or hydraulic conductivity of the subsurface. By doing so, the resulting groundwater table does not raise above the ground surface, which can easily happen when the hydraulic head is only calibrated at the emplacement hole (or close-by). Fixing the groundwater table versus not fixing it has shown to affect the groundwater travel time significantly.

The range of likely groundwater travel times at Long Shot as determined in this study is between 1,100 and 500,000 years. Wheatcraft (1995) estimated a groundwater travel time of 900 years in a finite element study of Long Shot, which compares well to results in this study. Hassan et al., (2002) performed stochastic modeling of Long Shot and in the 240 realizations performed almost 100 % showed a mass breakthrough within 2,200 years. The shortest mass arrival time was within 10 years. The main differences (except for the modeling approach) between the study by Hassan et al., (2002) and this study is that they used an anisotropy ratio of 1:10, and the effective porosity was up to three orders of magnitude smaller than in this study which would explain the short travel times of less than 10 years as estimated in their study.

In this study likely groundwater travel times at Cannikin range from 2,100 to four million years. This falls within the range that was determined by previous studies. From Darcy's law, age dating water, and infiltration parameter Fenske (1972) estimated the groundwater travel time to range between 3,300 and 4,400 years at Cannikin. Ballance (1970) estimated the groundwater travel times at Cannikin from hydraulic conductivities to range from more than hundred years to more than a million years. Hassan et al., (2002) and Hassan and Chapman (2006) performed stochastic modeling and at Cannikin approximately 85 of the 260 realizations did not show any mass breakthrough within the 2,200 years

timeframe and only 5 realizations have above 90 % breakthrough. Similar to Long Shot, the main differences between the study by Hassan et al., (2002) and this study is that an anisotropy ratio of 1:10 was used and the effective porosity was up to five orders of magnitude smaller than in this study.

Hassan and Chapman (2006) refined their model using the effective porosity and transition zone defined by Unsworth et al., (2007). They concluded that there was no radionuclides breakthrough to the marine environment within their modeling timeframe of 2,000 years at all three detonations. It is unknown how they defined the transition zone seeing as a saltwater concentration for the TZ as determined by MT was not documented.

Do these simulations confirm other studies seeing as the groundwater travel times compare well with earlier studies even though another method has been used? These results do not confirm other studies. Rather, it shows that more information is needed in order to decrease the uncertainty in the groundwater travel time. For example, Hassan et al. (2002) used a low value of effective porosity (yields short travel times) and a high anisotropy (yields long travel times) whereas this study used a high value of porosity (yields long travel times) and low anisotropy (yields short travel times), and this is more likely why the travel times compare well. If the same effective porosity were used in this study as was used by Hassan et al. (2002) the groundwater travel times would be significantly shorter than shown. Even though the results imply that the groundwater travel time are more than 1,000 years from the time of the detonation, more information of the subsurface is needed.

## Chapter 9 Conclusions

This study has shown that the groundwater travel times and seafloor arrival locations, can be estimated with groundwater modeling if the location of the transition zone as determined by magnetotellurics is available. It is important to note that just by measuring the TZ without knowing the actual saltwater concentrations, it is not possible to predict the groundwater travel time without doubt. The saltwater concentration for a TZ as determined by MT and the general subsurface characteristics could be quantified with groundwater modeling when geophysical constraints in combination with saltwater and hydraulic head measurements are available.

In general, the shape of the simulated transition zones compared to the shape of measured TZ compares better at Long Shot than at Cannikin. At both sites, the simulated shapes of the bottom TZ compares better than the top to measured TZ. At both sites, there is a dip of the top TZ at the east side of the island and an upturn of the bottom TZ on the west side of the island. These features could be the result of heterogeneities that change the shape of the TZ. At Long Shot, this was shown by including an andesite sill layer with an enhanced hydraulic conductivity and, at Cannikin, by assigning a higher hydraulic conductivity at the location of an assumed rubble chimney. The dips and upturns are more likely an artifact from MT due to the low resolution MT data at the island boundaries (Unsworth, 2007).

At some simulated scenarios, the saltwater concentrations for the top and bottom TZ range over 10,000 mg/l. It seems likely that MT can detect a saltwater concentration range greater than 10,000 mg/l therefore these scenarios were excluded and considered unlikely scenarios. At Long Shot, a scenario with a subsurface of an anisotropy ratio of 1:2 results in a more reasonable range of saltwater concentrations (less than 10,000 mg/l) than the isotropic scenarios and scenarios with a subsurface having an anisotropy ratio of 1:10. At Cannikin, a

more reasonable range of saltwater concentration was seen for an isotropic subsurface and an anisotropy ratio of 1:2.

At Long Shot, simulated saltwater concentrations and hydraulic heads compare best to measured saltwater concentrations and hydraulic heads when an anisotropy ratio of 1:10 is applied to the subsurface. Simulated hydraulic heads for the isotropic scenario and the scenario with a subsurface having an anisotropy ratio of 1:2 matches the shallow well measurement but not the deeper well measurements. It should be noted that there are limited saltwater and hydraulic head measurements at Long Shot. Comparisons to saltwater concentrations and hydraulic heads could give unreliable results. This is confirmed by the wide range of simulated saltwater concentrations that are seen at the isotropic and anisotropy ratio of 1:10.

At Cannikin, saltwater concentration measurements compare well with simulations for the isotropic scenarios. Shallow hydraulic head measurements compare well with scenarios that have a subsurface with an anisotropy ratio of 1:10, but not with other scenarios. Difficulties matching these measurements could be due to the fact that this well is located 1 km north of SGZ and outside the White Alice Creek basin. Shallow hydraulic heads from UAe-1 could not be matched with any scenarios, which could be explained by difficulties in the drilling and testing of this hole, making these measurements questionable. Deeper measured hydraulic heads compare well with the isotropic subsurface and the scenario with a subsurface that has an anisotropy ratio of 1:2. Hassan et al., (2002) also experienced difficulties matching shallow and deep head measurements in the same simulation.

These results imply that the subsurface at Long Shot has an anisotropy ratio of 1:2 and the subsurface at Cannikin has an isotropic subsurface or an anisotropy ratio of 1:2. This confirms the study by Fenske (1972) where it was reported that Amchitka Island could be considered homogeneous and isotropic below a depth of 400 mbsl.

The seafloor arrival locations move farther from shore with increased anisotropy. Particles in an isotropic subsurface will arrive closer to shore than particles with an anisotropic subsurface. At Long Shot, the maximum distance of seafloor arrival locations is approximately 1 km offshore and can be seen for a subsurface with an anisotropy ratio of 1:10. For a subsurface with an anisotropy ratio of 1:2, the seafloor arrival locations are a few hundred meters from shore and less than hundred meters for an isotropic subsurface. The seafloor arrival locations for the andesite sill scenarios are 350 m offshore. It was concluded that the subsurface most likely does not have an anisotropy ratio of 1:10, making it important to perform sampling closer to shore. It remains a possibility that the subsurface has an anisotropy ratio of 1:10 and, thus, some sampling should be performed at least 1 km offshore. At Cannikin, the particles arrive farther offshore compared to at Long Shot due to the deeper detonation. Seafloor arrival locations range from 550 m to 2,100 m offshore with the farthest distance from shore being for a subsurface with an anisotropy ratio of 1:10 and the closest from shore for the isotropic subsurface. The subsurface does most likely not have an anisotropy ratio of 1:10, thus more frequent sampling should be performed at 550 m and up to 1,100 m offshore. An anisotropy ratio of 1:10 was seen for some scenarios making it important to perform some sampling at least 2,100 m offshore.

The maximum distance of initial radionuclide distribution is unknown. At the Nevada Test Site, volatile radionuclides have been documented throughout the rubble at a minimum distance of five cavity radii vertically (Kersting, 1996). IAEA (1998a) reported that 10 % of  $^{233}\text{U}$  and  $^{236}\text{U}$  and 2 % of plutonium isotopes could be distributed in the rubble chimney. At Long Shot, it was shown that for an isotropic subsurface there is no significant difference between the groundwater travel time from the bottom of the cavity and from five cavity radii up into the rubble chimney. But, for an anisotropic subsurface, it was shown that there is a considerable difference in travel time between the two locations, making it

important to investigate the groundwater travel time from both locations. At Cannikin, the groundwater travel times vary significantly between particles originating at the bottom of the cavity and at five cavity radii up into the chimney for isotropic and anisotropic subsurface. Further studies should investigate groundwater travel times throughout the chimney

In this study, the influence on groundwater travel time for different dispersivities was investigated. At Long Shot there was a small saltwater concentration difference arising from different assumed dispersivities and no significant difference in groundwater travel time between dispersivities of 50 m, 100 m, and 200 m. In contrast, at Cannikin, even though there is only a minor effect on the saltwater concentration, there is a great difference in groundwater travel time for different dispersivities with longer travel times, for smaller dispersivities, and for increased anisotropy. Pohlmann et al., (2002) investigated the effect that dispersivity has on head and saltwater concentrations at Milrow. It was shown that the dispersivity has minor effects on concentrations. This study shows that even if the dispersivity has a minor impact on saltwater concentrations, it can have a significant difference in groundwater travel time with a greater effect the deeper the location of the transition zone. Large dispersivities should be included in groundwater travel time studies.

The shortest groundwater travel time at Long Shot for a subsurface with an anisotropy ratio of 1:2 is approximately 1,200 years. When an andesite sill layer with enhanced hydraulic conductivity is added to a conservative scenario (isotropic), the groundwater travel time decreases by 55 %. It has also been shown that once the width of the andesite sill layer reaches a total width of 4,000 m (2,000 m east and west of Long Shot), the groundwater travel time reaches a minimum and does not decrease further. In further modeling efforts, including an andesite sill layer with a total width of 4,000 m will result in the shortest groundwater travel time and thus the most conservative scenario.

At Cannikin, the shortest groundwater travel time for a likely scenario is an isotropic subsurface with a hydraulic conductivity of  $3.8 \times 10^{-7}$  m/s, where  $t_{\text{cavity}}$  and  $t_{5r}$  is 5,200 years and 2,100 years respectively. Adding an enhanced hydraulic conductivity to the rubble chimney for the likely scenario ( $K = 3.8 \times 10^{-7}$  m/s) decreases the groundwater travel times, but it also results in a recharge that is too high and a resulting saltwater concentration distribution that is too wide. It is important to look at the saltwater distribution throughout the depth to see whether it is reasonable when compared to the TZ as determined by MT. If there is a rubble chimney with an enhanced hydraulic conductivity, the hydraulic conductivity of the subsurface is most likely lower than  $3.8 \times 10^{-7}$  m/s, resulting in  $t_{\text{cavity}}$  and  $t_{5r}$  longer than 5,200 and 2,100 years respectively. It could also be that the chimney does not extend to the surface with a uniform hydraulic conductivity, or that an order of magnitude higher hydraulic conductivity compared to surrounding rock for the rubble chimney is too high, which would also result in longer groundwater travel times. As seen in the rubble chimney scenario, the saltwater concentration distribution changed dramatically to a range that is too wide making it important to note that when including heterogeneities, the distribution of the saltwater concentration should be investigated.

MT measurements show a reduced resistivity at the location of the cavity and chimney, which could be due to an enhanced porosity. The porosity as reported by Unsworth et al., (2007) was used throughout the cross section resulting in the groundwater travel time at Cannikin would be somewhat underestimated.

Adding Cannikin Lake to the simulation decreases the groundwater travel time with only a few percent for the isotropic scenario. This could change if the lake was applied to a scenario where the saltwater concentration is greater than 32,000 mg/l at a depth of 1,880 mbsl. It has been shown that the groundwater travel times increase significantly when the saltwater concentration is greater than 32,000 mg/l due to a significant increase in groundwater velocity.

It has been shown that it is important to fix the groundwater table throughout the island at the Long Shot profile. The groundwater travel time is 35 % longer at the Long Shot site when the groundwater table is not fixed. At Cannikin, the resulting groundwater travel time is more conservative when the groundwater table is not fixed to the groundwater surface. These results could change if a better topography can be obtained.

The saltwater concentrations for the top TZ is at 0 – 1 mg/l with an uncertainty range of 0 – 200 mg/l. The bottom TZ has a saltwater concentration of 32,800 to 33,000 mg/l with an uncertainty range between 30,100 to 33,000 mg/l. These saltwater concentrations can be used in further modeling studies of Amchitka Island. It is also possible that these saltwater concentrations could be used at similar island and seawater intrusion studies where there is available MT data of the subsurface.

DOE is planning a long-term monitoring program sampling biota at a time interval of five years. According to this study, the earliest groundwater travel time is 1,200 years from the time of the detonation and the longest groundwater travel time is 4 million years. In order to decrease this range, additional information about the subsurface is needed because this range is from already measured and estimated values of hydraulic conductivity and recharge at Amchitka. Unless we know better how the subsurface is constructed we cannot decrease the uncertainty of the groundwater travel time. If additional studies can be performed to achieve a better understanding of the subsurface, there is a possibility that the monitoring could be performed at a time interval longer than five years.

Given what we know today (excluding unknown heterogeneities and seismic events) combined with the results from this study, accepting the accuracy of assumptions in this approach, we can conclude that there is no imminent risk of contamination to the environment. It will be about 1,200 to 4 million years before any contamination reaches the marine environment and poses a risk to marine and human health. This study has also shown that more investigations of the

island are needed in order to determine the groundwater travel times to the marine environment seeing as heterogeneities can influence the groundwater travel time significantly.

## Chapter 10 Further work

Additional drilling on Amchitka Island is expensive and prohibited at certain locations, which makes supplementary information of the subsurface difficult to attain through hydrotesting. However, even without additional information on subsurface and meteorological parameters, further modeling could be performed. Only Long Shot and Cannikin were investigated due to limited information at the Milrow site. MT measurements at Milrow could be used in further modeling to confirm the saltwater concentration distributions for the TZ as determined in this study. Caution should be taken due to the limited data for this site. In addition, this study assumed a longitudinal transverse dispersivity ratio of 10. Other ratios could be investigated to see how the ratio affects the shape of the transition zone. It is also important to investigate further the influence dispersivities have on the groundwater travel times due to the effect seen at Cannikin. It is not apparent why different dispersivities at Cannikin do not show a difference in shapes of TZ. It is likely that this does not have an affect on the groundwater travel time but could need some further investigations.

In this study, the groundwater table was fixed to one meter below ground surface. It has been shown that there is a difference in groundwater travel time when the groundwater table is fixed to one meter below the ground surface at the island boundary compared to when it is not fixed and only calibrated close to the surface. It needs to be investigated further how much this affects the groundwater travel time. Such an investigation would be successful if the location of the groundwater table and topography data throughout the MT profiles could be determined. Topographic data could be collected at the next research expedition, whereas determining the groundwater table is more complex but feasible. The groundwater table could be measured by installing piezometers. These could be measured manually when visiting the island or pressure

transducers could be connected to data loggers where the information would be stored until downloaded or monitored via satellite.

When modeling, likely simulated scenarios can be determined by looking at the size of a simulated recharge. If this simulated recharge were greater than measured recharge the simulation would not be a likely scenario. Taking additional meteorological and hydrological measurements at the drainage basin for each site and performing water balances would result in a better understanding on recharge and thus help in determining if a simulated scenario is likely or not likely.

The simulated shape of the transition zones could not be matched entirely to the measured TZ. This indicates that there are unknown heterogeneities in the subsurface. If these heterogeneities have an enhanced hydraulic conductivity, it can decrease the groundwater travel time significantly, which was shown when an andesite sill layer and an assumed rubble chimney were included. Difficulties in matching the simulated data at the island boundaries is most likely due to the sparse data collected in 2004 at the island boundaries (Unsworth, 2007). Further measurements using MT or other seismic surveys could be performed to gain a better understanding of the subsurface. Many faults cross the island and if these experience an enhanced hydraulic conductivity, the groundwater travel time could decrease significantly. Further investigations should thus be performed perpendicular to the MT profiles collected in 2004 to see if faults possibly influence the travel paths close to the detonations. This was suggested for the 2004 expedition but due to limited time this was not performed (Unsworth et al., 2007).

Detecting the freshwater seepage zones would facilitate in understanding the subsurface and possible radionuclide seepage zones. Seafloor electromagnetic measurements in combination with other methods have been shown to be successful in mapping zones of freshwater (Hoefel and Evans, 2001). Continuous-resistivity profiling has also been demonstrated to be successful in

locating the freshwater – saltwater boundary (Belaval et al., 2003). These are two additional methods that could possibly be used to locate the freshwater seepage zones at the detonation sites.

There are many uncertainties when determining the groundwater travel time. Some uncertainties could be decreased if additional information at the sites was collected. What if the effective porosity is one order of magnitude less than estimated? Effective porosities as determined by MT compare well with effective porosities reported by Spitz and Moreno (1996) for generic volcanic tuff and basalt. This comparison may not mean much because these estimations of the effective porosities were not performed on Amchitka. If the effective porosity were one order of magnitude less than estimated, the groundwater travel time would also be one order of magnitude less than shown in this study and result in groundwater travel times of approximately 100 years. What if there are numerous layers with an enhanced hydraulic conductivity? These are all important aspects that need to be investigated in further studies in order to determine when and where radionuclides could be seeping out to the marine environment.

## Chapter 11 References

- Allen, B.A., S. L. Jr. Drellack, and M. J. Townsend, Surface effects of underground nuclear explosions. *U.S. Department of Energy Report DOE/NV/11718-122*, 1997.
- Anderson, M. P., Using models to simulate the movement of contaminants through groundwater flow systems, *CRC Crit. Rev. Environ. Control*, 9, 97-156, 1979.
- Archie, G. E., The electrical resistivity log as an aid in determining some reservoir characteristics. *Transactions of the American Institute of Mining, Metallurgical and Petroleum Engineers*, no. 146, 54-62, 1942.
- Ballance, W. C., Hydraulic tests in UA-1 and water inflow into an underground chamber, Amchitka Island, Alaska. *U.S. Geological Survey, USGS-474-72*, 1970.
- Ballance, W. C., Hydraulic tests in UAe-1, Amchitka Island, Alaska. *U.S. Geological Survey, USGS-474-102*, 1972.
- Ballance, W. C., and G. A. Dinwiddie, Hydraulic testing of hole UA-1-HTH-1, Amchitka Island, Alaska. *U.S. Geological Survey, USGS-474-144*, 1972.
- Belaval, M., J. W. Jr. Lane, D. P. Lesmes, and G. C. Kineke, Continuous-resistivity profiling for coastal groundwater investigations: three case studies, in *Symposium on the Application of Geophysics to Engineering and Environmental Problems (SAGEEP)*, April 6-10, 2003, San Antonio, Texas, Proceedings: Denver, Colorado, Environmental and Engineering Geophysical Society, CD-ROM, 14 p, 2003.
- Beteem, W. A., R. A. Young, C. L. Washington, and L. J. Schroder, Chemical analyses of water samples collected on Amchitka Island, Alaska, *USAEC Report USGS-474-135*, U.S. Geological Survey, 1971.
- Boardman, C.R. and J. Skrove, Distribution in fracture permeability of a granitic rock mass following a contained nuclear explosion, *J. Pet. Technol.*, 18, pp. 619-623, 1966.
- Carr, W. J. and W. D. Quinlivan, Progress report on the geology of Amchitka Island, Alaska. *U.S. Geological Survey, USGS-474-44 (Amchitka-5) (revised)*, 1969.

Castagnola, D. C., Tritium anomalies on Amchitka Island, Alaska Part I. Teledyne Isotopes *Report for the U.S. Atomic Energy Agency, Nevada Operations Office, NVO-1229-113 Part 1*, 1969.

Claassen, H. C., Hydrological processes and radionuclide distribution in a cavity and chimney produced by the Cannikin nuclear explosion, Amchitka Island, Alaska. *Geological Survey Professional Paper 712-D*, U.S. Geological Survey, Washington, DC, p. 28, 1978.

Cooper H. H., Jr., F. A. Kohout, H. R. Henry, R. E., Glover, Sea water in coastal aquifers. Relation of salt water to fresh water. *Geological Survey Water-Supply Paper 1613-C*. United States Government Printing Office, Washington, 1964.

Dasher, D., W. Hanson, S. Read, S. Faller, D. Farmer, W. Efurud, J. Kelley, and R. Patrick, An assessment of the reported leakage of anthropogenic radionuclides from the underground nuclear test sites at Amchitka Island, Alaska, USA to the surface environment. *Journal of environmental radioactivity*. (60) 165-187, 2002.

Diersch, H.-J. G., FEFLOW: Finite element subsurface flow and transport simulation system. In *FEFLOW 5.2 User's Manual*, Berlin, Germany: WASY, Institute for Water Resources Planning and Systems Research Ltd, 2002.

DOE, see U.S. Department of Energy.

EPA, see U.S. Environmental Protection Agency.

Fenske, P. R., Event-related hydrology and radionuclide transport at the Cannikin Site, Amchitka Island, Alaska. Desert Research Institute, *Center for Water Resources Research, Report 45001, NVO-1253-1*, 1972.

Fetter, C. W., *Applied Hydrogeology*. 2nd ed. New York: Macmillan Publishing Company, 1988.

Fitts, C. R., *Groundwater Science*. San Diego: Academic Press, 2002.

Garber, M. S., A method for estimating effective porosity in a rubble chimney formed by an underground nuclear explosion, *U.S. Geological Survey, Prof. Paper 750-C*, Denver, CO, 1971.

Gard, L. M., Hale, W. E., Geology and hydrology of the Long Shot Site, Amchitka Island, Alaska, *Technical Letter: Long Shot-1*, United States Department of the Interior Geological Survey, 1964.

Gonzalez, D. D., L. E. Wollitz, G. E., Brethauer, Bathymetry of Cannikin Lake, Amchitka Island, Alaska, with an evaluation of computer-mapping techniques. *U.S. Geological Survey. USGS-474-203*, 1974.

Gonzalez, D. D., Hydraulic effects of underground nuclear explosions, Amchitka Island, Alaska. Ph.D. Dissertation, Colorado State University, Fort Collins, Colorado, 141p.,1977.

Hassan, A., K. Pohlmann, J. Chapman, Modeling groundwater flow and transport of radionuclides at Amchitka Island's underground nuclear tests: Milrow, Long Shot, and Cannikin. Las Vegas, NV. *Desert Research Institute Publication No. 45172, DOE/NV/11508-51*, 2002.

Hassan, A. and J. Chapman, Verification and uncertainty reduction of Amchitka underground nuclear testing models. Las Vegas, NV. *Desert Research Institute Publication No. 45172, DOE/NV/13609-46*, 2006.

Hazleton-Nuclear Science Corporation, Interim ground-water safety feasibility, project Long Shot. *Earth Sciences Section Hazleton-Nuclear Science Corporation Report HNSTR-1229-123*, Palo Alto, California, 1964.

Hoefel, F. G., and R. L. Evans, Impact of low salinity porewater on seafloor electromagnetic data: A means of detecting submarine groundwater discharge. *Estuarine, Coastal and Shelf Science* 52, 179-189, 2001.

Hu Q., D. K. Smith, T. Rose, L. Glascoe, C. Steefel, M. Zavarin, Radionuclide mobility at the Nevada Test Site. *Office of Civilian Radioactive Waste Management of the Department of Energy. Report UCRL-TR-2000953.*, 2003.

IAEA, The radiological situation at the atolls of Mururoa and Fangataufa, Technical Report, Volume 3, Inventory of radionuclides underground at the atolls. International Atomic Energy Agency, Austria, 1998a.

IAEA, The radiological situation at the atolls of Mururoa and Fangataufa, Summary Report, Report by an advisory committee. Interim (unedited) version. International Atomic Energy Agency, Austria, 1998b.

Johnson, M., C. Stewart, Results from the Amchitka Oceanographic Survey, in Powers, C.W. et al., Editors, 2005. Biological and Geophysical Aspects of Potential Radionuclide Exposure in the Amchitka Marine Environment. Consortium for Risk Evaluation with Stakeholder Participation, Institute of Responsible Management, Piscataway, NJ, 2005.

Johnson, M., Personal communication, Fairbanks, Alaska, 2005.

Kersting, A., The state of the hydrologic source term. *Lawrence Livermore National Laboratory, report UCRL-ID-126557*, 1996.

Knox R. C., D. A. Sabatini, and L. W. Canter, *Subsurface transport and fate processes*. Lewis Publishers, Boca Raton, Florida, 1993

Lee, W. H. and L. M. Gard, Summary of the subsurface geology of the Cannikin site, Amchitka Island, Alaska. *U.S. Geological Survey, USGS-474-132 (Amchitka 6-4)*, 1971.

Luszczynski, N.J., 1961. Head and flow of ground water of variable density. *Journal of Geophysical Research. Volume 66 No. 12*, 1961.

McKeown, F. A., R. A. Young, W. F. Williams, and G. E. Brethauer, Geologic effects of the Long Shot explosion, Amchitka Island, Alaska. *U.S. Geological Survey, Technical Letter: Long Shot-3*, 1967.

Merritt, M. L., Physical and biological effects, Cannikin. *U.S. Atomic Energy Commission, report NVO-123*, Nevada Operations Office, Las Vegas, Nevada, 106p., 1973.

Merritt, M. L., R.G. Fuller, editors, *The environment of Amchitka Island, Alaska*. Energy Research and Development Administration, Technical Information Center, 1977.

Myers, J. D., The Geology, Geochemistry and Petrology of the recent Magmatic Phase of the Central and Western Aleutian Arc. Unpublished manuscript, 1994.

Perry, R. B., and H. Nichols, Bathymetry of Adak Canyon, Aleutian Arc, Alaska. *Geological Society of America Bulletin, v. 76, no.3*, 1965.

Pohlmann, K. F., A. E., Hassan, and J. B. Chapman, Modeling density-driven flow and radionuclide transport at an underground nuclear test: Uncertainty analysis and effect of parameter correlation. *Water Resources Research, Vol. 38, NO. 5. 10.1029/2001WR001047*, 2002.

Powers, C. W., J. Burger, D. Kosson, M. Gochfeld, and D. Barnes, eds., et al (see author list on page iii), *Biological and Geophysical Aspects of Potential Radionuclide Exposure in the Amchitka Marine Environment*. Consortium for Risk Evaluation with Stakeholder Participation, Institute for Responsible Management, Piscataway, New Jersey, 2005.

Ryan, H. F., and D. W. Scholl, Geologic implications of great interplate earthquakes along the Aleutian Arc: *Journal of Geophysical Research*, v. 98, p. 22,135-22,146, 1993.

Schroder, L. J. and W. C. Balance, Summary of chemical and radiochemical monitoring of water for the Cannikin event, Amchitka Island, Alaska, Fiscal year 1972. *U.S. Geological Survey, USGS-474-167*, 1973.

Silva R. J. and H. Nitsche, Actinide environmental chemistry. *Radiochimica Acta* 70/71:377-396, 1995.

Smith, D. K., and W. L. Bourcier, The production and dissolution of nuclear explosive melt glasses at underground test sites in the Pacific region. *Lawrence Livermore National Laboratory, Report UCRL-JC-130095*, 1998.

Spitz, K., and J. Moreno, *A practical guide to groundwater and solute transport modeling*. New York, NY, John Wiley & Sons, Inc, 1996.

SRTM, <http://srtm.usgs.gov/> Accessed February 15, 2005.

SRTM, <http://srtm.usgs.gov/> Accessed November 7, 2006.

Unsworth, M., W. Soyer, V. Tuncer, Magnetotelluric measurements for determining the subsurface salinity and porosity structure of Amchitka Island, Alaska, in Powers, C.W. et al., Editors, 2005. *Biological and Geophysical Aspects of Potential Radionuclide Exposure in the Amchitka Marine Environment*. Consortium for Risk Evaluation with Stakeholder Participation, Institute of Responsible Management, Piscataway, NJ, 2005.

Unsworth, M., W. Soyer, V. Tuncer, A. M. Wagner, D. L. Barnes, Environmental and hydrogeological assessment of the Amchitka Island Nuclear test site (Alaska) with magnetotellurics, *Geophysics* 10.1190/1.2539353, 2007.

Unsworth, M., Personal communication via e-mail, Fairbanks, Alaska, 2007.

USGS, see U.S. Geological Survey.

U.S. AEC, *Project Cannikin*. United States Atomic Energy Commission, 1971.

U.S. Army Corps of Engineers and U.S. Geological Survey, Project Long Shot Amchitka Island, Alaska, Geologic and Hydrologic Investigations *Main Report (Phase 1)*. *Unnumbered report*, 1965.

U.S. Department of Energy, United States Nuclear Tests July 1945 through December 1992. *U.S. Department of Energy, Report DOE/NV-209 (Rev. 15)*, 2000.

U.S. Department of Energy, Subsurface completion report for Amchitka underground nuclear test sites: Long Shot, Milrow, and Cannikin. *U.S. Department of Energy, National Nuclear Security Administration, Nevada Site Office. DOE/NV-1106-REV. 1*, 2006a

U.S. Department of Energy, Long-term surveillance and maintenance plan for the U.S. Department of Energy Amchitka, Alaska, Site. *U.S. Department of Energy Office of Legacy Management, Report DOE-LM/GJ1 131-2006*, 2006b

U.S. Environmental Protection Agency, Long term hydrological monitoring program: Amchitka, Alaska 1997. Washington, DC: *EPA Radiation and Indoor Environments National Laboratory, EPA-402-R-98-002*, 1998.

U.S. Geological Survey, Geologic and hydrologic effects of the Milrow event, Amchitka Island, Aleutian Islands, Alaska. *U.S. Geological Survey, Report USGS-474-71*, 1970.

U.S. Geological Survey, Geological and hydrological effects of the Cannikin underground nuclear explosion, Amchitka Island, Aleutian Islands, Alaska. (Amchitka-33). *United States Department of the Interior Geological Survey, USGS-474-148*, 1972.

Voss, C. I., A finite-element simulation model for saturated-unsaturated fluid-density-dependent ground-water flow with energy transport or chemically-reactive single-species solute transport. *U.S. Geological Survey Water-Resources Investigations Report 84-4369*, 1984.

Wheatcraft, S. W., Sea water intrusion model of Amchitka Island, Alaska. Nevada Operations Office, *U.S. Department of Energy, Report DOE/NV/10845-59*, 1995.